2009-07-09

Ion Transport Behaviors Upstream and Downstream from the Sampling Cone of an Inductively Coupled Plasma Mass Spectrometer

Haibin Ma
Brigham Young University - Provo

ION TRANSPORT BEHAVIORS UPSTREAM AND DOWNSTREAM FROM

THE SAMPLING CONE OF AN INDUCTIVELY COUPLED PLASMA MASS

SPECTROMETER

by

Haibin Ma

A dissertation submitted to the faculty of

Brigham Young University

In partial fulfillment of the requirements for the degree of

Doctor of Philosophy

Department of Chemistry and Biochemistry

Brigham Young University

August 2009

BRIGHAM YOUNG UNIVERSITY

GRADUATE COMMITTEE APPROVAL

of a dissertation submitted by

Haibin Ma

This dissertation has been read by each member of the following graduate committee and

by majority vote has been found to be satisfactory.

_____   _____
Date   Paul B. Farnsworth, Chair

_____   _____
Date   David V. Dearden

_____   _____
Date   Steven R. Goates

_____   _____
Date   Eric T Sevy

_____   _____
Date   Ross L. Spencer

BRIGHAM YOUNG UNIVERSITY

As chair of the candidate's graduate committee, I have read the dissertation of Haibin Ma in its final form and have found that (1) its format, citations and bibliographical style are consistent and acceptable and fulfill university and department style requirements; (2) its illustrative materials including figures, tables, and charts are in place; and (3) the final manuscript is satisfactory to the graduate committee and is ready for submission on to the university library.

_____   _____

Date   Paul B. Farnsworth

                                                             Chair, Graduate Committee

Accepted for the Department

                                                         _____

                                                             David V. Dearden

                                                             Graduate Coordinator

Accepted for the College

                                                         _____

                                                             Thomas W. Sederberg

                                                             Associate Dean, College of Physical and

                                                             Mathematical Science

ABSTRACT

ION TRANSPORT BEHAVIORS UPSTREAM AND DOWNSTREAM FROM THE

SAMPLING CONE OF AN INDUCTIVELY COUPLED PLASMA MASS

SPECTROMETER

Haibin Ma

Department of Chemistry and Biochemistry

Doctor of Philosophy

Inductively coupled plasma - mass spectrometry (ICP-MS) is the technique of choice

worldwide for trace elemental determinations because of its excellent ionization ability,

low detection limits and fast analysis speeds. However, the ICP-MS still suffers from

some disadvantages, such as spectral overlap and severe matrix effects. Matrix effects or

interferences, partly arise from changes in the analyte transmission through the interfacial

region between the ICP and mass spectrometer with changes in sample matrix. Better

understanding of the transmission behaviors of analyte through the sampling and

skimmer cones will provide the insights needed to alleviate matrix interferences and to

improve the interface design between the ICP and mass spectrometer.

Laser induced fluorescence is a highly sensitive, non-invasive and element specific

detection method. The research herein endeavors to explain the transport behaviors of

analytes upstream and downstream from the sampling cone in an ICP-MS. The final goal

of this research is to improve the consistency and efficiency with which ions are transported from an ICP source to a mass analyzer.

Several issues related to analyte transmission through the sampling and skimmer cones have been explored and discussed in this dissertation. First, it is found that the existence of the sampling cone not only disturbs the local thermodynamic equilibrium of the plasma, but also changes the spatial distributions and number densities of analyte species. Second, it has been verified that the spread of analyte species in the first vacuum stage is mass-dependent and can be explained by ambiploar diffusion theory. Finally, the current research suggests that the transmission efficiencies of the skimmer cone are impacted by the nebulizer flow and first vacuum stage pressure of the ICP-MS.

To better elucidate the analyte transport behaviors from the plasma to the ion detector in an ICP-MS, more investigation needs to be carried out. Further research, such as the entire measurements of analyte transmission efficiency through the skimmer cone, the variation of doubly charged ions under different plasma operational conditions, and the functions of argon metastable atoms on analyte ionization inside the plasma will require much additional work.

TABLE OF CONTENTS

1. INTRODUCTION

1.1. Introduction to Inductively Coupled Plasma – Mass Spectrometry

Inductively coupled plasma - mass spectrometry (ICP-MS), which features several outstanding capabilities, including good ionization ability, low detection limits and excellent selectivity, has been used routinely in research laboratories and for industrial applications for precise, ultra-trace element detection and component analysis.[1] In 2005, more than 5000 ICP-MS systems had been installed worldwide, covering a diverse range of applications including chemical, environmental, geochemical, biochemical, semiconductor, clinical, nuclear, and metallurgical areas.[2]

1.1.1. The fundamental aspects of ICP-MS

Although specific designs of commercially-produced ICP-MS instruments vary, they all share the same fundamental components: a sample introduction system, a plasma torch, an interfacial region, an ion focusing system, a mass separation device, an ion detector, and a personal computer.[2] Many ICP-MS instruments also include collision/reaction cells to overcome the formation of polyatomic spectral interferences originating from the combination of argon, solvent and sample-based ionic species.

During an ICP-MS analysis, the sample is nebulized to a fine aerosol and carried by argon gas into the ICP torch, where it is atomized and ionized. Then the analyte ions are drawn into the mass separation device via the interface, which consists of two similar metallic cones, called the sampler and the skimmer. Each cone features a small size orifice, typically 0.4~1.2 mm. After the skimmer cone, ions pass through to the ion optics, where the ion beam is electrostatically focused and guided into the mass separation device. Finally, an ion detector converts the ions into an electrical signal,

which is processed by a computer.

1.1.2. Atomization and ionization of analytes inside the plasma

Three components are required to form an inductively coupled plasma: a radiofrequency (RF) generator, a coupling coil and a fused silica torch. When argon flows through the fused-silica torch, the rapid changes in the magnetic field generated by the load coil connected with the RF generator will induce eddy currents in electrons and ions seeded into the gas with a Tesla coil. During this process, resistance to the eddy current produces Joule heating, lifting the temperature of argon gas. When the temperature reaches the ionization temperature of the gas, the process is self-sustaining and a plasma forms.[3]

Sample aerosol from the nebulizer is carried into the plasma in a central gas flow. The hot plasma heats the aerosol, removes any remaining solvent, and causes sample atomization followed by ionization.

It has been reported that electron impact, charge transfer, and Penning ionization are the important excitation and ionization mechanisms in an ICP, although which one is the predominant mechanism is still being debated.[4,5,6] Some researchers have suggested that charge transfer between different elements and argon atoms are possible excitation/ionizations mechanisms inside the plasma.[7,8,9] Others have stated that Penning ionization dominates excitation/ionization processes for ionization of most analytes, particularly when matrices with low second ionization potentials exist in the sample. [5,10,11]

1.1.3.   Ion transmission through the interfacial region of an ICP-MS

The interface, which bridges the atmospheric-pressure ionization source and the high-vacuum mass detector, is one of the critical parts in an ICP-MS.[12,13] Analyte ions generated in the plasma are successively extracted through regions of decreasing pressure, as illustrated in Fig. 1.1.
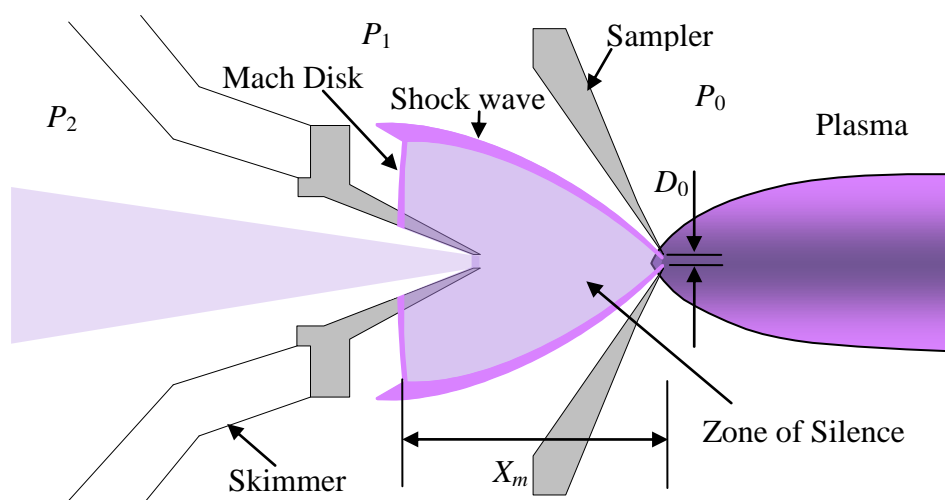
Fig 1.1 Schematic of a typical ICP-MS interface, where the analytes are transported from the plasma to the second vacuum stage, and D_0 is the diameter of the sampler orifice; P_0, P_1 and P_2 are the pressures of the plasma, first and second vacuum stages, respectively; X_m is the distance from the tip of the sampler cone to the Mach disk

A supersonic free jet forms when plasma expands through the sampling cone adiabatically. The random movement of the particles inside the plasma is then converted into directed motion. The flow field behind the sampler consists of a "zone of silence", which is terminated by a Mach disk and surrounded by a barrel shock.[14]

As shown in Equation 1-1,[15] the distance from the sampler cone to the Mach disk (X_m) is proportional to D_0 and the ratio of P_0 to P_1, which are defined in Fig. 1.1:

$$\frac{X_m}{D_0} = 0.67(\frac{P_0}{P_1})^{1/2} \quad (1\text{-}1)$$

In the supersonic jet, the number density of particles drops when the axial position increases.[16] The typical pressure of the first vacuum stage is a few Torr.

Subsequently, after the plasma passes through the skimmer cone, its pressure decreases to approximately 10^{-3} Torr (P_2). Before the skimmer cone, particles with different charges are balanced. After the skimmer cone, the electrons move out of the plasma flow due to their higher mobility, which results in electron depletion. Thus, a space charge effect, which is Coulombic repulsion of positive ions within a high charge density region, occurs behind the skimmer cone.[17] The space charge effect defocuses the ions within the skimmer and prevents the mass spectrometer from giving a true spectrum of the ions of the plasma.[3,18]

Behind the skimmer cone, a series of ion focusing lenses are installed to deliver as many positive analyte ions as possible to the mass separation device.[19,20]

1.2. Capabilities and limitations of ICP-MS technique

The ICP-MS has prominent merits over other atomic spectral techniques in elemental analysis. Compared with other ionization sources, such as direct current plasmas (DCP) and microwave induced plasmas (MIP), ICP-based techniques have better reproducibility. The gas kinetic temperature of the ICP can reach 6000 K, and effectively ionize more than 90% of all the elements.[2] Compared with other elemental analysis techniques, such as atomic absorption spectrometry (AAS) and ICP-Optical Emission Spectrometry (ICP-OES), ICP-MS has clear characteristic advantages in multi-element monitoring, speed of analysis, low detection limits, and isotopic

analysis capability. The ICP-MS offers extremely low detection limits, in the sub part per trillion range for most metal elements, usually 3~4 orders of magnitude better than ICP-OES. ICP-MS also features a linear dynamic range reaching 10^8, and good applicability to a wide range of sample types and sampling conditions.

However, the ICP-MS still suffers from spectral overlap and severe matrix effects. Spectral overlap, which originates mostly from isobaric interferences, and polyatomic or molecular spectral interferences, can be partly alleviated by use of reaction/collision cells or use of a high- resolution mass spectrometer. [3] Degradation of analytical performance due to matrix effect, which is caused by the changes in sample compositions, remains another weakness of ICP-MS, although some methods, such as internal standardization or standard addition, can be adopted to eliminate or overcome this interference.[21] This problem is particularly troublesome when the matrix component is concentrated. Typically, the maximum total dissolved solids in the sample should be below 0.1%. Otherwise, matrix effects can become very pronounced and the sample can accumulate on sampling and skimming cones, preventing transport of analyte ions from the plasma to the mass detector.[22] In addition, the precision and accuracy for lighter elements suffers heavily from the interference of the heavier elements in the solution.

In an ICP-MS, several processes, such as solution nebulization, aerosol transfer from nebulizer to the plasma, atomization and ionization processes inside the plasma, and transport through ICP-MS vacuum interface, contribute to matrix interferences.[23] Until now, much work has been done to better understand the matrix interference in an ICP-MS.[2,3] Full characterization of analye transport behavior through the interfacial region between ICP and Mass spectrometer can facilitate us alleviate the

matrix interference significantly. Interest in consistent generation and delivery of ions from plasma to mass spectrometer has motivated fundamental studies of sampling and skimming processes. So far, many studies have been conducted on characterizing or reducing matrix interference from the ICP-MS interfacial region by different research groups.[3,5,13] However, some important issues still remain in our understanding of the ion extraction and transport processes through the interface of an ICP-MS. Fundamental studies of the causes of these problems could be helpful for alleviating the severity of matrix and other interferences.

1.3. Sensitivity deterioration due to transmission losses through the interface

Sensitivity, which denotes the capacity of an instrument or method to discriminate small concentration differences of analytes, is an important aspect in trace elemental analysis.[24] If an ICP-MS is to provide optimum analytical performance, the analyte ions must be transmitted through the vacuum interface efficiently and consistently.[6,25] Reactions or processes that change the composition of the analyte should be avoided completely.[13]

The sensitivity of an ICP-MS is largely dependent on the fraction of ions created in the source that are transported from the plasma to the mass spectrometer.[26] Due to the pressure drop in the interfacial region of an ICP, usually from atmospheric pressure to 10^{-3} Torr, transport of ions from ICP to MS is inefficient. Only a small fraction of analyte ions can be collected by ion focusing lenses and reach to the mass detector.[27] Furthermore, Any variation in ICP operating parameters can change the amount entering the sampling orifice, changing the sensitivity of the whole instrument.[28] In addition, the high RF power required by ICP can cause a decrease in sensitivity due to the space charge effect of highly ionized argon and high electron

density inside the plasma.[29]

1.4. Factors impacting ions transport through the interface

In this section, matrix and other interferences arising from the interfacial region in ICP-MS applications will be categorized and discussed on the basis of their influence on the ion transmission in an ICP mass spectrometer.

1.4.1.   Matrix interference inside the plasma

The success of ICP-MS applications argues that the knowledge about the ICP as an emission source can be used to understand the ICP as ion sources.[30] However, atomization and ionization mechanisms of analytes in the inductively coupled plasma are not fully understood.[7,8,31] Neither Penning ionization nor charge transfer mechanisms can completely explain the phenomena related to ionization mechanisms observed inside the plasma.[32,33]

Matrix effects are thought to be more severe in ICP-MS than in ICP-OES.[3] Furthermore, many studies have been dedicated to explaining the mechanisms responsible for the matrix effects inside the plasma.[34,35] Several factors control matrix effects arising from an ICP-OES, such as nebulizer flow, RF power, and different sample introduction systems. In addition, the presence of easily ionized elements (EIEs) is a significant matrix concern inside the plasma.[36,37] The existence of EIEs can enhance the energy transfer between the plasma and analytes, thus impacting the atomization and ionization processes. Therefore, high concentrations of EIEs can not only increase either electron number density or electron temperature of the plasma,[38] but also can change the signal intensity of analytes in the plasma,[39] which is related to the amount of ionized analytes and affect the sensitivity in both ICP-OES and

ICP-MS.[40,41,42]

1.4.2.　Influence of the sampling cone

When a low temperature, water-cooled sampling cone is inserted into the plasma, the local thermodynamic equilibrium of the plasma is disturbed slightly.[43] Furthermore, significant differences between the performance of ICP-OES and ICP-MS suggest that the presence of the vacuum interface in ICP ion source changes the plasma, which affect the analytical performance of ICP-MS.[30]

Early researchers thought the properties of bulk plasma were relatively unchanged by the presence of the sampling cone.[44] Subsequently, relying on Thomson and Rayleigh scattering, and line-of-light emission techniques, Hieftje's group compared radial distributions of species densities and temperatures at 6, 7 and 8 mm above the load coil in the presence and absence of the sampling cone.[23] The presence of the cone lowered plasma temperatures and reduced electron densities. They also showed that the matrix in the sample solution lowers the ion number densities in both cases, especially at high central gas flow rate. Furthermore, the sampling cone has a significant influence on spatial distribution and number densities of electrons, analyte atoms and ions.[10,43]

1.4.3.　Diffusion loss downstream from the sampling cone

After the sampling orifice, the bulk gases, including the plasma, analyte atoms and ions, undergo an isentropic, supersonic expansion. During this process, the mean velocities of species in samples should be proportional to the reciprocal of the molar or number average molecular weight in that mixture. The composition of the plasma downstream from the sampling cone is similar to that at the orifice.

There are many parameters affecting the ion transmission efficiency through the sampling cone in an ICP-MS. Some of them are sample composition, RF power, nebulizer flow, and torch shield configuration[45] Using a monodisperse dried microparticulate injector technique, Olesik found that the existence of the sampling cone has a significant impact on the velocities of plasma species.[46] Macedone et al. measured the ion trajectories and variation of plasma composition in the first vacuum stage of an ICP-MS and demonstrated that collisions are a critical factor determining the composition of the plasma entering the skimmer orifice.[47,48]

1.4.4.   Space charge effect related to skimming process

To ensure optimum ion transmission efficiency of the skimming process, the position of the skimmer cone is critical. Unfortunately, in a typical ICP-MS, a shock wave always exists at or near the skimmer orifice, perturbing plasma flow and driving the skimming process far from ideal. Ion currents just behind the skimmer are dramatically lower than those predicted by a gas dynamic model.[49]

Behind the skimmer cone, electron number density drops abruptly and is highly impacted by masses of matrix elements.[50] It was found that ion radial distribution behind the skimmer was mass-dependent.[51,52] In addition, Due to the existence of the shock wave at the tip of the skimmer cone, even when the skimmer orifice enlarged to 2 mm in diameter, the centerline number intensities were still about half those of an ideally skimmed beam.[53]

Theoretically, the space charge effect is severe with highly concentrated solutions; heavy ions cause most matrix effects and force light ions off axis.[54] It has been reported that a three aperture vacuum interface in ICP-MS can minimize space charge

effects, matrix effects, and mass bias without severely limiting sensitivity. This kind of interface can also reduce the formation of shock waves upstream and the space charge effect downstream from the skimmer cone.[55,56] Houk[57,58] improved ion transmission efficiency and analytical sensitivities of an ICP-MS across the full mass range by introducing electrons into the ion beam. The added electrons reduced space charge effects in the second vacuum stage.

Axial and radial distributions of different ions downstream from the skimmer cone have also been recorded in our lab.[59~62] Relying on a reference located outside the interface at the tip of the sampling cone, the researchers also found that the transmission efficiencies of analyte through the whole interfacial region were suppressed by the addition of matrix components.

1.5. Research background and proposed work

This research is designed to better understand the processes controlling ion transport through the vacuum interface of an ICP-MS. The work has concentrated on the following five issues.

1.5.1.   The effects of sampling cone on the plasma

The cold sampling cone has a significant influence on the spatial distribution of atomic and ionic analytes inside the plasma, thus impacting the amount and proportions of analytes directed to the ICP-MS detector.[23] The work described herein relied on laser induced atomic and ionic fluorescence and CCD imaging techniques to measure the spatially resolved distribution of specific analyte atoms and ions inside the plasma. A series of plasma operating conditions in the presence and absence of the sampling cone were used in this research, to better understand the comprehensive

effects of the sampling cone on the atomization and ionization of the analytes inside the plasma.

1.5.2.   Spatial investigation of analytes just upstream from the sampling cone

The spatial distribution of analytes just upstream from the sampling cone is critical for verification of simulation models used to predict transport behaviors, such as diffusion, atomization and ionization processes of analytes in the mass spectrometer-connected plasma. Due to limitations of an earlier experimental setup, spatial distribution information within a 1 mm region just upstream from the sampling cone was unreliable because of a scattering interference from the tip of the sampling cone.[63] A novel excitation laser arrangement was adopted to overcome the scattering interferences from the surface of the sampling cone, thus more reliable spatial distributions of analyte ions and atoms were recorded to test the simulation model being developed by our collaborators in the physics department.

1.5.3.   Mass-dependent spread of ions behind the sampling cone

A paper by Reis[64] concluded that when a free-jet binary gas passes through an orifice, the enrichment of the heavier species is an artifact of a probe effect. This provided a potential hint to explain the mass-bias in the first vacuum stage of an ICP-MS instrument. A comprehensive understanding of the sources of mass bias is critical for isotopic analysis.

Relying on a similar hardware setup to that described in reference 47, the spatial distributions of barium and calcium ions 10 mm downstream from the sampling cone and just at the sampling orifice were measured. The mass dependent diffusion of ions

behind the sampling cone in an ICP-MS was demonstrated experimentally.

1.5.4. Temperature and velocity measurement in the first vacuum stage

Based on Doppler shifts in fluorescence excitation spectra, the velocities of argon metastable atoms were repeatedly measured in the first vacuum stage of an ICP-MS in our group. The initial measurements revealed that two different populations of analytes existed at the mouth of the skimmer: one was heated but moved slowly, another was cold but moved fast.[59] Measurements were extended to the first vacuum stage by Radicic et al.,[13] who studied the velocities and temperatures of argon atoms as a function of spatial position within the mach disk and barrel shock, as functions of nebulizer flow, RF incident power, water loading, plasma and auxiliary gas flow.

Herein, nearly simultaneous velocity and temperature measurements of mass-similar calcium ions and argon atoms behind the sampling cone were carried out. The data were used to examine the effects of charge on gas flow through the first vacuum stage of an ICP-MS.

1.5.5. Ion transmission through the skimmer cone of an ICP-MS

Shock waves formed on or near the tip of the skimmer impact the skimming process significantly. The supersonic expansion, including the zone of silence, shock wave, and Mach disk in the first vacuum stage have been characterized in our lab[61] by fluorescence probing metastable argon atoms, which showed a bimodal velocity distribution of the probe atoms.

To better understand the origins of the disturbance and its effect on ion

transmission through the skimmer, hardware was developed that allowed simultaneous measurements of densities immediately upstream and immediately downstream from the tip of the skimmer cone. Relying on the laser induced fluorescence technique, we measured the ion number densities upstream and downstream from the skimmer cone under different incident powers, nebulizer flows, and sample compositions, and a variety of first vacuum stage pressures. By comparing the ratio of ion number densities at the tip of the skimmer cone and just behind the skimmer cone, the total ion transmission efficiencies through the skimmer cone were calculated.

1.6. Investigation method

The investigation of spatial distributions of analytes inside the plasma source and the interfacial region between the plasma and mass spectrometer is difficult due to the high temperature of the plasma and space limitations in the load coil, sampling and skimmer cones.[60,62] Several techniques have been adapted to study the ion transmission through the interfacial region of an ICP-MS.

An ion deposition technique with nickel mesh was the first tool our lab used to demonstrate the spatial distribution of analyte ions in the second vacuum stage of an ICP-MS.[59] Similarly, a graphite target was used to capture the ions extracted by the skimming cones in an ICP-MS.[66]

The Langmuir probe is another useful tool to measure the electron temperature and density, the space and floating potentials in the interfacial vacuum region of an ICP-MS.[50,67] Unfortunately, neither ion deposition nor the Langmuir probe is an ideal tool due to their insertion of a metal mesh or electrode into the plasma beams, thus

perturbing the ion flow.

Thomson and Rayleigh scatterings are reliable techniques to investigate the gas-kinetic temperature, electron number density and temperature in inductively coupled plasma.[5] Unfortunately, these techniques require an expensive instrumental setup, and a delicate calibration process, and suffer from severe light scattering interferences from particles inside the plasma. In addition, Thomson scattering requires a Gaussian distribution of analyte particles, which is not strictly correct in ICP, thus causing over- or under-estimation of electron temperature and number density.[3]

The laser induced atomic and ionic fluorescence technique is a non-invasive, species-selective, highly sensitive and real-time diagnostic method to probe the spatial distributions of atoms and ions in the plasma and interfacial regions between an ICP and a mass spectrometer.[7, 47] In this technique, only fluorescence resulting from the targeted atoms or ions can produce a signal that can be detected. Noise from scattered light can be minimized by careful selection of test analytes and optical design.

1.7. Research instrumentation

The study of ion transport through the interfacial region of an ICP-MS is an ongoing effort in our lab, which is focused on the ion transmission processes and matrix effects in the interfacial vacuum stage between the inductively coupled plasma and mass spectrometer.[47,48]

Many references[13,45,47, 63] from our lab have given a detailed description of the instruments used in this research. Briefly, a mock-up stage has been constructed for probing and imaging the spatial distributions of ions and atoms upstream and

downstream from the sampling and skimmer cones of an ICP-MS. An Excimer laser with XeCl gas is used to pump dye lasers, which are tuned to excite analyte ions and atoms. The fluorescence produced by the target analyte atoms and ions can be either detected by a photomultiplier tube or an intensified, gated, and high resolution CCD detector.

During each individual project, some modifications to the experimental setup have been carried out to fit the specific research requirements, which will be described in the individual chapters.

1.8. References

[1] Rosen. A. L., Hieftje G. M., *Spectrochimica. Acta Part B*, 59, **2004**, 135

[2] Robert T., *Practical Guide to ICP-MS*, Marcel Dekker, Inc., New York, **2004**

[3] Montaser, A. Golightly, D. W., *Inductively Coupled Plasmas in Analytical Atomic Spectrometry*, 2nd, VCH Publisher, Inc. **1992**

[4] Farnsworth P. B., Woolley, A., Omenetto, N, Matveev, O., *Spectrohimica Acta Part B*, 54, **1999**, 2143

[5] Chan, G. C.-Y., Hieftje, G. M., *Spectrochimica Acta Part B*, 61, **2006**, 642

[6] Niu. H., Houk, R. S., *Spectrochimica. Acta Part B*, 51, **1996**, 779

[7] Farnsworth, P. B., Smith, B. W., Omenetto, N., *Spectrochimica Acta Part B*, 46, **1991**, 843

[8] Ogilvie C. M., Farnsworth, P. B., *Spectrochimica Acta, Part B*, 47,**1992**, 1389

[9] Farnsworth, P. B., Omenetto N., *Spectrochimica Acta Part B*, 48, **1993**, 809

[10] Lehn, S. A., Hieftje, G. M., *Spectromchimica Acta Part B*, 58, **2003**, 1821

[11] Chan, G. C.-Y., Hieftje G. M., *Spectromchimica Acta Part B*, 59, **2004**, 1007

[12] Douglas D. J., French, J. B., *J. Anal. At. Spectrom.*, 3, **1988**, 743

[13] Radicic, W. N., Olsen J. B., Neilson R. V., Macedone J. H., Farnsworth P. B., *Spectrochimica. Acta Part B*, 61, **2006**, 686

[14] Scoles, G., Bassi, D., Buck U., Laine D. C., Atomic and Molecular Beam Methods, V1, Oxford University Press, **1988**

[15] Hieftje G. J. Vickers G. H., *Analytica Chimaca Acta*, 216, **1989**, 1

[16] Niu. H., Houk, R. S., *Spectrochimica. Acta Part B*, 49, **1994**, 1283

[17] Allen L. A., Leach J. J., Houk R. S., *Anal. Chem.*, 69, **1997**, 2384

[18] Gillson G. R., Douglas D. J., Fulford J. E., Halligan K. W., Tanner S. D., *Anal.*

Chem., 60, **1988**, 1472

[19] Tan S. H., Horlick G., *J. Anal. At. Spectrom.*, 2, **1986**, 745

[20] Tanner S D., *Spectrochimica. Acta Part B*, 47, **1992**, 809

[21] Todoli, J. L., Gras L., Hernandis V., Mora J., *J. Anal. At. Spectrom.*, 17, **2002**, 142

[22] Olivares J. A. Houk, R. S., *Anal. Chem.*, 58, **1986**, 20

[23] Lehn, S. A., Huang, M., Warner, K. A., Gamez G., Hieftje G. M., *Spectrochimica. Acta Part B*, 58, **2003**, 1647

[24] Skoog D. A., Holler F. J., Nieman T. A., *Principles of Instrumental Analysis*, 5th, Harcourt Brace & Company, **1998**

[25] Vickers G. H., Wilson D. A., Hieftje G. M., *Spectrochimica. Acta Part B*, 45, **1990**, 499

[26] Macedone, J. H., Farnsworth, P. B., *Spectrochimica Acta Part B*, 61, **2006**, 1031

[27] Dziewatkoski M. P., Daniels L. B., Olesik J. W., *Anal. Chem.*, 68, **1996**, 1101

[28] Cicerone, M. T., Farnsworth P. B., *Spectrochimica Acta Part B*, 44, **1989**, 897

[29] Sakata K., Yamada N., Sugiyama N., *Spectrochimica Acta Part B*, 56, **2001**, 1249

[30] Ma, H., Taylor N., Farnsworth P. B., *Spectrochimica Acta Part B*, **2009**, doi:10.1016/j.sab.2009.04.006

[31] Chan, G. C.-Y., Hieftje G. M., *Spectromchimica Acta Part B*, 63, **2008**, 619

[32] Mermet J. M., *Acad. Sci., B*., 281, **1975**, 273

[33] Schram D. C., Raaymakers I. J. M. M., B. van der Sijde, Schenkelaars H. J. W., Boumans P. W. J. M., *Spectrochimica Acta Part B*, 38, **1983**, 1545

[34] Blades M. W., Horlick, G., *Spectrochimica Acta Part B*, 36, **1981**, 881

[35] Olesik, J. W., Williamson E. J., Appl. Spectrosc., 43, **1989**, 1223

[36] Wu M., Hiefjie G. M., *Spectrochimica Acta Part B*, 49, **1994**, 141

[37] Xu Q., Mattu G., Agnes G. R., *J. Anal. At. Spectrom.*, 16, **2001**, 715

[38] Kalnicky D. J., Fassel V. A., Kniseley R. N., *Appl. Spectrosc.*, 31, **1977**, 137

[39] Sesi N. N., Hieftje G. M., *Spectrochimica Acta Part B*, 51, **1996**, 1601

[40] Oelsik, J. W., Hobbs S. E., *Spectrochimica Acta Part B*, 52, **1997**, 353

[41] Van de Sande, M. J., Wan Eck, P., Gamero, A., Van der Mullen, J. J. A. M., *Spectrochimica Acta Part B*, 58, **2003**, 457

[42] Van de Sande, M. J., Wan Eck, P., Gamero, A., Van der Mullen, J. J. A. M., *Spectrochimica Acta Part B*, 58, **2003**, 783

[43] Lehn, S. A., Warner K. A., Huang M., Hieftje G. M., *Spectrochimica. Acta Part B*, 57, **2002**, 1739

[44] Grain J. S., Smith R. H., Houk R. S., *Spectrochimica. Acta Part B*, 45, **1990**, 249

[45] Macedone, J. H., Gammon, D. J., Farnsworth P. B., *Spectrochimica Acta Part B*, 56, **2001**, 1687

[46] Steward, I. I., Hensman C. E., Olisik J. W., *Appl. Spectrosc.*, 54, **2000**, 164

[47] Macedone, J. H., Mills A. A., Farnsworth P. B., *Appl. Spectrosc.*, 58, **2004**, 463

[48] Macedone, J. H., Farnsworth, P. B., *Spectrochimica Acta part B*, 61, **2006**, 1031

[49] Gillson G. R., Douglas D. J., Fulford J. E., Halligan K. W., Tanner S. D., *Anal. Chem.*, 60, **1988**, 1472

[50] Niu. H., Houk, R. S., *Spectrochimica. Acta Part B*, 46, **1991**, 805

[51] Li, G., Duan Y., Hieftje G. M., *J. Anal. At. Spectrom.*, 30, **1995**, 841

[52] Burgoyne T. W., Hieftje G. M., Hites R. A., *Anal. Chem.*, 69, **1997**, 485

[53] Olney T. N., Chen. W., Douglas D. J., *J. Anal. At. Spectrom.* 14, **1999**, 9

[54] Tan S. M., Horlick G., *J. Anal. At. Spectrom.*, 2, **1987**, 745

[55] Tanner, S. D., Cousins L. M., Douglas D. J., *Appl. Spectrosc.*, 48, **1994**, 1367

[56] Tanner, S. D., Douglas D. J., French J. B., *Appl. Spectrosc.*, 48, **1994**, 1373

[57] Praphairaksit N., Houk R. S., *Anal. Chem.*, 72, **2000**, 2351

[58] Praphairaksit N., Houk R. S., *Anal. Chem.*, 72, **2000**, 2356

[59] Chen. Y., Farnsworth, P. B., *Spectrochimica. Acta Part B*, 52, **1997**, 231

[60] Duersch B. S., Chen Y., Ciocan A., Farnsworth P. B., S*pectrochimica. Acta Part B*, 53, **1998**, 569

[61] Patterson J. E., Duersch B. S., Farnsworth P. B. *Spectrochimica. Acta Part B*, 54, **1999**, 537

[62] Duersch B. S., Farnsworth P. B. *Spectrochimica. Acta Part B*, 54, **1999**, 545

[63] Mills A. A., Macedone, J. H., Farnsworth, P. B., *Spectrochimica Acta Part B*, 61, **2006**, 1039

[64] Reis V. H., Fenn J. B., *J. Chem. Phys.*, 39, **1963**, 3240

[65] Ogilvie C. M., Farnsworth, P. B. *Spectrochimica. Acta Part B*, 47, **1992**, 1389

[66] Burgoyne, T. W., Hieftje, G. M., Hites R. A., *Anal. Chem.*, 69, **1997**, 485

[67] Chambers D. M., Poehlman J., Yang P., Hieftje, G. M., *Spectrochimica Acta Part B*, 46, **1991**, 741

2. SPATIAL INVESTIGATION OF BARIUM ATOMS AND IONS AT THE TIP OF THE SAMPLING CONE OF AN ICP-MS

2.1. Introduction

To improve the sensitivity of an ICP-MS, analyte ions must be transmitted from the plasma through the interfacial region as efficiency as possible.[1,2] Inside the plasma, analyte components are motivated by gas flow and diffusion.[3]

The operating parameters of ICP have significant effects on the analyte signals.[4] The basic experimental variables associated with plasma are plasma gas flow, auxiliary gas flow, nebulizer flow, incident power and sampling depth.[5] Much work has contributed to understand the spatial distributions of analyte species upstream from the sampling cone under different operating conditions.[3,6,7]

In recent work,[8,9] our lab mapped number density distributions of barium ground state atoms, ground state ions, and metastable ions in the region between the load coil and the sampling cone of an ICP-MS under conditions of different RF incident power, nebulizer flow and sample compositions. These studies demonstrated that the spatial distributions of analyte ions at the sample cone vary significantly with different operating conditions, changing the transport efficiencies of analyte through the whole interfacial region.

The successful development of a simulation model that can be used to describe the transport behaviors of analyte species from the plasma to the mass detector in an ICP-MS is based on its being verified by reliable experimental data. However, there is a significant divergence between the experimental values and the simulated results from a simple fluid dynamic model flowing from a homogenous ideal gas. The

density drops of different analyte species along the centerline inside the plasma begin earlier and are more extreme than the results simulated by the simple fluid model.[9]

To simulate the behavior of analyte flowing through the sampling orifice, the spatial distributions of analyte just at the tip of the sampling cone, which determine the quantity of analytes reaching the detector, are crucial. Unfortunately, due to limitations of previous experiments, studies could not obtain credible spatial distribution information within the 1 mm region just upstream from the sampling cone. When the side-on excitation laser got close to the tip of the sampling cone, laser scattering and reflection interferences from the sampling cone had the potential of affecting the measured results. To collect reliable experimental data closer to the cone, the scattering of the excitation laser should be minimized to reduce the impact on ionic and atomic fluorescence imaging.

In this section, a novel experimental setup was adopted to excite and image the barium ground state atoms, ground state ions and metastable ions upstream from the sampling cone under different nebulizer flows and incident powers. The emphasis was placed on the spatial distributions of barium atoms and ions at or near the tip of the sampling cone. The data were expected to test the simulation being developed by coworkers from the physics department.[10]

2.2. Experimental

2.2.1.   Instrumental setup

The basic experimental setup used in this research has been described in detailed by many previous papers from our lab.[8,9,11] Briefly, an ICP generator (Elan 500 ICP-MS, Perkin Elmer, Norwalk, CT) with a short quartz torch (450-05, Precision

Glassblowing of Colorado, Centennial, CO) was used to maintain and direct the

plasma onto a sampling cone (VG-1001-Ni, Spectron, Ventura, CA) with

1-mm-diameter orifice mounted on an aluminum chamber. The sampling cone was

water-cooled. The chiller water for the sampling cone was provided by an HX 150

recirculating chiller (Thermo NESLAB, Fortsmouth, NH).

Some modifications were carried out to fit the requirements of the new specific

experimental objectives. As shown in Fig 2.1, instead of mapping atomic and ionic

fluorescence through the sampling cone, as described in reference 9, we sent the

excitation lasers through the back of the sampling cone. This approach required some

care to minimize large scattering from the walls of the sampling orifice. The skimmer

cone was removed in this experiment due to the limited space behind the sampling

orifice. The distance between the sapphire window and the sampling cone was about
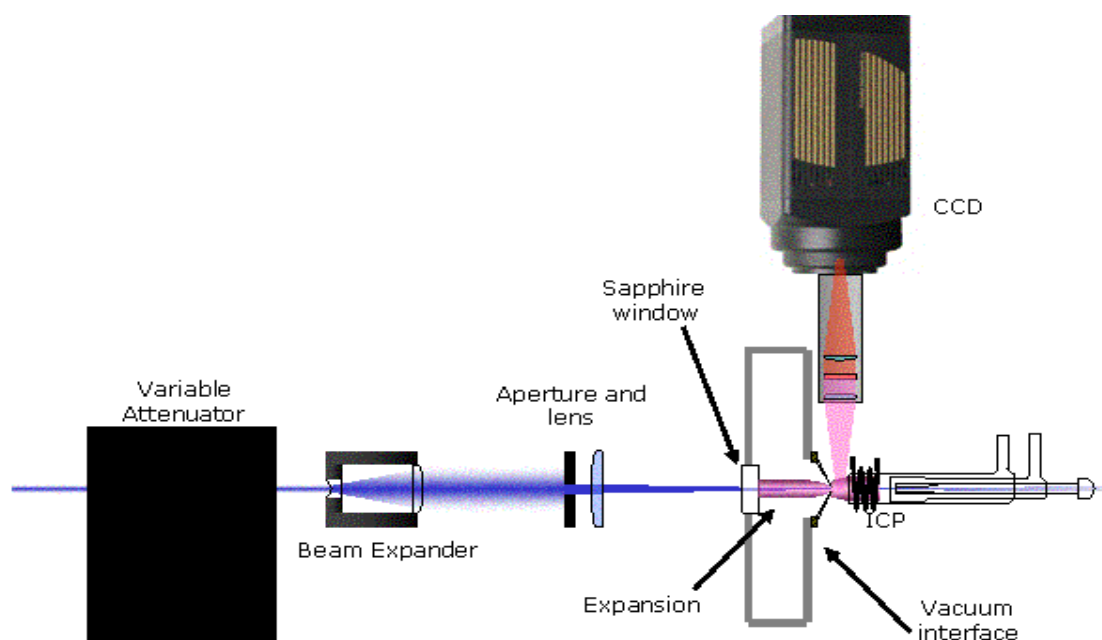
50 mm.

Fig 2.1 Schematic of experimental setup

A XeCl Excimer laser (LPX 200, Lambda Physik, Ft. Lauderdale, FL) was used

to pump SCANmate dye laser system (Lambda Physik, Ft. Lauderdale, FL). A high-energy variable attenuator (M-935-10, Newport, CA) was inserted to adjust the intensity of the dye laser, which was used to just saturate the analyte fluorescence while minimizing laser scattering interferences. After the attenuation, a beam expander (Newport, Irvine, CA) was used to produce a uniform laser beam, which passed through an iris with 1 mm-in-diameter aperture. A 2-inch-diameter lens with a 16-inch focal length was used to focus the beam to a diameter less than 1 mm. The laser finally passed through the sampling orifice, then the plasma, and into the injector of the torch. The gated intensified CCD detector (7361-0001, Princeton Instruments, Trenton, NJ) was mounted on the vacuum stage, and used to image a line of fluorescence produced by the analyte beam as it passed through the plasma.

2.2.2. Analyte and Operating conditions

The analyte used in this research was 10 ppm barium solution, which was prepared from solid barium chloride (reagent-grade, Fisher Scientific, Hampton, NH). An ultrasonic nebulizer (ATX-100, Cetac, Omaha, NE) and a desolvation system (U-5000, Cetac, Omaha, NE) were used to aspirate the barium solution into the plasma. The ICP instrument operating parameters are listed in Table 2.1, unless otherwise specified. The vacuum of the first stage was pumped by two mechanical pumps (VL3514, Duniway Stockroom Corp. CA) and measured by a PIRANI thermocouple pressure gauge (HPS, Instruments Inc. San Diego, CA).

Table 2.1 Instrumental operating conditions

Incident power	1250 Watts
Reflected power	< 5 Watts

Outer gas flow	12 L min^{-1}
Intermediate gas flow	0. 4 L min^{-1}
Sample uptake rate	1 mL min^{-1}
First stage vacuum pressure	~ 1 Torr
Sampling depth (Distance from load coil to sampling cone)	10 mm

2.2.3. Fluorescence wavelength

During the experiments, the dye laser was tuned to transitions at 614.171 nm (Rhodamine B, LC6100, Lambda Physik, Ft. Lauderdale, FL), 455.403 nm (Coumarin 460, Exciton, Dayton, OH), and 350.111 nm (DMQ, Exciton, Dayton, OH) to excite barium metastable ions, ground state ions, and ground state atoms, respectively.

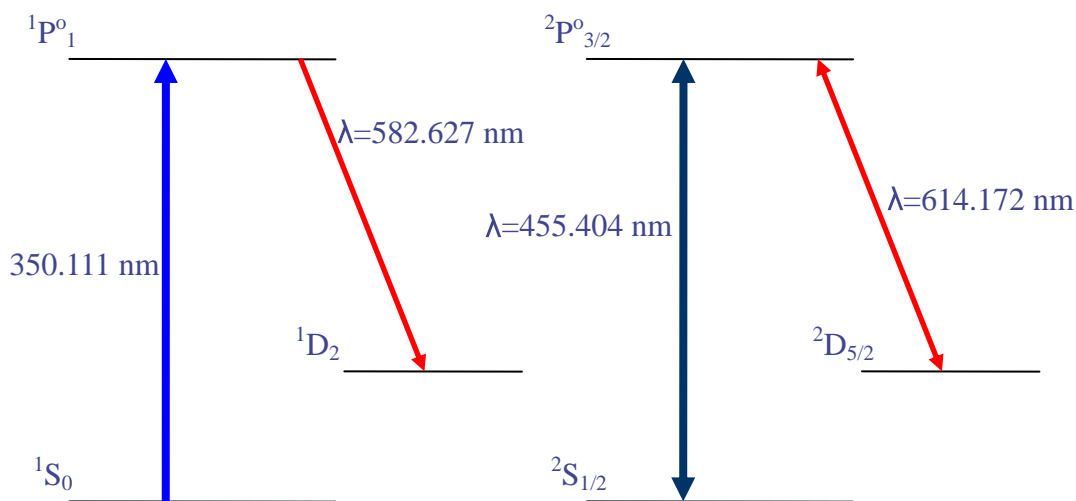Fig 2.2 Fluorescence schemes of barium atoms (left) and ions (right) used. For measurements of metastable state ions, the excitation and emission transitions were switched.

Fig 2.2 shows the excitation and emission fluorescence wavelengths used in this experiment. The barium ground state atom fluorescence was isolated with a 582.68 nm interference filter (010FC36-25/582.68, Andover, Salem, NH). The barium ground

state ion fluorescence was isolated with a 614.2 nm interference filter (614.2/1-25.4-Barr，Barr Associates, Westford, MA). The barium metastable ion fluorescence was isolated with a 455.4 nm interference filter (F03-455.4-4-1.00, CVI, Albuquerque, NM).

2.2.4.   Data collection and processing

The atomic and ionic fluorescence produced by barium species were collection by an intensified, gated CCD detector, which was controlled by its controller (ST133A, Princeton Instruments, Trenton, NJ). The CCD detector has a square sensor array with 512×512 pixels on 24 μm centers. With a lens system consisting of an objective lens (AC254-100-A1, Thorlabs, Newton, NJ) that has a 10 cm focal length, an interference filter, and an identical lens with a 10 cm focal length, the images were focused onto the CCD device. All lenses were achromatic doublets with a 400–700 nm anti-reflection coating. During this experiment, the delay and gate width of CCD under gated mode were optimized by most intense response of a series of ionic fluorescence images.

To eliminate noise arising from the fluctuations of sample quantities delivered by the ultrasonic nebulizer, the data presented in this paper were time averaged. 2000 laser shots were integrated to produce barium ground state and metastable ions; 5000 laser shots were integrated for ground state atom imaging.

Because each image contained both laser-induced fluorescence and plasma background emission, an emission image with same off-peak laser shots (the laser was detuned about 5 nm from the peak excitation wavelengths), recorded immediately after the fluorescence imaging, was recorded and subtracted from the corresponding

image including the excited fluorescence and emission background. Fig. 2.3 shows a processed ionic fluorescence signal image with incident power of 1250 Watts and nebulizer flow of 1.33 L/min. Similar fluorescence images were obtained from the metastable ions and ground state atoms.

As displayed in Fig 2.3, the fluorescence signal has a smaller diameter than the sampling orifice, which is 1 mm at room temperature. The symmetry and narrow width of fluorescence signal suggests that the laser scattering from the sampling orifice was minimized.

The images were processed in MathCad to determine the centerline spatial distributions of barium ground state ions, metastable ions and ground state atoms. The position of sampling cone tip was defined as the zero on the X axis. To eliminate the noise caused by single row of pixels, the centerline intensities are the averages of rows closest to the centerline.
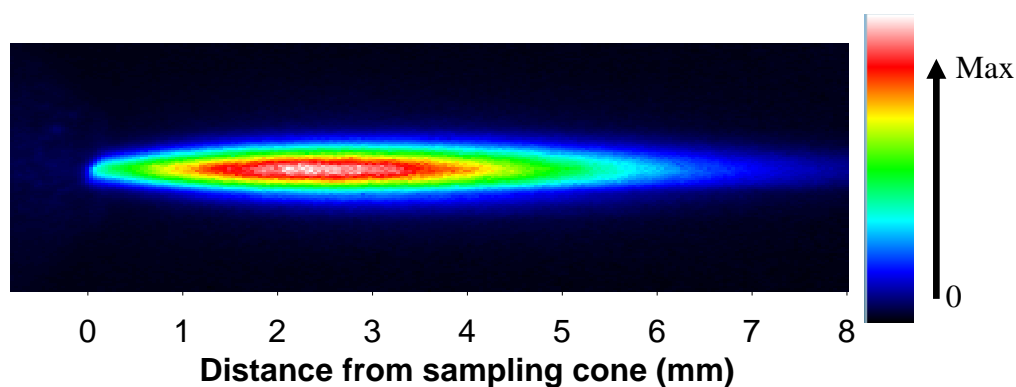

Fig 2.3 Demonstrated signal of barium ground state ion

2.3. Results and discussion

The temperature of the plasma changes with varied incident power and nebulizer flow. Therefore, the position of the sampling cone's tip, which is the origin of the X

axis in the following plots, changes slightly due to varying degrees of thermal expansion. The distance between the sampling orifice and the load coil is shortened to less than 10 mm. This variation was partly corrected by adjusting the origin to correspond to the tip of the sampling cone. The position of the sampling cone tip was defined as the origin of the Z axis. Because we were only concerned with the spatial distribution of barium species just upstream from the sampling cone, the z axis was truncated at 9 mm.

2.3.1.   Reproducibility of experimental results

For each spatial distribution of barium ions and atoms, three identical experiments were run and the data were averaged. The error bars in the plots are the calculated standard deviations of triplicate measurements.
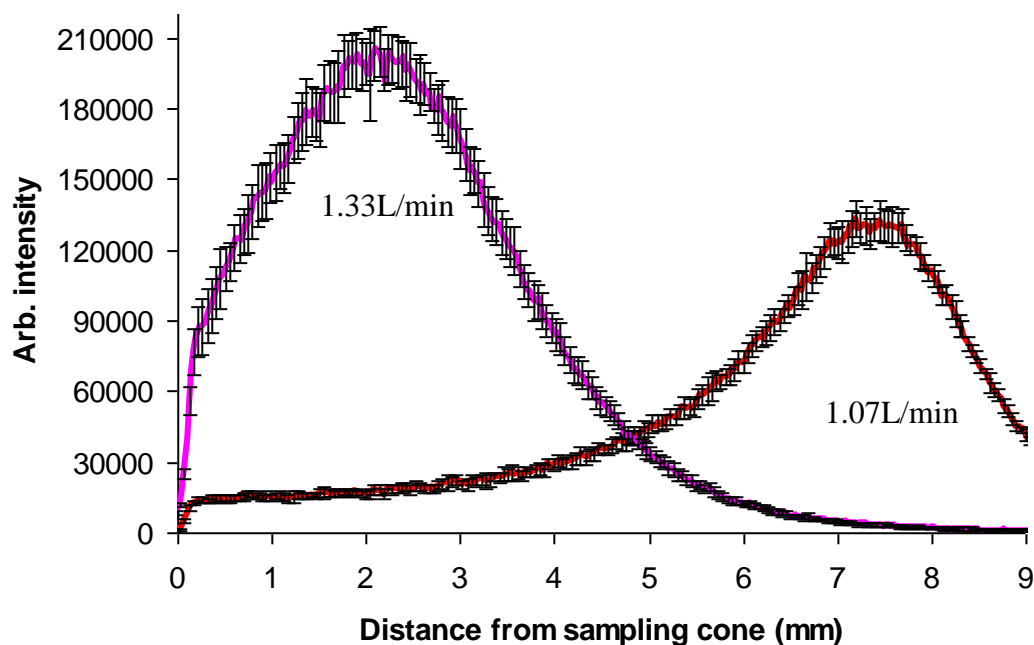

Fig 2.4 Reproducible fluorescence signal - barium ground state ions

Fig 2.4 demonstrates some results for the barium ground state ion with error bars.

As shown, the experimental results have good reproducibility. Similar experimental reproducibilities were also found in other ionic and atomic results under all operating conditions. To show the spatial distribution clearly and avoid clutter, the error bars for the triplicate measurements were not displayed after Fig 2.4.

2.3.2.   Axial centerline distribution of atoms and ions

Typically, in an ICP source analytical instrument, liquid samples are first aspirated and transported into the plasma source, where analytes are vaporized, then atomized and ionized.[12] Usually, a particle has to be atomized before it can be ionized, and the atomization temperature is lower than that required by ionization.[13] This phenomenon was also verified by the current experimental results. As shown in Fig 2.5, the atomization process happens lower in the plasma than the ionization process when analytes leave the plasma torch. The peak intensity of atoms also appears earlier than the peaks of ions. The same trends were observed under other operating conditions.
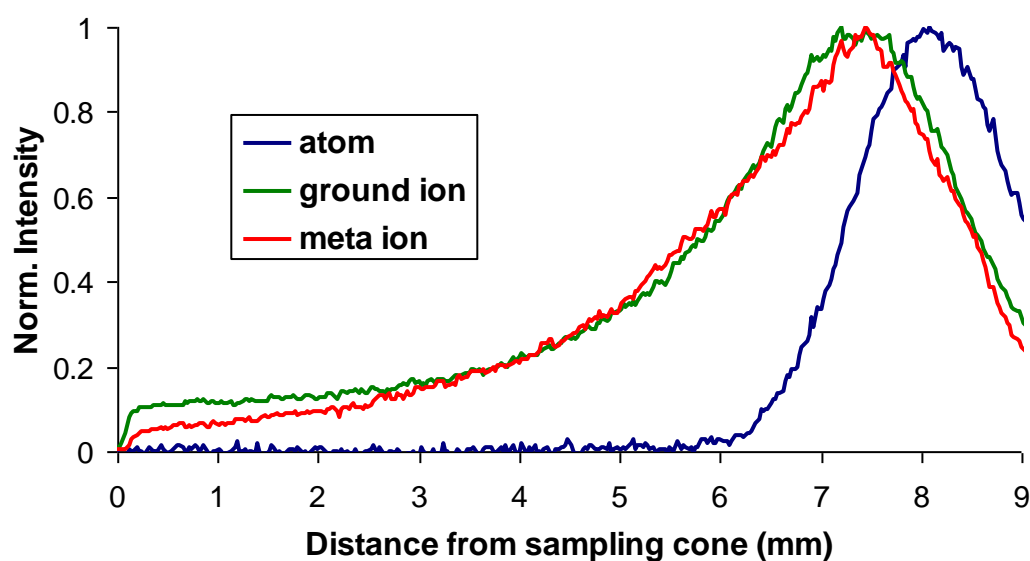
Fig 2.5 Spatial distribution of atoms and ions under 1250 W, 1.07 L/min. The signals

were normalized to their respective maximum values

2.3.3. Impact of RF power and nebulizer flow

The spatial distribution of analytes upstream from the sampling cone of an ICP-MS is strongly influenced by the RF incident power and nebulizer flow. They do not dramatically affect flow velocity of analytes in the central channel, but change the temperature and density gradients of the plasma.[14] In this research, the axial distribution of barium ground state ions, metastable ions and ground state atoms under different incident powers (850 W & 1250 W) and nebulizer flows (1.07 L/min & 1.33 L/min) were mapped and shown in Fig 2.6.

Atom

Ground state ion
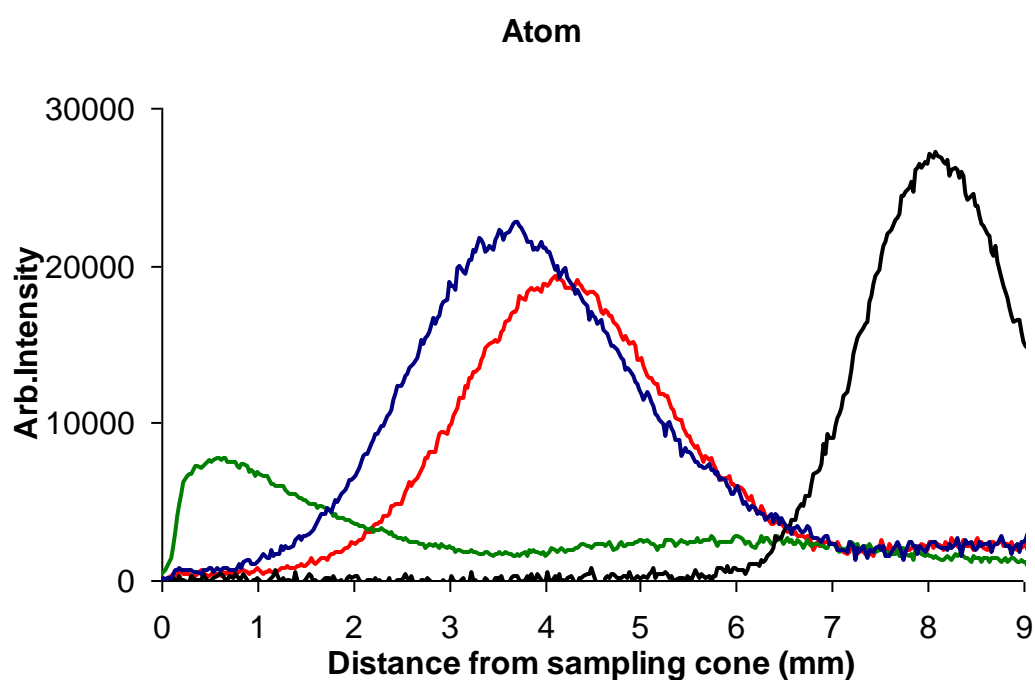
Metastable ion

Fig 2.6 Axial distribution of ground state atoms, ground state and metastable ions under a series of nebulizer flow and incident power; (———) 1250 W, 1.07 L/min; (———) 1250 W, 1.33 L/min; (———) 850 W, 1.07 L/min; (———) 850 W, 1.33 L/min

The experimental results not only provided credible axial distributions of barium

species just at the tip of the sampling cone in an ICP-MS, but also gave a good verification of the previous work.[8] The data will be used to verify the Monte Carlo model being developed.

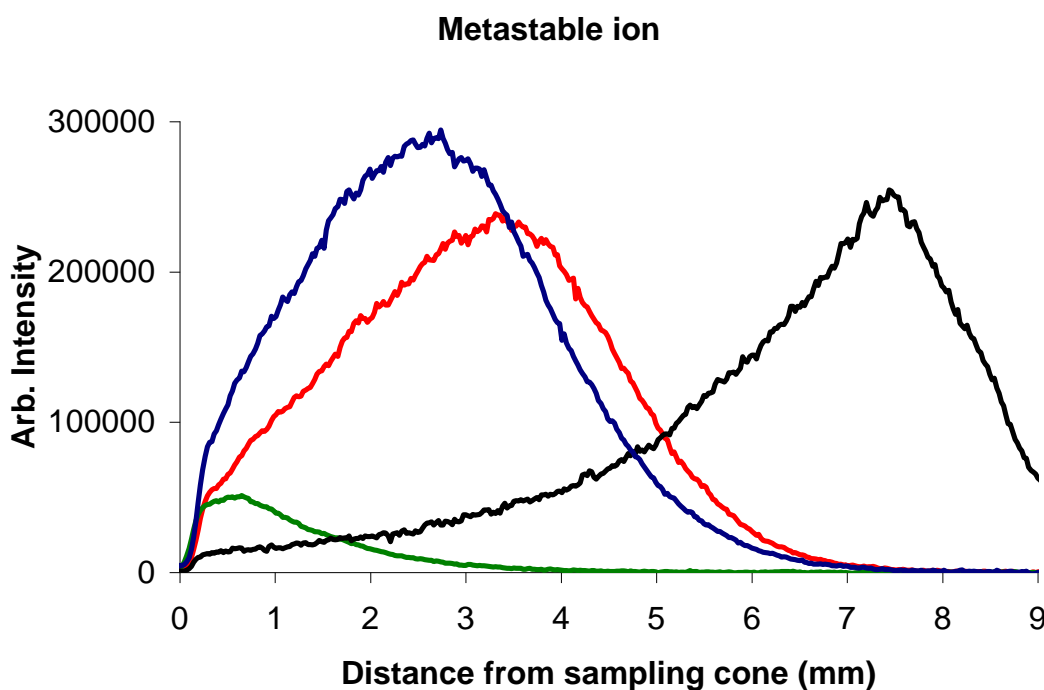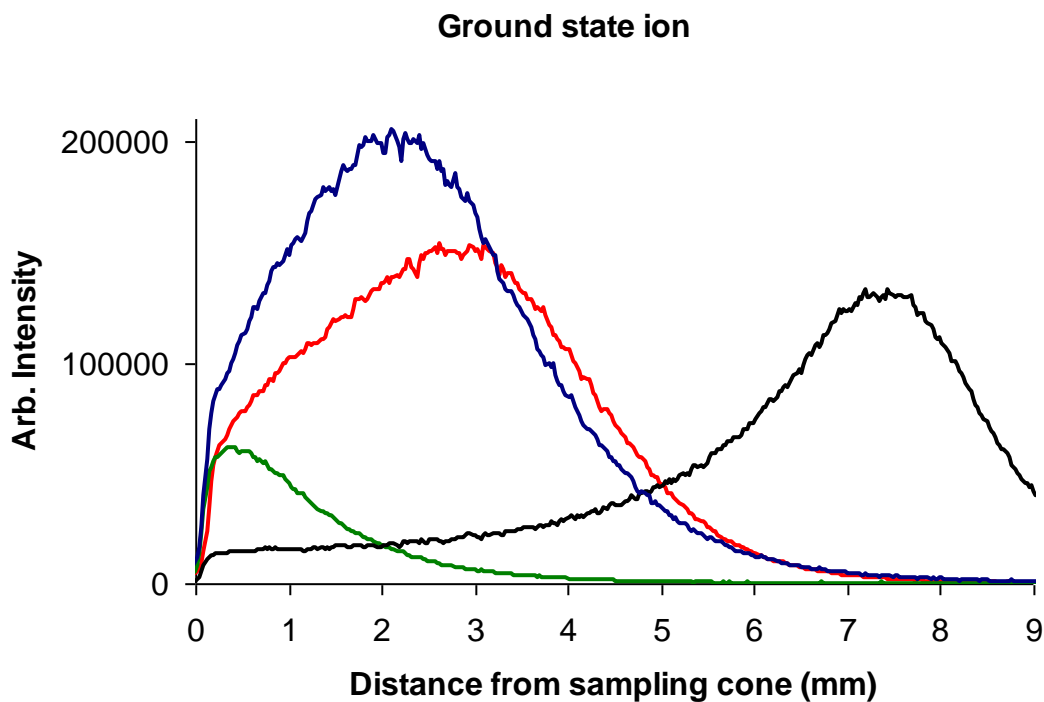In addition, as shown in Fig. 2.6, the peak intensities of these three species under 1250 W and 1.33 L/min were higher than these under 850 W and 1.07 L/min, indicating that the plasma has a higher atomization and ionization efficiency with higher incident power and nebulizer flow, although it is speculated that the lower nebulizer flow increases the dwell time of analyte species inside the plasma.

2.3.4. Temperature variation inside the plasma

The Boltzmann distribution, which is used to describe the partitioning of ionic or atomic species occupying a set of energy states, is a function of the plasma temperature.[13] The higher the ratio of the partition is, the higher the temperature of the plasma. The Boltzmann distribution equation for the fractional number of particles $N_i \, / \, N$ with different energy state E_i can be written as

$$\frac{N_i}{N} = \frac{N_i}{\sum\limits_i N_i} = \frac{g_i e^{-E_i/(k_B T)}}{\sum\limits_i g_i e^{-E_i/(k_B T)}} \quad (2\text{-}1)$$

where k_B is the Boltzmann constant, T is the plasma temperature, g_i is the degeneracy, and N is the total number of particles. By comparing the arbitrary number densities of metastable ions and ground state ions, we can gain insight into the temperature variation of the plasma under different operating conditions.

Fig 2.7, which shows the ratio of metastable ions to ground state ion under different operating conditions, illustrates such a comparison of number densities.

Because of low signals of metastable ion near the load coil and high noise at an incident power of 850 W and a nebulizer flow of 1.33 L/min, the ratio for these conditions was plotted only for the 5 mm immediately upstream from the sampling cone.

First, as expected, the decreases of RF incident power or increases of nebulizer flow can both cool the central channel, and delay the atomization and ionizations of analytes inside the plasma, as shown in the region close to the load coil, 4-9 mm in Fig 2.7.

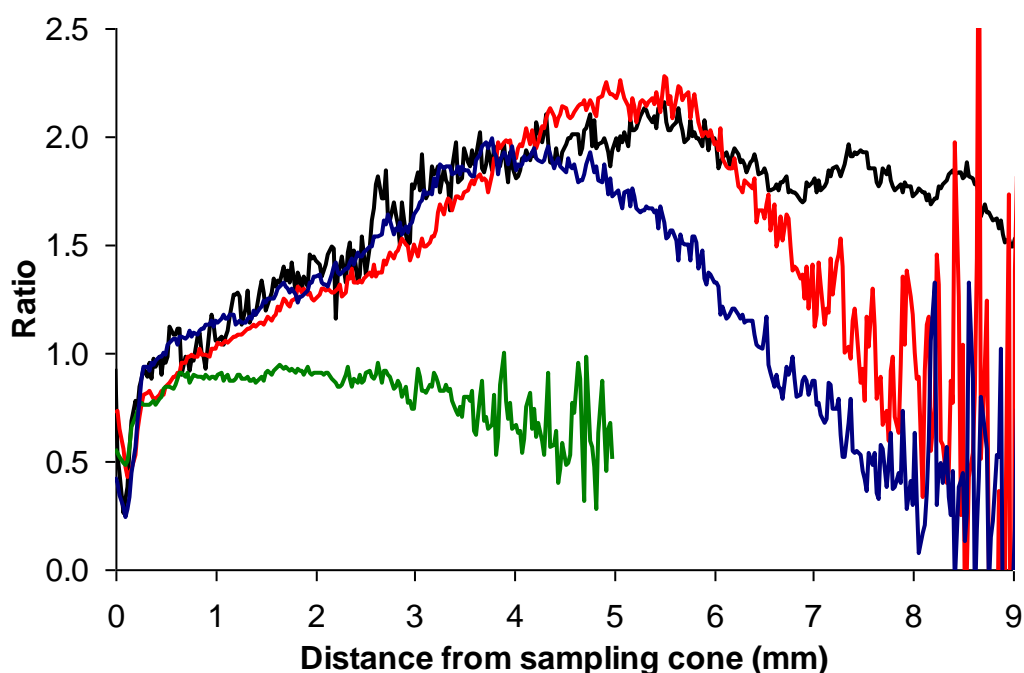Fig 2.7 Ratios of metastable ions to ground state ions under different operating conditions, (——) 1250 W, 1.07 L/min; (——) 1250 W, 1.33 L/min; (——) 850 W, 1.07 L/min; (——) 850 W, 1.33 L/min

Second, Fig 2.7 also shows that when the incident power was low and nebulizer flow was high (850 W, 1.33 L/min), the atomization and ionization inside the plasma were both incomplete. The ratio of metastable ions and ground state ions was low

throughout the plasma.

Then, it is not surprising that the plots of two conditions (850 W, 1.07 L/min) and (1250 W, 1.33 L/min) in Fig 2.7 are similar, since the plots of atomization and ionization in these conditions are similar. Furthermore, when the incident power was high while nebulizer flow was low, 1250 W and 1.07 L/min, the plasma has a higher temperature near the load coil. Therefore, the atomization and ionization processes happened in the region close to the torch.

Finally, we also note that three of four plots were overlapped 0-4 mm upstream from the sampling orifice. We speculate that in this region, the temperature of the plasma is highly influenced by the water-cooling sampling interface, instead of the operating conditions of the plasma. Please refer to chapter 3 for a detailed discussion of this subject.

2.3.5.   Recombination of atoms inside the plasma

Another consideration is the recombination of ions and electrons inside the plasma. The recombination can significantly change the number densities of atoms and ions inside the plasma. Therefore, the axial distributions of barium ground state atoms with a series of nebulizer flow under optimum incident power (1250 W) were recorded, as shown in Fig 2.8.

As we can see from Fig 2.8, after the atomization process inside the plasma was completed, the axial quantities of atoms approached zero near the sampling cone. In the range of nebulizer flows we used, it seems that there was no recombination of electrons and ions near the sampling cone, where the temperature of plasma decreased due to the existence of the sampling cone. Further, due to the continuous radial

diffusion inside the central plasma channel, the peak intensities of barium atoms decreased with the increase of the nebulizer flow.
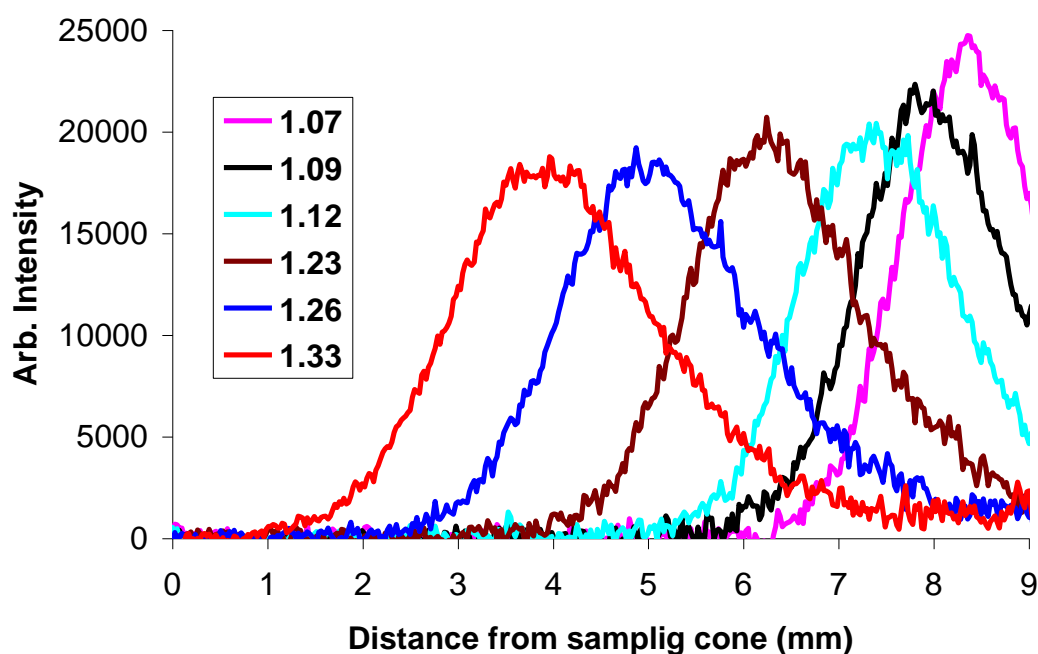
Fig 2.8 Axial distributions of ground state atoms under a series of nebulizer flows (Unit: L/min)

2.4. Conclusions

The laser induced atomic and ionic florescence technique is a non-invasive and powerful method for the study of analyte ion and atom transmission in the vacuum interfacial region between the ICP and mass spectrometer.

The novel laser excitation scheme used in this research guaranteed the mapping of spatial distributions of ionic and atomic fluorescence just at the tip of the sampling cone. The experimental results were comparable with the previous results. The data can be used to verify the simulation model being developed.

2.5. References

[1] Stewart I. I., Hensman C. E., Olesik, J. W., *Appl. Spectrosc.*, 54, **2000**, 164

[2] Lehn S. A., Warner K. A., Gamez G., Huang M., Hieftje, G. M., *Spectrochim. Acta, Part B*, 58, **2003**, 1647

[3] Chambers D. M., Poehlman J., Yang P., Hieftje G. M., *Spectrochim. Acta, Part B*, 46, **1991**, 741

[4] Niu H., Houk R. S., *Spectrochim. Acta, Part B*, 51, **1996**, 779

[5] Montaser, A. Golightly, D. W., *Inductively Coupled Plasmas in Analytical Atomic Spectrometry*, 2nd, VCH Publisher, Inc. **1992**

[6] Longerich H. P., Fryer B. J., Strong D. F., Kantipuly C. J., *Spectrochim. Acta, Part B*, 42, **1987**, 75

[7] Holiday A. E., Beauchemin D., *Spectrochim. Acta, Part B*, 59, **2004**, 291

[8] Macedone, J. H., Gammon D. J., Farnsworth P. B., *Spectrochim. Acta, Part B*, 56, **2001**, 1687

[9] Mills A. A., Macedone J. H., Farnsworth P. B., *Spectrochim. Acta, Part B*, 61, **2006**, 1039

[10] Spencer R. L., Krogel J., Palmer J., Payne A., Sampson A.*, Spectrochim. Acta, Part B*, 64, **2009**, 215

[11] Duersch B. S., Chen Y., Ciocan A., Farnsworth P. B., *Spectrochim. Acta, Part B*, 53, **1998,** 569

[12] Robert T., *Practical Guide to ICP-MS*, Marcel Dekker, Inc., New York, **2004**

[13] Ingle J. D. Jr., Crouch S. R., *Spectrochemical Analysis*, Prentice Hall, New Jersey, **1988**

[14] Cicerone M. T., Farnsworth P. B., *Spectrochim. Acta, Part B*, 44, **1989**, 897

3. THE EFFECT OF THE SAMPLING CONE ON SPATIAL DISTRIBUTIONS OF BARIUM IONS AND ATOMS IN AN ICP-MS

3.1. Introduction

The ICP is an effective ion source used worldwide for trace elemental analysis. In an ICP-MS, a metallic water-cooled interface is installed between the ICP and the mass spectrometer to deliver representative analytes from the plasma to the mass detector.[1] Until now, many research efforts have concentrated on better understanding the ion transport through the interfacial region of an ICP-MS.[2,3,4]

However, the understanding of plasma as an ion source used in ICP-MS analysis is largely dependent on literature that focuses on the fundamental study of ICP as an excitation and emission source used in atomic emission spectrometry. Clearly, the influence of an interface between the ICP and the MS should not be neglected, since the performance differences between ICP-AES and ICP-MS are significant, which also indicates that the influence of an interface on the atomization and ionization of analytes inside the plasma should be investigated completely.

Much work[5,6,7] has been carried out to understand the influence of ICP-MS sampling cone on the characteristics of the plasma in Hieftje's group. Relying on Thomson and Rayleigh scattering techniques, Lehn et al.[5] demonstrated that the sampling cone of an ICP-MS caused changes in the plasma several millimeters upstream from the sampling cone. Analyte emission intensities were depressed because of the presence of the sampling interface. In follow-up studies,[6,7] Hieftje's group examined the effect of the interface on the plasma under a variety of plasma operation conditions. The results they published clearly showed that the sampling cone has a significant impact on the plasma far upstream from the sampling cone.

However, their data are based on point-by-point measurements, which are easily influenced by long-term instability and poor reproducibility of a typical ICP-MS instrument.

Furthermore, the fluorescence intensity of analyte ions and the influence of matrix compositions depend on which type of nebulizer system is used. The nebulizer also impacts the excitation and ionization temperatures of ions, the ion-to-atom ratio, and the electron number densities in the plasma.[8] Usually, the aspiration and transport efficiency of the ultrasonic nebulizer for analytes is about 2~5 times higher than that of the pneumatic nebulizer under the same experimental conditions. Therefore, the type of nebulizer has to be defined in the experimental section.

In this research, we used planar laser-induced fluorescence, which has been proven to be a successful tool for rapid acquisition of two-dimensional images of the plasma with high resolution,[12] to image the spatial distributions of barium atoms and ions downstream from the load coil. By analyzing the data obtained, we provide a comprehensive picture of how the sampling cone affects the characteristic of the plasma. In addition, to aid in the interpretation of the experimental results, the velocities of analyte atom particles inside the plasma were measured in the presence and absence of the sampling cone.

3.2. Experimental

The ICP and imaging instruments used in this research have been thoroughly described in previous publications from our lab.[9,10,11,12] Only a few modifications were carried out to ensure the success and reproducibility of the experiments.

3.2.1. Fluorescence imaging

The excitation laser system was the same as described in chapter 2. The excitation wavelengths for barium metastable ions, ground state ions, and ground state atoms were tuned to 614.171 nm, 455.403 nm, and 350.111 nm, respectively. A ~15-meter optical fiber (AS400/420 UVAN, FiberTech Optica Inc., Kitchener, Ontario) was used to transmit output pulses of the dye laser to the plasma. At the end of the optical fiber, laser light was collimated by a fused silica plano-convex singlet lens (01 LQP 007, Melles Griot, Rochester, NY). The collimated light was then focused in one dimension by a plano-convex cylindrical fused silica lens (CLCX-25.4-50.9-UV, CVI Laser, Albuquerque, NM) to form planar light parallel to the plasma centerline. The produced fluorescence signals were isolated by the appropriate bandpass filters, as described in chapter 2.

If not otherwise specified, the aqueous samples were introduced to the plasma by a pneumatic nebulizer system. At a nebulizer flow rate of 1.09 L min^{-1}, 7 mg min^{-1} of water was delivered to the plasma. The chiller water for the sampling cone was provided by an HX 150 recirculating chiller (Thermo NESLAB, Fortsmouth, NH).

The CCD was mounted on the stage of the plasma torch, as shown in Fig 3.1, to minimize the positioning variation of the CCD imaging system relative to the load coil and the plasma. In addition, during the experiments, the plate holding the sampling cone was dismounted to reflect the condition of the absence of the sampling cone. If not mentioned specifically, the sampling depth, the distance between the load coil and sampling cone, was 10 mm.

In the experiments without the sampling cone, the mechanical pumps used to

maintain the vacuum in the first vacuum stage were stopped, and the sampling cone was removed from the chamber stage. The stage holding the load coil and plasma torch was pushed back about 100 mm from the position shown in Fig 3.1.
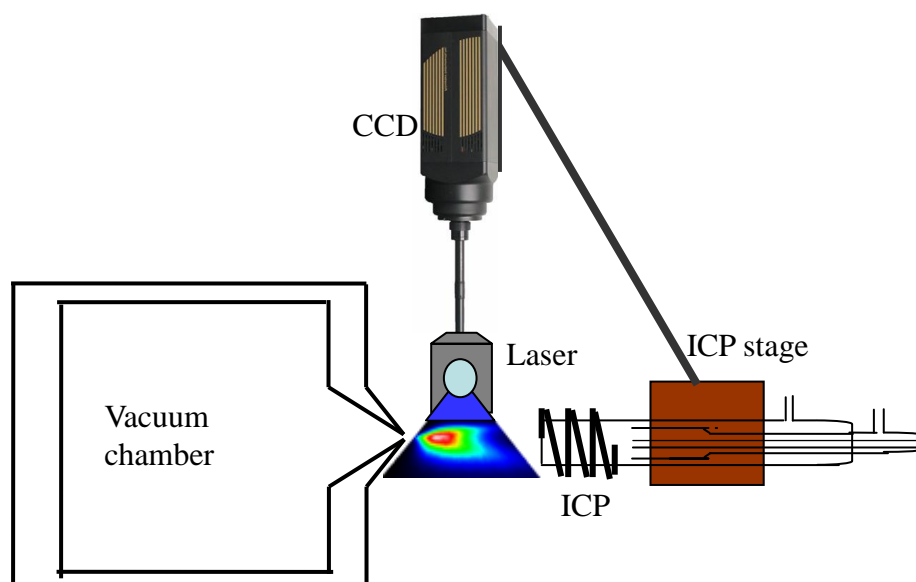
Fig 3.1 Demonstration of experimental setup in the presence the sampling cone

3.2.2.   Measurement of particle velocity inside the plasma

To aid in the interpretation of the experimental results, the velocities of particles along the plasma centerline were measured in the presence and absence of the sampling cone by Nick Taylor, a researcher in our group. Dr. Taylor's results are included here because they were essential in interpreting the fluorescence data.

The principle of the velocity measurements has been described by Cicerone and Farnsworth.[13] Briefly, vaporizing analyte particles create a high local concentration of analyte in the plasma that show up as spikes in the time-dependent atomic emission. By recording the time-dependent emission profiles of these vapor clouds separated by a fixed distance based on the time of flight between the two sampled locations, we can

calculate the flow velocity of particles inside the plasma.

Fig. 3.2 shows the schematic of the experimental setup for particle velocity measurements inside the plasma in the presence of the sampling cone. The ICP setup was identical to that described above. Calcium atomic emission signals were monitored by two fibers, located in the focal plane of the collection optics and separated by 1.28 mm. The output of the fibers was coupled to identical 0.2 meter monochromators (H20, Horiba Jobin Yvon, Edison, NJ), which were tuned to the Ca I resonance line at 422.7 nm and equipped with photomultiplier tubes (R928, Hamamatsu, Bridgewater, NJ). The PMT outputs were amplified with matched current amplifiers (Model 428, Keithley Instruments, Cleveland, OH) and digitized by a digital oscilloscope (Lecroy, Wavesurfer, Chestnut Ridge, NY).
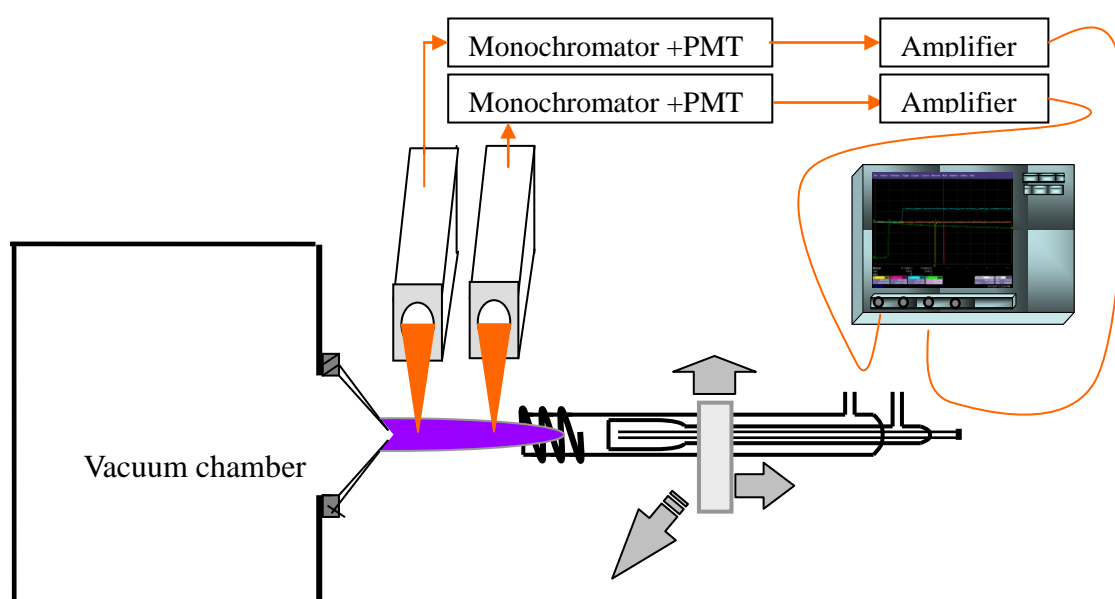

Fig 3.2 Experimental setup for particle velocity measurement inside the plasma. Two optical systems were used to collect analyte fluorescence, which is isolated by two monochromators and finally recorded by an oscilloscope

A 100 ppm calcium solution, which was prepared from analytical reagent calcium carbonate powder (Mallinckrodt, Paris, KY) was aspirated into the plasma. The waveform signals were processed in Matlab, and the velocities were computed as the ratio of the distance between two fibers to the time difference displayed by the peaks of the cross correlation functions.

3.2.3. Analytes

Solid reagent-grade barium chloride (Fisher Scientific, Hampton, NH) was used to prepare 10 ppm and 25 ppm barium chloride solutions. The different matrix solutions were diluted to equimolar concentrations because it seems that matrix effects are largely dependent on the total molar concentration of concomitant species. 33.5 ppm lithium solutions were prepared from lithium nitrate (solid reagent-grade lithium nitrate, Mallinckrodt, Paris, KY) with 10 ppm and 25 ppm barium solutions, respectively. Similarly, 1000 ppm lead solutions were prepared from lead nitrate (Crystal reagent-grade lead nitrate, Chemical MFG. Corp., Redondo Beach, CA) with 10 ppm and 25 ppm barium solutions respectively. All the solutions were diluted by 18 MΩ de-ionized, distilled water (Milli-Q RG, Millipore, Bedford, MA).

For barium ground state and metastable state ion measurements, a 10 ppm barium chloride solution was aspirated into the plasma. However, in the ground state atom experiments, due to low atom number densities and the low transition probability of the selected atomic fluorescence line, a 25 ppm barium chloride solution was used.

3.2.4. Data collection

The fluorescence imaging of the plasma can tell us the variation in analyte ionic and atomic number densities along any axial or radial line through the images. Data

were collected at the region of 0 ~ 10 mm region downstream from the plasma torch in the presence and absence of the sampling cone. During the entire experiment, a shear flow of compressed air was used to protect the CCD lens from heating by the plasma. The CCD, triggered by a photodiode (DET210, Thorlabs, Newton, NJ) positioned inside the dye laser box, was gated to coincide with the excited atomic and ionic fluorescence pulses. The delay and gate width of the CCD, 77 ns and 25 ns, respectively, were adjusted to give the maximum fluorescence signals.

To prevent the results from being affected by laser scattering and shot-to-shot variations of laser intensity, laser irradiances used for each analytes species were adjusted to just above the saturation threshold. For each experimental measurement, the saturation of the laser was checked by the method used in chapter 2.

To reduce the signal fluctuations arising from the fluctuations of sample quantities delivered by the pneumatic nebulizer and from the fluctuations in the plasma itself, the data presented in this paper were averages of multiple laser shots. 2000 laser shots were integrated to produce a single fluorescence image of barium ground and metastable state ions; 5000 laser shots were integrated for imaging of ground state atoms.

In this research, each image contained laser-induced fluorescence and plasma emission background. Therefore, an emission image with same number of CCD imaging shots with detuned off-peak laser excitation was recorded immediately after the fluorescence imaging. The final signal images were generated by subtracting the background emission from the corresponding fluorescence images. Fig 3.3 shows the representative images of barium ions in the presence and absence of the sampling cone. The incident power and nebulizer flow were 1250 Watts and 1.09 L/min,

respectively.

Definition of the axial origin is critical to compare the spatial distributions of ions and atoms upstream from the sampling cone in the presence and absence of the sampling cone.[12] In this research, the position of the torch was defined as zero for the x axis. Unfortunately, it is hard to identify the position of the plasma torch precisely. An easy alternative is to figure out the position of the tip of the sampling cone. Once the orifice of the sampling cone was located in the fluorescent images, the edge position of the torch could then be obtained by subtracting 10 mm (the sampling depth). As described in chapter 2, the thermal expansion of the nickel sampling cone could cause some errors on the definition of X origin, were neglected in my treatment of the data.
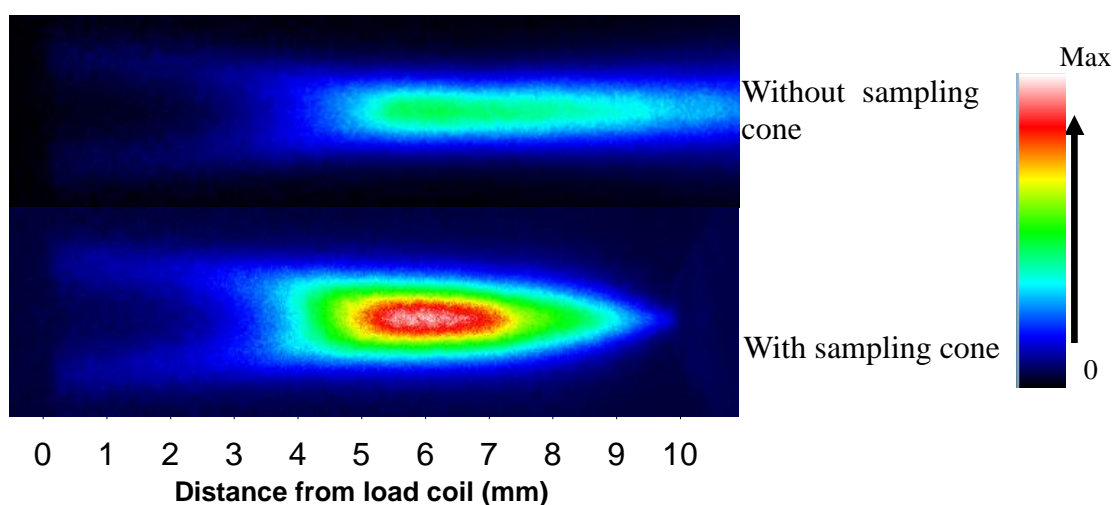

Fig 3.3 Representative fluorescent images of barium ground state ions with and without the sampling cone

3.3. Results and discussions

The original CCD images were converted to ASCII format and processed by Winview (Princeton Instruments, Roper Scientific Inc. Trenton, NJ) and Mathcad. For

axial and radial profile analysis of atom and ion number densities, triplicate experiments were run to calculate the standard deviations of these measurements. The central lines of each image were averaged and plotted. Error bars were not included in axial and radial distributions of barium species, to avoid too much clutter unless otherwise indicated.

3.3.1. Reproducibility of barium fluorescence signals

Averaged results from three runs, with error bars showing standard deviations, are plotted in Fig 3.4. The operational conditions were nebulizer flow of 1.09 L/min and incident power of 1250 Watts.
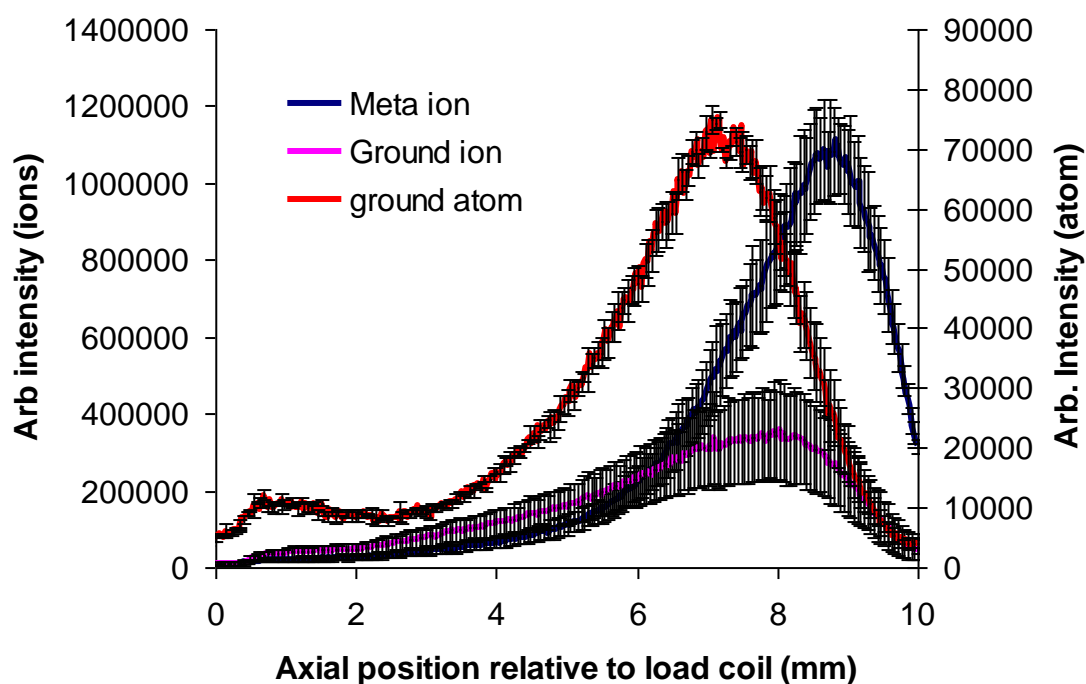

Fig 3.4 Representative data with error bars of barium species

As displayed, the error bars of ground state atoms and metastable ions are small. The variation of ground state ions in the triplicate measurements is a little larger, but tolerable.

3.3.2.   Impact of nebulizer flow on axial distributions of barium species

As shown in previous work,[12] the temperature of the ICP is strongly dependent on the plasma operating conditions. Changes in nebulizer flow and incident power cause similar changes in the spatial distribution of different barium species in the plasma. Therefore, in this research, only different nebulizer flows were adopted to demonstrate the effect of the sampling cone on the plasma. The incident power of the ICP was set to 1250 W for all experimental conditions. Three flow rates, 0.97 L/min, 1.09 L/min and 1.21 L/min were used in the presence and absence of the sampling cone of an ICP-MS. Fig. 3.5 shows the influence of nebulizer flow rates on the axial distributions of barium ground state ion, metastable ions, and ground state atoms.

Ground state ion

Metastable ion
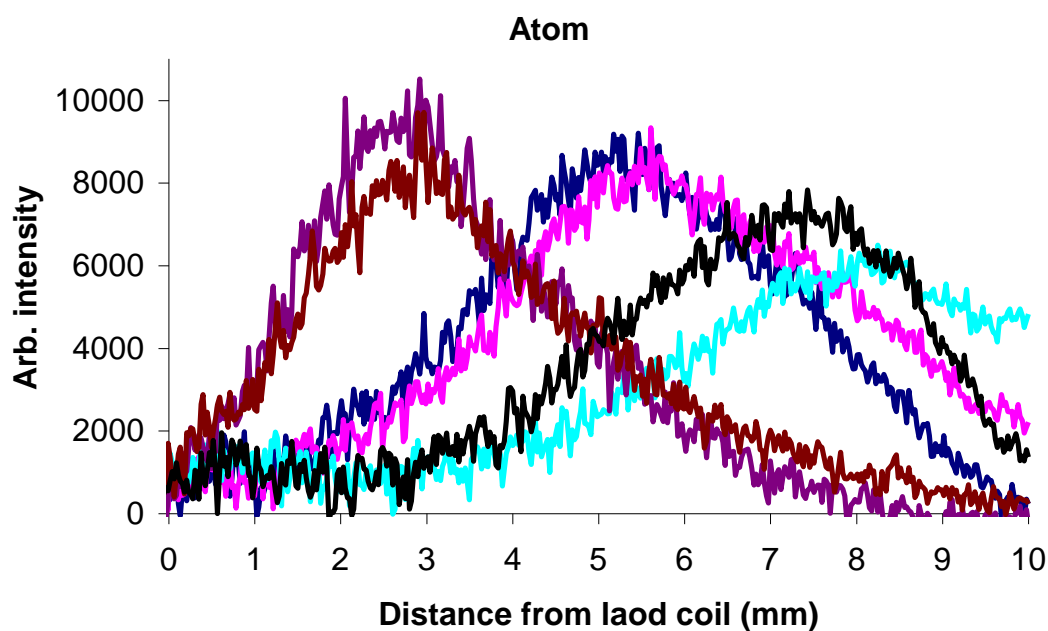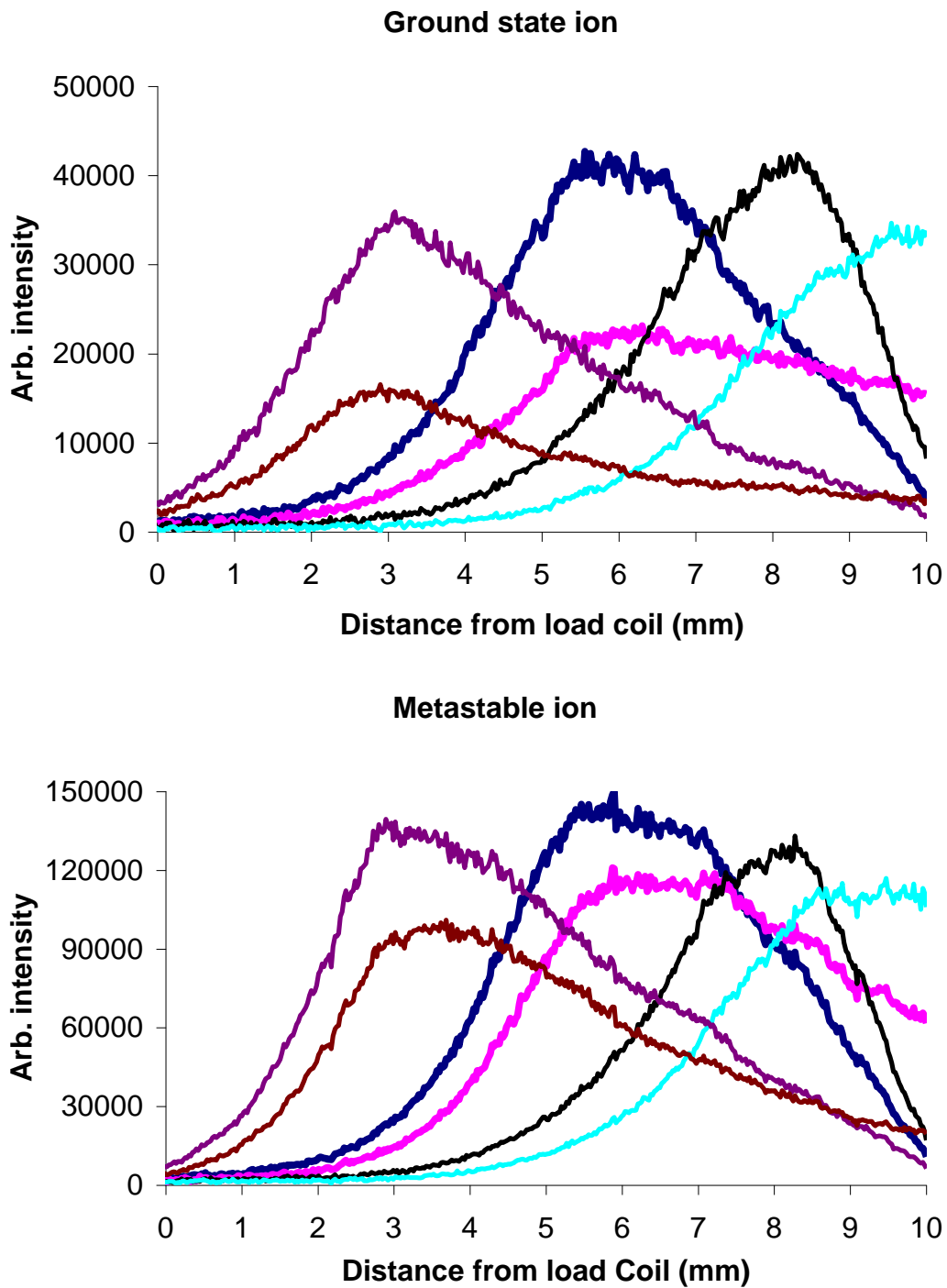

Fig 3.5 Axial distributions of barium species under different experimental conditions in the presence and absence of the sampling cone; (———) 0.97 L/min with cone, (———) 0.97 L/min without cone (———) 1.09 L/min with cone, (———) 1.09 L/min without cone, (———) 1.21 L/min with cone, (———) 1.21 L/min without cone

The axial profiles of atom and ion densities in the plasma are noteworthy. It has

been reported [2] that the flow velocity of gases in central channel of the plasma downstream from the load coil does not change dramatically with changes of the nebulizer gas flow, but the temperature and density gradient that the analyte experiences as it is directed through the channel changes with different nebulizer flow rates.

Although we did not measure the temperature of the plasma directly, the ratios of metastable ion densities to ground state ion densities can indicate temperature variation of the plasma. Higher ratios mean higher excitation temperatures. As plotted in Fig 3.6 and Fig 3.7, the increase of the nebulizer flow and the presence of the sampling cone decreases the temperature of the plasma dramatically.
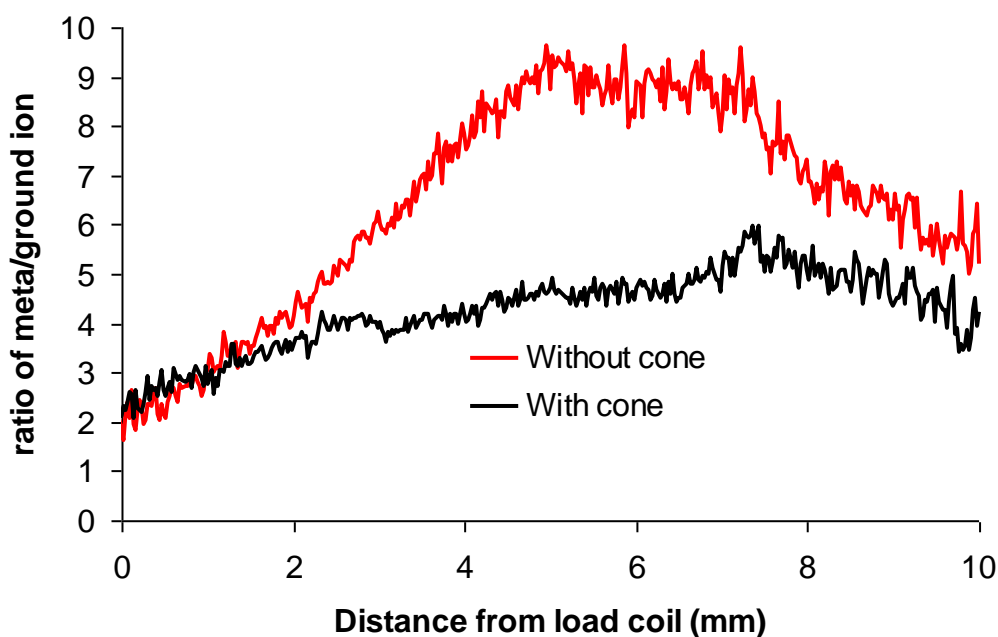

Fig 3.6 Ratios of metastable ion to ground state ion under nebulizer flow of 0.97 L/min

For atomization processes, the temperature required is much lower than for ionization. Therefore, the insertion of the sampling cone does not cause much change

in the spatial distribution of atomic species at low nebulizer flow. The central channel is sufficiently hot that atomization is completed low in the plasma. As shown in Fig 3.5, when nebulizer flow increases, the plasma temperature drops and the atomization process delays to higher in the plasma. When the nebulizer flow is very high, the atomization is incomplete, and the insertion of the sampling cone decreases the number density of barium atoms.
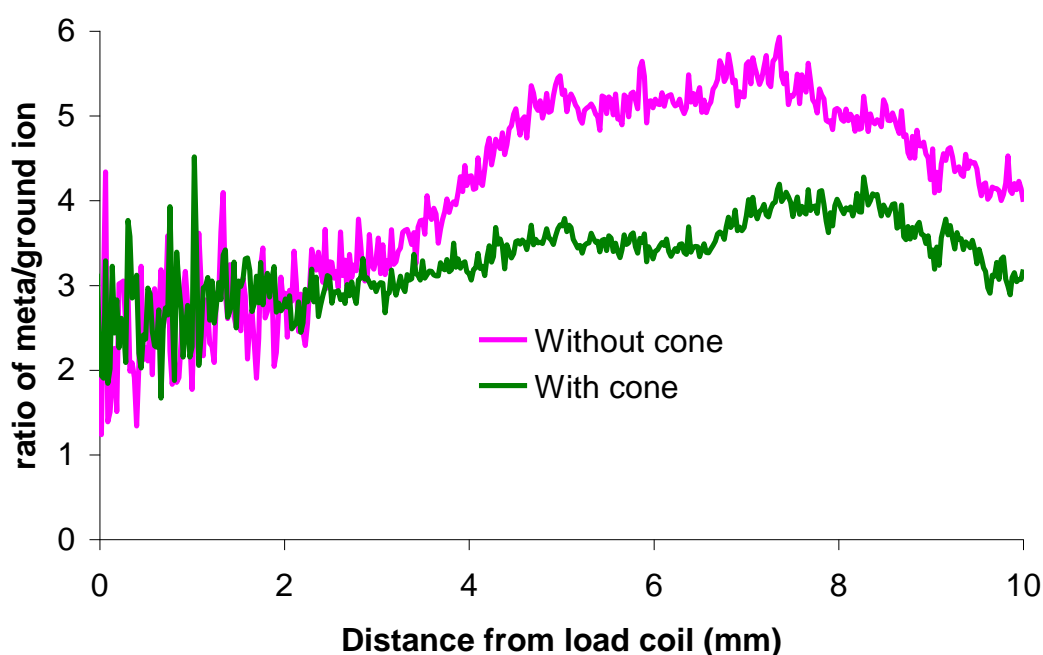
Fig 3. 7 Ratios of metastable ion to ground state ion under nebulizer flow of 1.09 L/min

For ionization, the sampling cone has a profound influence on the spatial distributions of analyte species inside the plasma. The presence of the sampling cone decreases the number density of detected species of ions near the sampling cone, and increases the number density of species near the load coil, with crossover points at 7~9.5 mm downstream from the load coil under different nebulizer flows. It is convenient to divide the influence of the sampling cone into two regions: the 0-3 mm

immediately upstream from the sampling cone in which the presence of the sampling cone decreases the number density of ionic species, and the 0-7 mm downstream from the load coil where ion number density rises. The reasons for the observed changes will be discussed in the following sections.

3.3.2.1.   Ionization near the sampling cone

The drop in number density near the sampling cone is partially caused by the temperature drop due to the insertion of the sampling cone. Near the sampling cone, the temperature is relatively low, and recombination of ions and electrons occurs. Indirect evidence has been published recently. Macedone and Farnsworth[14] reported that ion-electron recombination in the supersonic expansion happens immediately downstream from the sampling cone.

Another reason for the fall of barium ionic number density is the acceleration of the plasmas gases into the sampling orifice due to the pressure difference between the plasma and the first vacuum stage. Using the technique introduced in reference 13, we measured the centerline flow velocities of analyte species in the presence and absence of the sampling interface, to provide a directed measurement of the effect of the sampling cone on the acceleration of particles inside the plasma. The measuring setup has been introduced in section 3.2.2. The principle will be described briefly.

The time-dependent calcium emission spectra from the plasma, which are collected by the two optics systems and defined as upstream and downstream signals, are displayed in Fig 3.8. The velocity (v) of particles was calculated by the distance between two collection points (L) and time difference (t) recorded by the oscilloscope:

$$\nu = \frac{L}{t} \qquad\qquad (3\text{-}1)$$
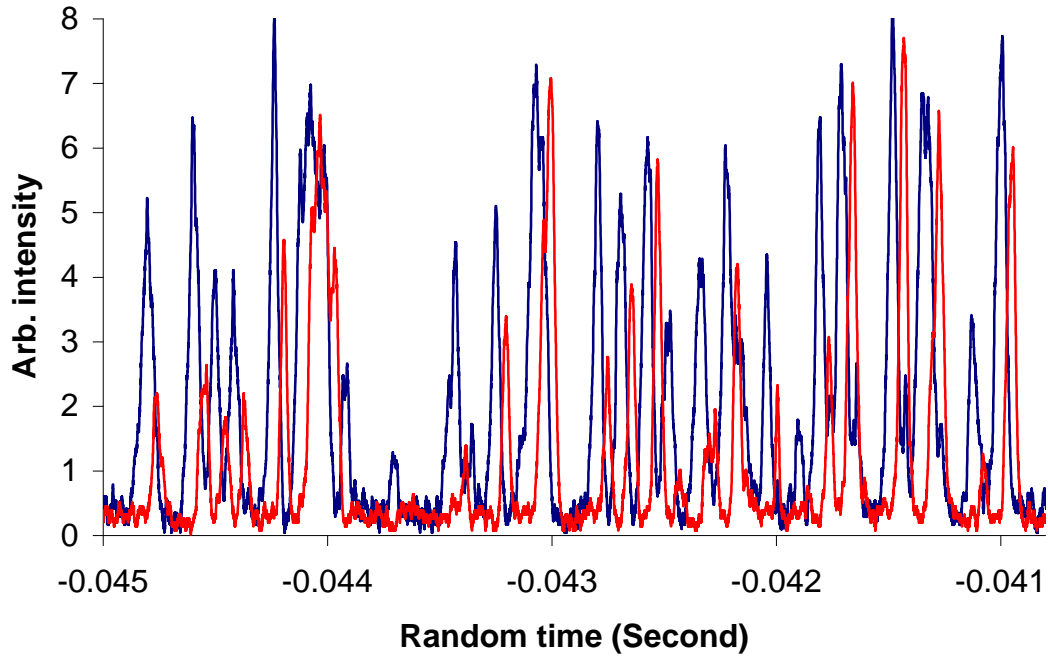
Fig 3.8 Recorded spectra for velocity measurements inside the plasma; (———)
upstream, (———) downstream

Fig 3.9 shows the velocities in the presence and absence of the sampling cone.
The error bars represent the standard deviations of triplicate measurements. As we can
infer from the plots, the pressure difference does accelerate the particles inside the
plasma, and most of the acceleration occurs in the 3 mm upstream from the sampler
cone, near where the crossover points are observed.

Fig 3.9 Velocity of particles inside the plasma in the presence and absence of the sampling cone; (■) with cone, (◆) without cone

3.3.2.2. Ionization near the load coil

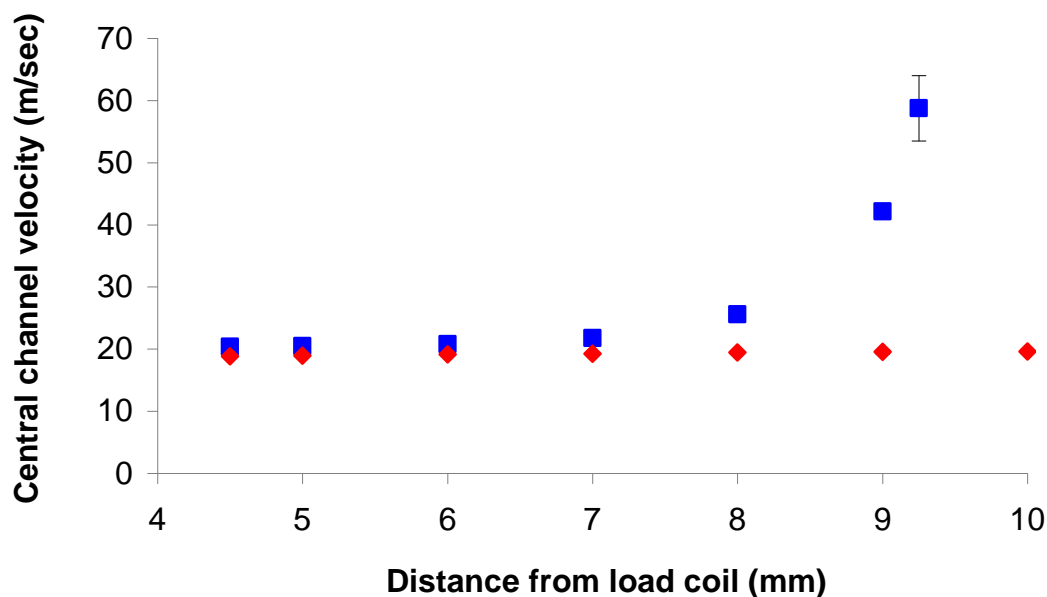The number density of ionic species increases near the load coil due to the presence of the sampling cone in this research. It is difficult to explain the experimental results since many assumptions are needed.

First, there are significant differences between our results and the data obtained in Hieftje's group.[4,5] There were no large differences among number densities of analytes observed in their research. Under some specific experimental conditions, the number densities even increase when the sampling interface is removed. One possible explanation is the difference of experimental configuration and analytes used between two labs. Some differences are listed in Table 3.1.
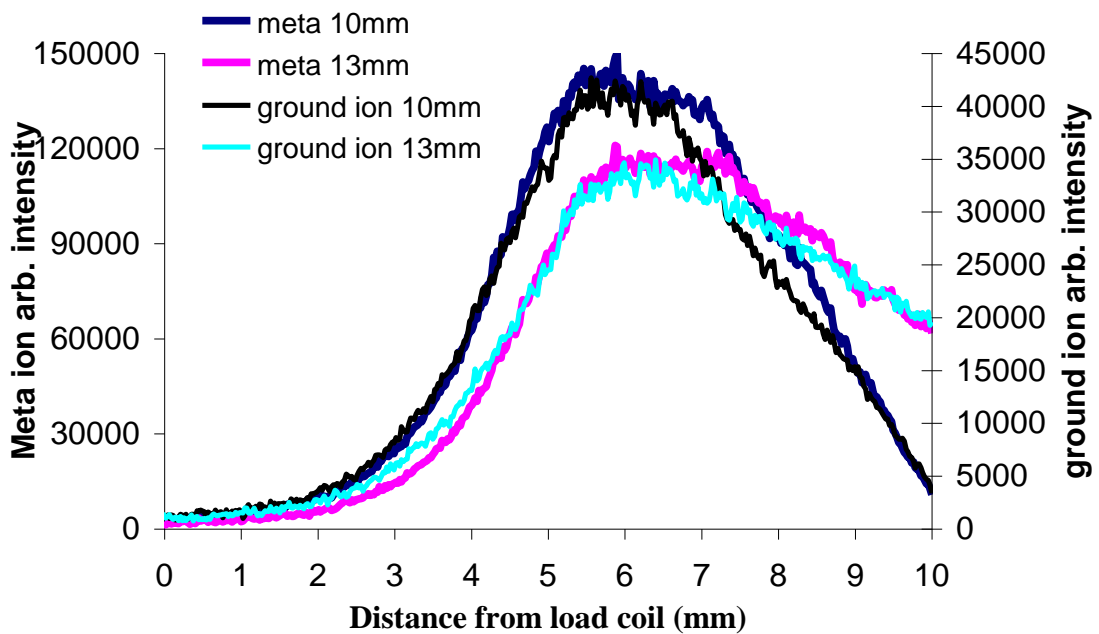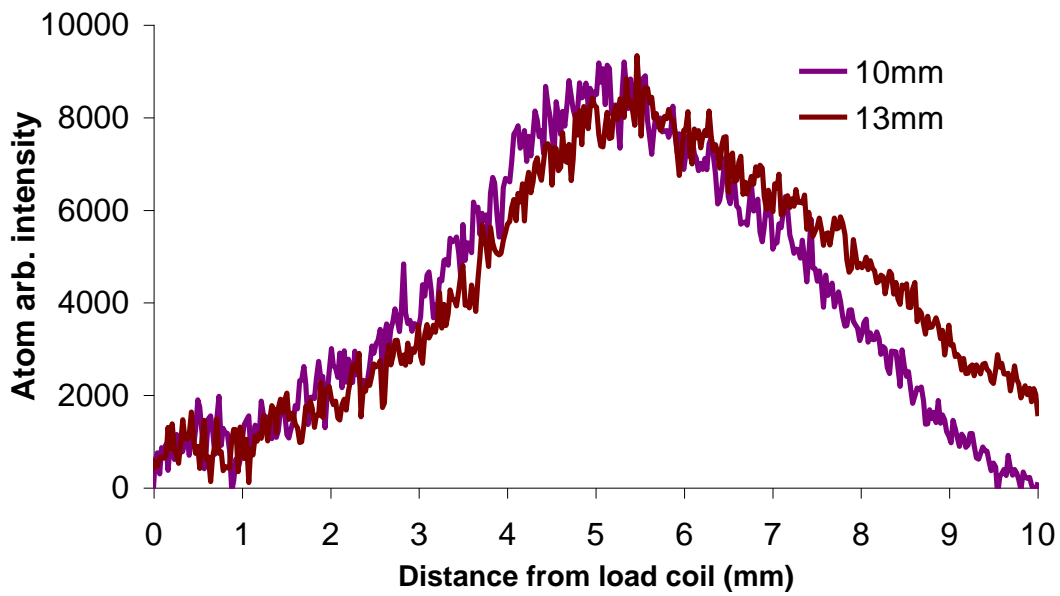
Fig 3.10 Axial distributions of barium ions and atoms at different sampling depths,

10mm vs 13mm

One different parameter that can be easily minimized is the sampling depth used

in two different configurations. However, when we changed the sampling depth used

in this experiment, the results did not change very much, as shown in Fig 3.10. The
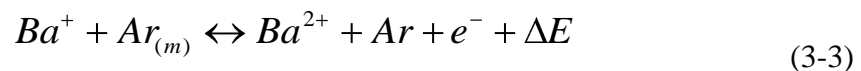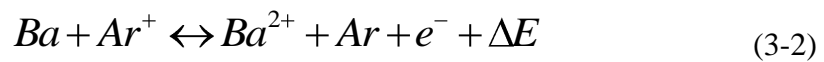
results from the two labs still do not agree.

Table 3. 1 Comparison of experimental features used in this work and reference 4

	This work	Reference 4
Load coil ground	Center tapped	Ground at downstream end
Torch orientation	Horizontal	Vertical
Sampling depth	10 mm	13 mm
Torch injector diameter	1.5 mm	1.2 mm
Analyte	Ba	Ca, Sr

To explain the experimental results we obtained, we assume possible mechanisms for the conversion between singly and doubly charged barium ions. This conversion can account for the differences seen in the data obtained from different experiments. It is important to realize that the fluorescence imaging technique we used in this experiment is blind to any form of the analyte other than the specific states being probed by the laser. The measurements are generally based on the assumption that the plasma is in local thermodynamic equilibrium, and the bulk of the atoms and ions are in ground state and can be described by a Boltzmann distribution. However, when a cooled sampling interface is inserted into the plasma, these assumptions may not be correct.

The shift of the following reactions can be used to account for the increase of singly charged barium species in the presence of the sampling orifice:

$$Ba + Ar^+ \leftrightarrow Ba^{2+} + Ar + e^- + \Delta E \tag{3-2}$$

$$Ba^+ + Ar_{(m)} \leftrightarrow Ba^{2+} + Ar + e^- + \Delta E \tag{3-3}$$

$$Ba^+ \leftrightarrow Ba^{2+} + e^- + \Delta E$$

It is speculated that the increase of barium ionic signal is largely due to the conversion of barium doubly-charged ions to singly-charged ions primarily from the reverse of equation 3-4. However, high densities of barium doubly charged ions are not observed in spectra recorded in the ICP-MS. One plausible explanation is that during the transmission from the plasma to the mass detector, the ion-electron recombination rates of doubly charged ions are significantly higher than these of singly charged ions.[15]
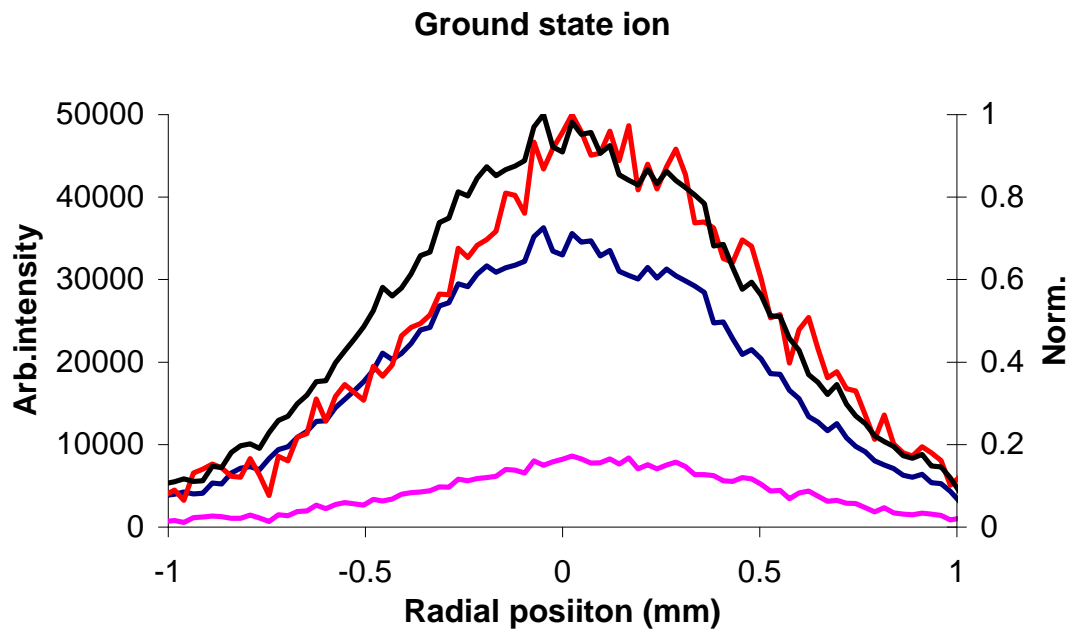
3.3.3.   Radial distribution of barium species inside the plasma

Another factor that might account for the increase of ionic signal in the presence of the sampling cone is the radial spread. The existence of the sampling cone and the vacuum of the first stage may narrow the radial distribution of analyte species. By combining the radial distribution with axial number densities, we can estimate the number densities of analyte species in a specific volume inside the plasma.

Therefore, in this section, the radial intensities and normalized distributions of barium ground state atoms, ground state ions, and metastable ions 5mm downstream from the load coil in the presence and absence of the sampling cone are plotted in Fig 3.11. The incident power and nebulizer flow used were 1250 Watts and 1.09 L/min, respectively.

As displayed, at the observed radial positions, the radial distributions of analyte species do not become narrow due to the presence of the sampling cone. The radial spreads of analytes in the presence and absence of the sampling cone are similar. The

same trends were also observed in the other operating conditions. The increase of singly charged ions 0-7 mm downstream from the load coil cannot be explained by the low radial spread rate of analyte species inside the plasma.

Atom

Ground state ion

Metastable ion
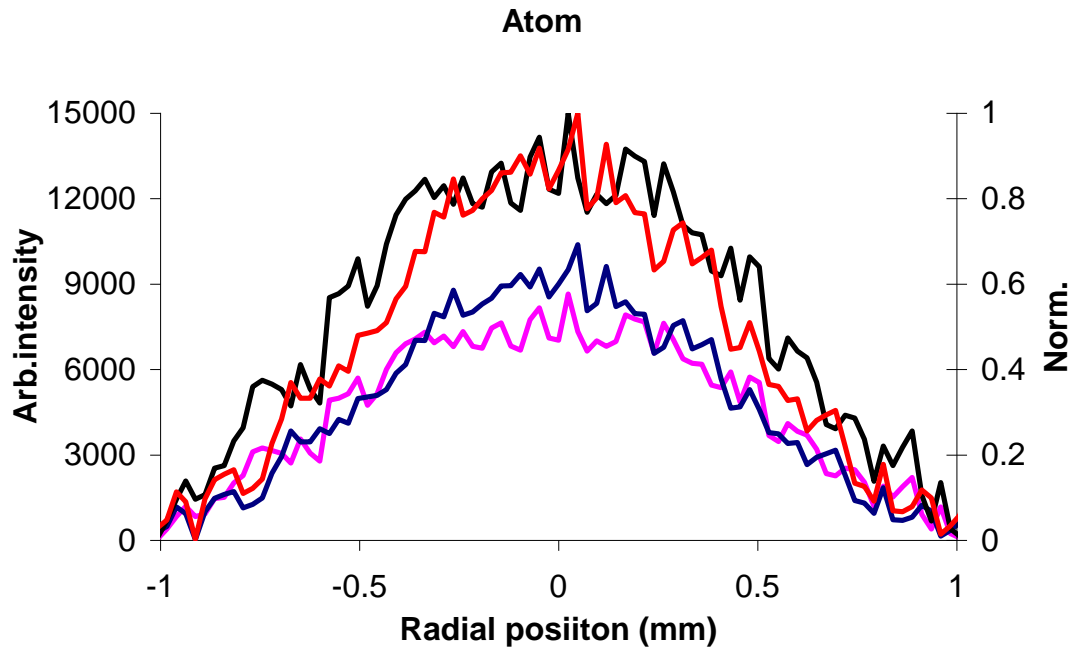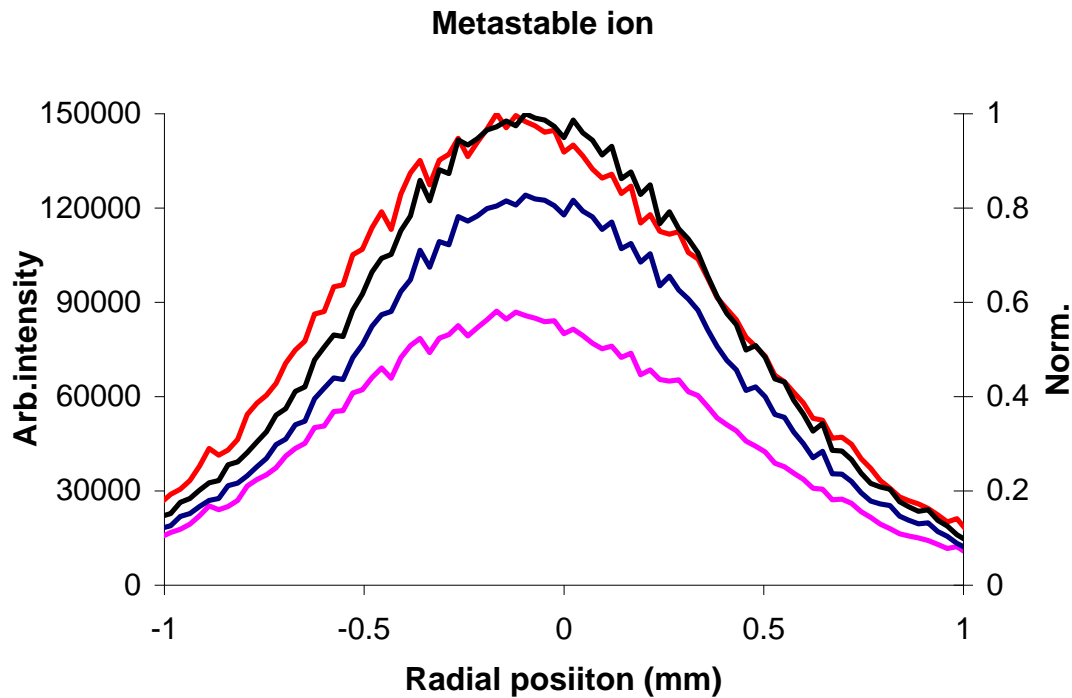
Fig 3.11 Radial distribution of barium species 5 mm downstream the load coils in the presence and absence of the sampling cone; (———) with cone, (———) without cone; (———) normalized intensity with cone, (———) normalized intensity without cone

3.3.4. Impact of matrix effects with and without the sampling cone

It is reported [12] that the addition of matrix species, both lithium and lead, suppressed or reduced fluorescent emission intensities of barium ionic species high in the plasma. As shown in Fig 12, the phenomena are consistent with the data in reference 12. The same trends with intensification of ionic signal several millimeters downstream from the load coil are obtained, although the drops caused by the introduction of lithium are more significant than these for lead.

However, the introduction of the matrix components can't explain the huge difference of barium ion number densities in the presence and absence of the sampling cone shown in this research. We still assume that the conversion between the singly charged and doubly charged barium ions dominates the phenomena

observed in this research. Further study is needed on the function of doubly charged ions inside the plasma.

Atom

Ground state ion

Metastable ion
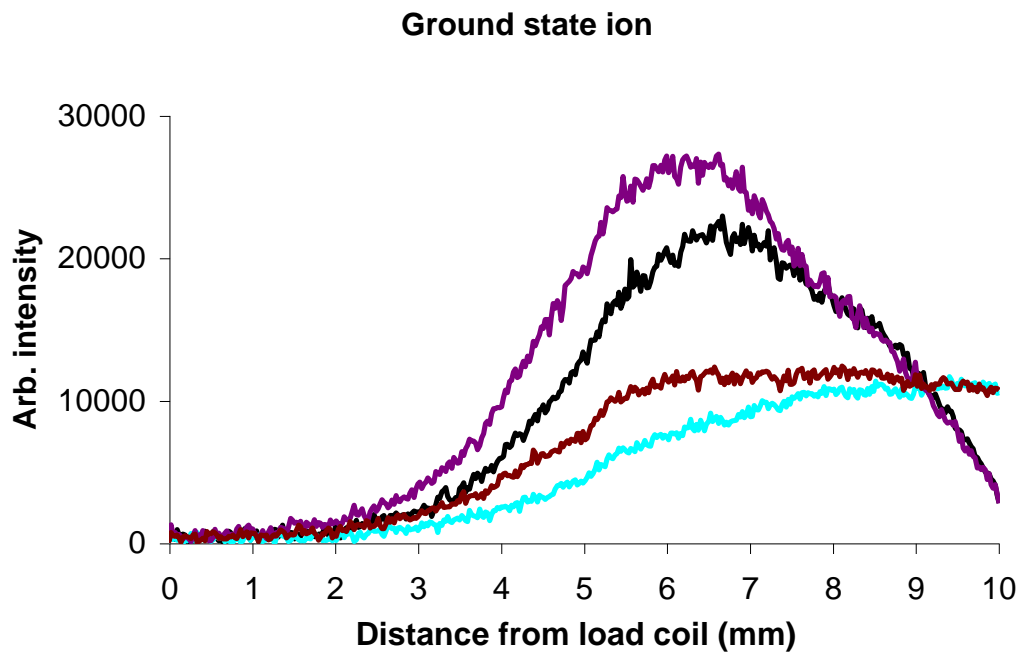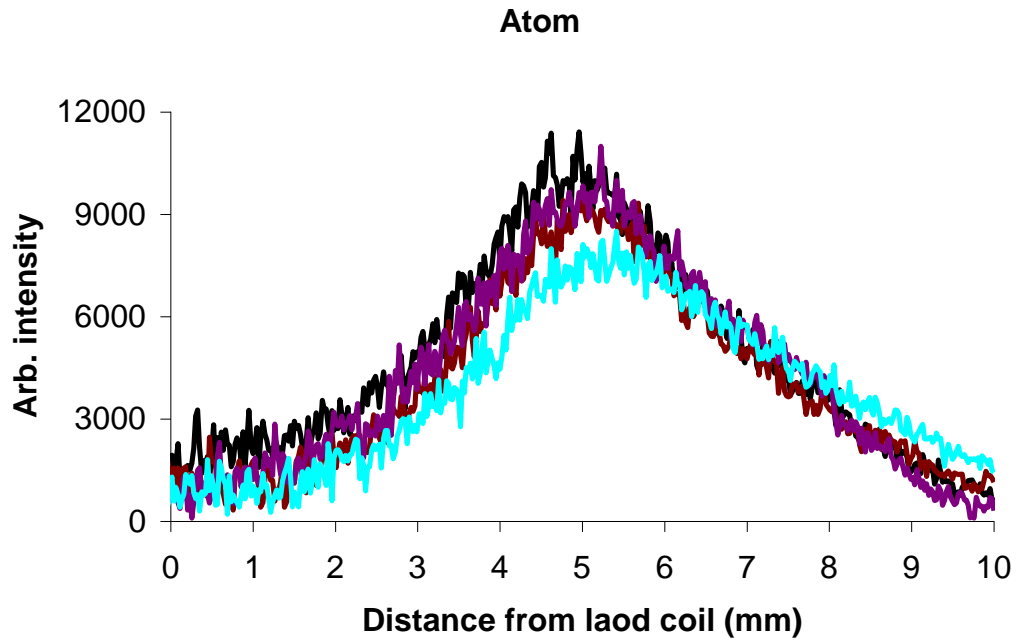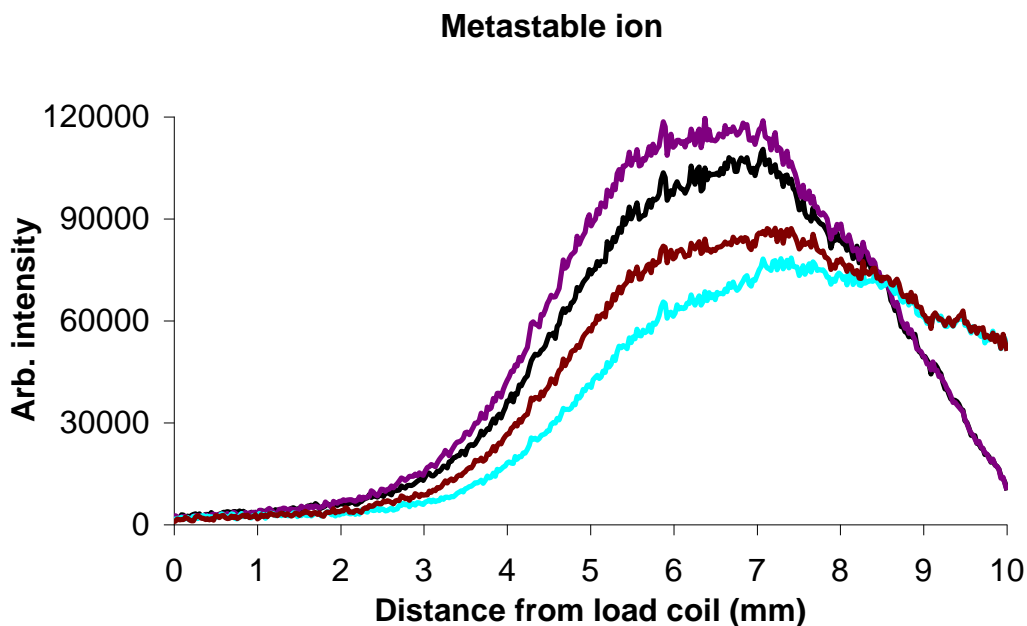
Fig 3.12 Impact of matrix effect on axial distributions of barium ions and atoms under 1250 W, 1.09 L/min; (———) Lithium with cone, (———) Lithium without cone; (———) Lead with cone, (———) Lead without cone

3.3.5.   Poorly reproducible results with ultrasonic nebulizer

Similar experimental schemes were carried out with the ultrasonic nebulizer. Unfortunately, higher aspirating efficiency did not create better signal-to-noise ratios for ground state ions. On the contrary, it was found that the variations of ground state ions and metastable ions under repeated experiments were unacceptable, as shown in Fig 3.13. Therefore, no further work was carried out on the experimental results obtained from aspirations using the ultrasonic nebulizer. Future work requires a more stable ionic signal with a better ultrasonic nebulizer system.

Atom
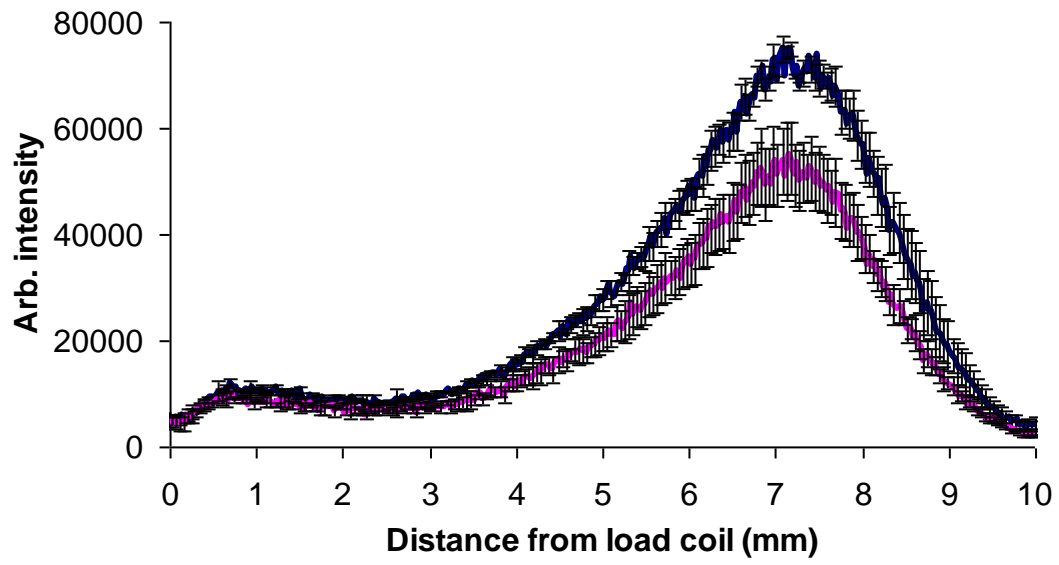
Ground state ion
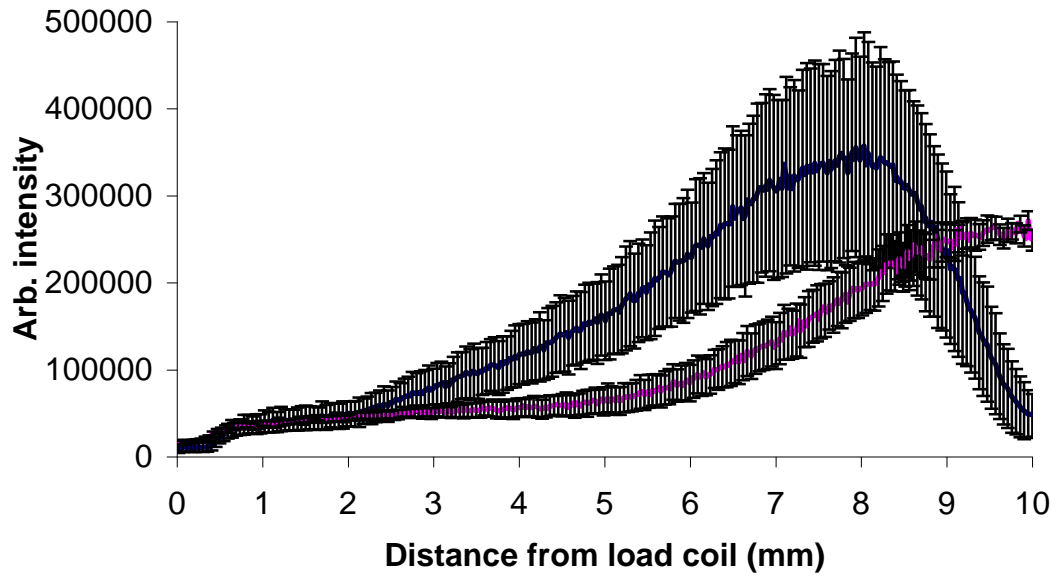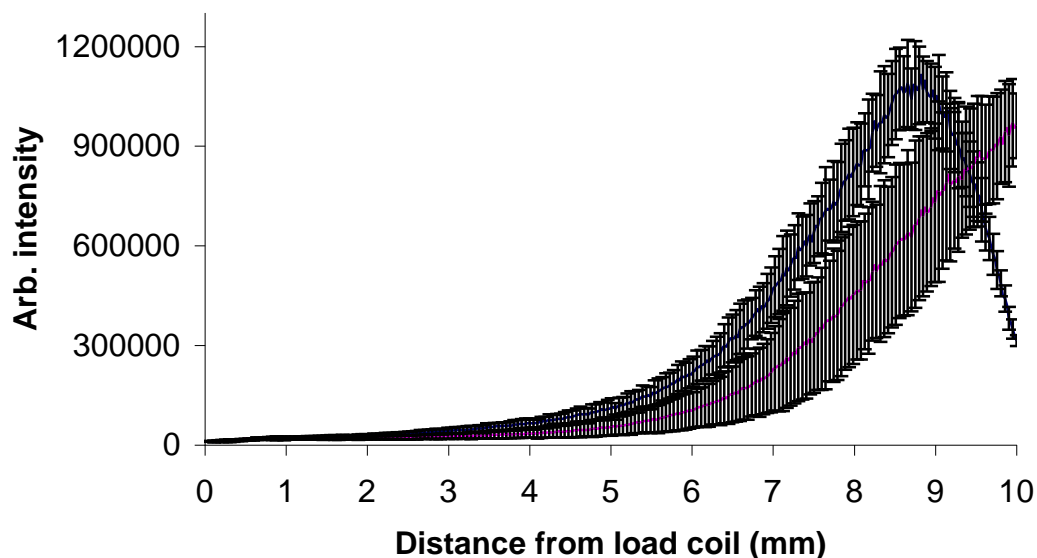
Metastable ion

Fig 3.13 Representative signals with error bars of barium ground state and metastable ion, ground state atoms in the presence and absence of the sampling cone, incident power 1250 W, nebulizer flow 1.09 L/min, (——) with cone, (——) without cone

3.4. Summary and conclusions

Relying on laser induced fluorescence techniques, spatial distributions of barium ground state atoms, ground state ions, and metastable ions downstream from the load coil in the presence and absence of the sampling cone were imaged.

The insertion of the sampling interface has a profound influence on the axial distributions of analyte species. The atomic and ionic fluorescence signals drop 3 mm upstream from the sampling cone in the presence of the sampling cone. The decrease can be attributed to the temperature drop of the plasma and the acceleration of the first stage's vacuum. However, in the region of 0-7 mm downstream from the load coil, the number densities of singly charged barium ions are intensified significantly. This can't be explained either by wider radial spread or matrix interference. We interpret those

increases as conversions between neutral atoms, singly charged ions, and doubly

charged ions. Our data both from fluorescence techniques and ICP-MS measurement

indicate the efficient production of barium doubly charged ions in the plasma.

3.5. References

[1] Douglas D. J., French J. B., *J, Anal. At. Spectrum.*, 3, **1988**, 743

[2] Stewart I. I., Hensman C. E., Olesik J. W., *Appl. Spectrosc.*, 54, **2000**, 164

[3] Holliday A. E., Beauchemin D., *Spectrochim. Acta, Part B*, 59, **2004**, 291

[4] Lehn S. A., Huang M., Warner K. A., Gamez G., Hieftjie G. M., *Spectrochim. Acta, Part B*, 58, **2003**, 1647

[5] Lehn S. A., Warner K. A., Huang M., Hieftje G. M., *Spectrochim. Acta, Part B*, 57, **2002**, 1739

[6] Gamez G., Lehn S. A., Huang M., Hieftje G. M., *Spectrochim. Acta, Part B*, 62, **2007**, 357

[7] Gamez G., Lehn S. A., Huang M., Hieftje G. M., *Spectrochim. Acta, Part B*, 62, **2007**, 370

[8] Borkowska-Burnecka J., Lesniewicz A., Zyrnicki W., *Spectrochim. Acta, Part B*, 61, **2006**, 579

[9] Duersch B. S., Chen Y., Ciocan A., Farnsworth P. B., *Spectrochim. Acta, Part B*, 53, **1998**, 569

[10] Macedone J. H., Gammon D. J., Farnsworth P. B., *Spectrochim. Acta, Part B*, 56, **2001**, 1687

[11] Macedone J. H., Mills A. A., Farnsworth P. B., *Spectrochim. Acta, Part B*, 58, **2004**, 463

[12] Mills A. A., Macedone J. H., Farnsworth P. B., *Spectrochim. Acta*, *Part B*, 61, **2006**, 1039

[13] Cicerone M. T., Farnsworth P. B., *Spectrochim. Acta, Part B*, 44, **1989**, 897

[14] Macedone, J. H., Farnsworth P. B., *Spectrochim. Acta, Part B*, 61, **2006**, 1031

[15] Chan G. C. Y., Hieftjie, G. M., *Spectrochim. Acta, Part B*, 61, **2006**, 642

4. MASS-DEPENDENT SPREAD OF IONS IN THE FIRST VACUUM STAGE OF AN ICP-MS

4.1. Introduction

In an ICP-MS, the analyte species are ionized by the plasma, sampled and skimmed by the sampling cone and skimming cone sequentially, then transmitted through the ion optics, and finally measured by the mass detector.[1] A comprehensive understanding of ion transmission in the first vacuum stage of an ICP-MS can facilitate development of theoretical models used to simulate analyte transport behaviors, improve the interface design, reduce the severity of matrix effects and increase the transmission efficiency of analyte from the plasma to the mass detector. During the sampling process, differential ion losses due to mass-dependent radial diffusion remain a concern.

Whether the heavy elements are enriched relative to lighter ones on the passage of a gas mixture through the sampling cone of an ICP-MS is still under debate. The current gas-dynamic theory model used to describe ion movement in the continuum flow in the first vacuum stage is mostly based on the assumption that the temperature and density of the plasma drop during the sampling process, but the overall composition remains unchanged.[2]

Many early papers state that the free jet behind the nozzle generally favors the heavier species.[3,4,5,6] However, Reis[7] confirmed that the enrichment of heavy molecules in the sampling process was an artifact and could be explained by probe effects. The prevalent models of the supersonic expansion do not account for charge-induced effects. Previous experiments[8] suggests that some movement of the ions is due to electric fields that arise in the first vacuum stage. In this chapter, I

describe experiments designed to identify mass-dependent behavior in the supersonic expansion in an ICP-MS.

Two analytes having different masses but similar first ionization potentials, barium and calcium ions, were adopted as test analytes. The spatial distributions of these analyte ions at the sampling cone and 10 mm downstream from the sampling cone under different incident powers and nebulizer flows were compared to display the mass-dependent spread of ions in an ICP-MS interfacial region. The radial distribution of ions at the tip of the skimmer cone is important because only the central part of the distribution passes through the skimmer cone into the second vacuum stage. Flat distributions lead to poor transport efficiency through the first vacuum stage, while distributions that are peaked on the expansion axis lead to higher transport efficiencies.

The results of my experiments will be compared to a Monte Carlo simulation model being developed by collaborators in the physics department at the BYU. The comparison will provide insights into the origins of mass biases in the first vacuum stage of an ICP-MS.

4.2. Experimental

4.2.1. Probed species and analyte solution

Dye lasers were tuned to transitions at 393.366 nm (PBBO, Lambda Physik, Ft. Lauderdale, FL) and 455.404 nm (Coumarin 460, Exciton, Dayton, OH) to excite the calcium and barium ions, respectively, as shown in Fig 4.1. The calcium ion fluorescence was isolated with a 1.1 nm bandpass filter with wavelength centered at 854.3 nm. The barium ground state ion fluorescence was isolated with a 614.2 nm (1

nm band pass) filter (614.2/1-25.4，Barr Associates, Westford, MA).
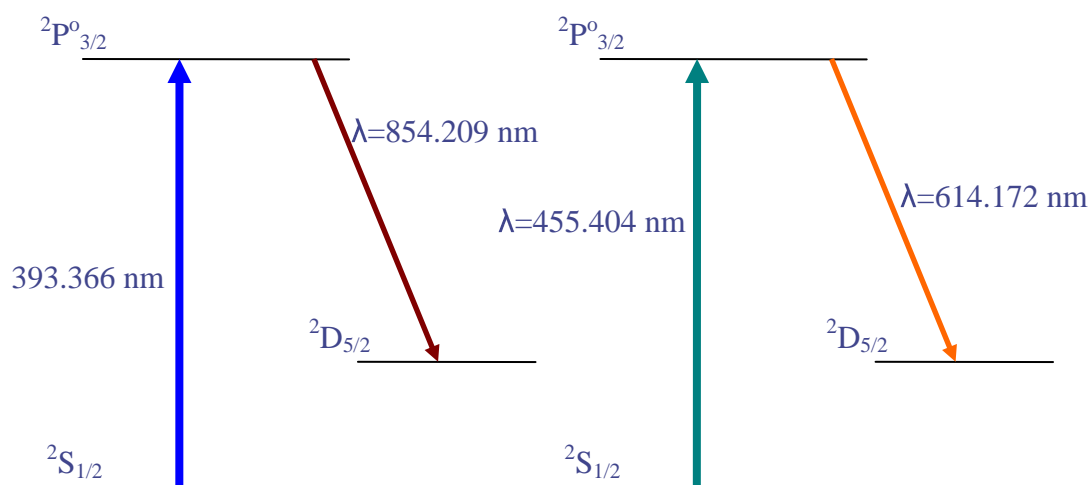
Fig 4.1 Energy level diagram of Ca (II) (left) and Ba (II) (right) used

4.2.2. Instrumentation

The fundamental instrumental setup used in this research has already been described in the previous chapters of this dissertation and other publications from our research group.[9,10] The ICP parts, including the RF generator, the plasma torch and the sampling cone, were identical to those described in the section 2, chapter 2. Only the modifications of the experimental setup are described. Two instrumental setups were adopted to map the spatial distribution of calcium and barium ions at the sampling orifice and 10 mm downstream from the sampling cone in this research, as shown in Fig 4.2 and 4.3, respectively.

Fig 4.2 shows the experimental setup for imaging the spatial distribution of analyte ions at the tip of the sampling cone. A 25-mm-diameter sapphire window (02 WSA 008, Melles Griot, Rochester, NY) was mounted on an aluminum flange, which was water-cooled. The distance between the sapphire window and the sampling cone was 52 mm. The planar excitation laser, which just skimmed the tip of the sampling

cone, was mounted on the vacuum chamber stage. The intensified gated CCD behind the sapphire window was used to record the analyte's fluorescence emitted at the sampling orifice. Because the excited ionic fluorescence was collected through the sampling orifice, the scattering interference from the tip of the sampling cone, which was discussed in chapter 2, was not a significant concern.
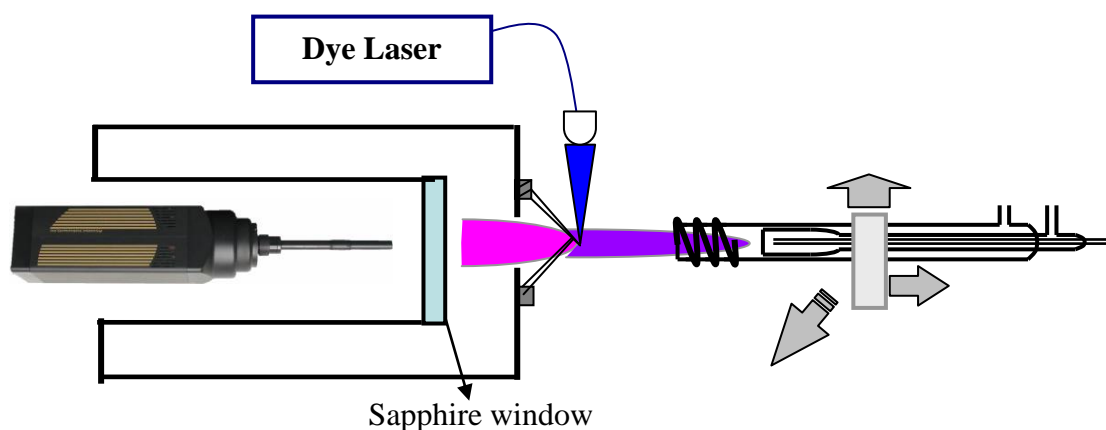

Fig 4.2 Experimental setup for fluorescence imaging at the sampling orifice
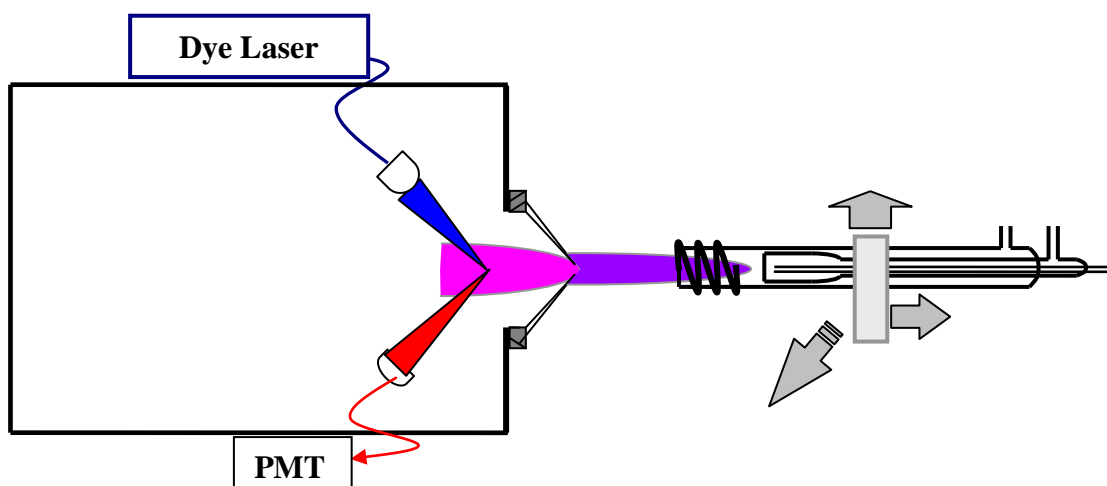

Fig 4.3 Experimental setup for fluorescence measurement 10 mm downstream from the sampling orifice

Fig 4.3 shows the experimental setup for radial distribution detection of analyte 10 mm behind the sampling cone. During this process, a 0.4 mm optical fiber was used to deliver the excitation laser to the vacuum chamber, and to collect emission fluorescence to a photomultiplier tube (R928 Hamamatsu, Bridgewater, NJ), which signal was amplified by a fast amplifier (model 310, Sonoma Instruments, Santa Rosa, CA) and averaged by a gated boxcar integrator (SR 250, Stanford Research system, Sunnyvale, CA). Finally, the signal was recorded by an A/D converter (PCI-6110, National Instruments, Austin, TX) and displayed on a personal computer.

4.2.3.   Plasma operating condition and analytes

The operating conditions of the ICP were the same as listed in table 1, chapter 2. The 10 ppm barium solution used in this experiment was prepared from anhydrous barium chloride powder (Spectrum Chemical Mfg. Corp., Gardena, CA). The 25 ppm calcium solution was made from solid calcium carbonate (AR grade, Mallinckrodt Inc., Paris, KY). The matrix lithium solution was obtained from granular lithium nitrate (AR. Mallinckrodt Specialty Chemicals Co., Paris, KY). All the solutions were aspirated into the plasma by an ultrasonic nebulizer (ATX-100, Cetac, Omaha, NE) and desolvation system (U-5000, Cetac, Omaha, NE).

4.2.4.   Data collection and processing

To ensure the results were not impacted by the variation of the dye laser energy output, the laser intensity was checked to ensure its irradiance was above the saturation thresholds of each analyte species before the images or data were recorded.

When the spatial distributions of analyte species were mapped at the sampling orifice, the CCD was gated to coincide with the laser pulses and the gate width was

set to 40 ns. For each experiment, 1000 shots were summed to generate one single image of fluorescence signal and one emission background, respectively. To create the final image, the emission background was subtracted from the image that included both fluorescence and emission. The subtracted fluorescence signal was then converted to ASCII and the spatial distributions of analytes were extracted by a MathCad program.

A point-by-point excitation and collection laser-induced fluorescence system was used to record the spatial distribution of barium and calcium fluorescence at the position 10 mm downstream from the sampling cone. A LabView (National Instruments, Austin, TX) program was used to control the optics to scan in the vertical direction from 7 mm to -7 mm. The point-by-point increment was 0.5 mm. At each point, 100 shots were recorded and time-averaged to produce a single fluorescence signal. The signals displayed on the PC were relative and dependent on the voltage imposed on the PMT and the gain of the amplifier.

4.3. Results and discussion

4.3.1.   Influence of different nebulizer flows on the spatial distribution of analytes at the sampling orifice

The operating conditions of the plasma, such as nebulizer flow and incident power, have a high impact on the spatial distribution of analyte species at the sampling orifice. As previously explained, changes of nebulizer flow or incident power can produce similar effects on the plasma. Therefore, only the variation of the nebulizer flow was adopted to check its influence on the extraction efficiency of the sampling cone. The plasma incident power was fixed to 1250 Watts.

Fig 4.4 displays the fluorescence images of barium ions at the sampling orifice under different nebulizer flows. The color displayed in the images represents the variation of ionic fluorescence response for different nebulizer flows. The fluorescence of each image was normalized to the maximum intensity obtained for the entire series of images.

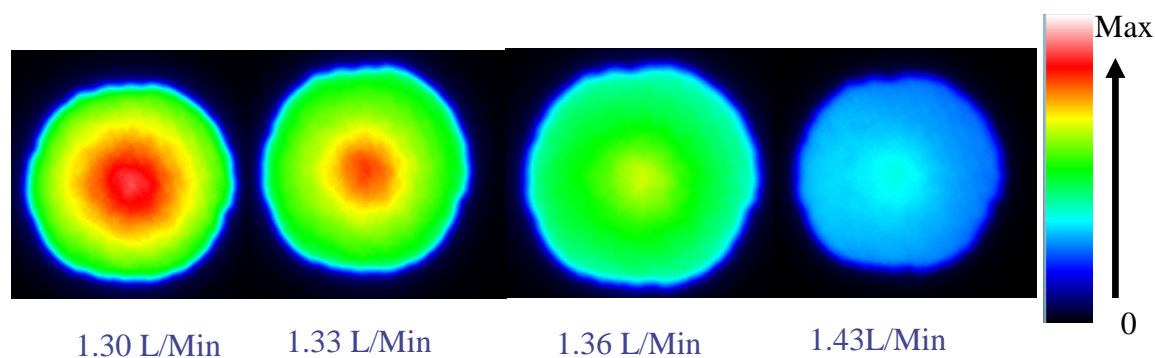1.30 L/Min   1.33 L/Min   1.36 L/Min   1.43L/Min

Fig 4.4 Spatial distribution of barium ions at the sampling orifice under different nebulizer flows
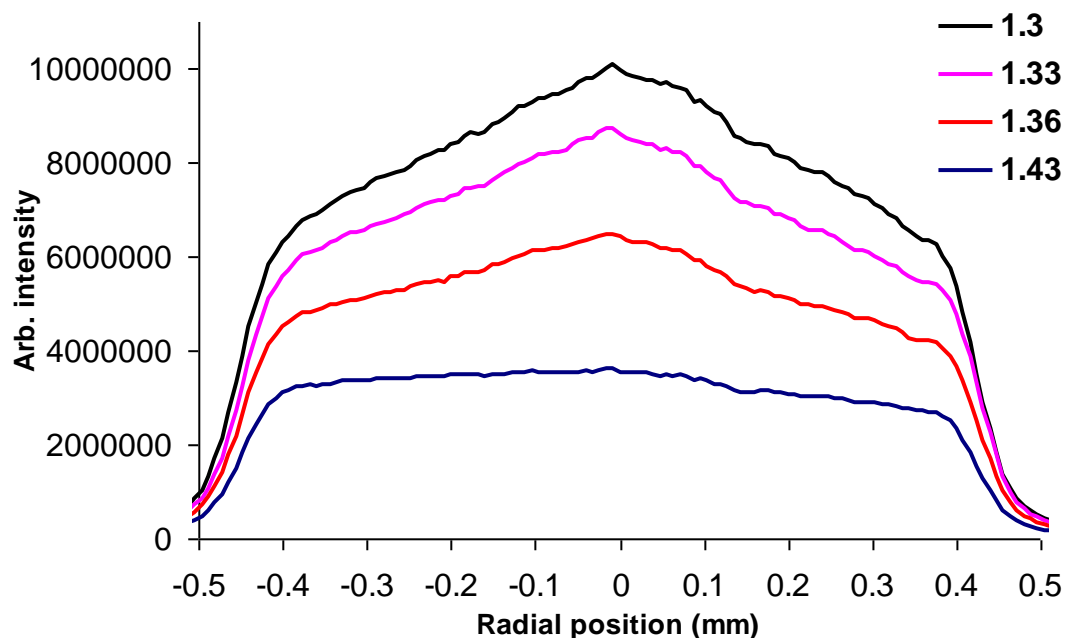

Fig 4.5 Demonstrated spatial distribution of barium ions at the sampling orifice under different nebulizer flows (unit: L/min)

Radial distributions of barium ions under different nebulizer flows were extracted from the images and plotted, as shown in Fig 4.5. As demonstrated by the plots, when the nebulizer flow increases, the ionization of analyte becomes incomplete, the fluorescence response of barium ion decreases, and the spatial distribution of barium ions became flat. For a detailed explanation, please refer to reference 10.

4.3.2. Spatial distributions of barium and calcium at the sampling orifice

In this section, error bars in each plot representing the standard deviations of triplicate measurements were displayed to reflect the reproducibility of the experimental results.

The spatial distributions of calcium and barium ions at the sampling orifice are expected to be similar because of their close first ionization energies. In this section, nebulizer flows of 1.36 L/min for barium and 1.33 L/min for calcium were used. It was shown that under these nebulizer flows, the fluorescence signals and radial distributions of barium and calcium ions at the sampling orifice were both ideal in the preliminary experiments. Therefore, the extracted cross-sectional spatial distribution of calcium and barium ions under 1.33 L/min and 1.36 L/min, respectively, were normalized and plotted in Fig 4.6. Considering the error bars, the match between the radial distribution of barium and calcium ions at the sampling orifice was quite good. If any difference exists, the radial distribution of calcium ions was a littler narrower than that of barium ions.
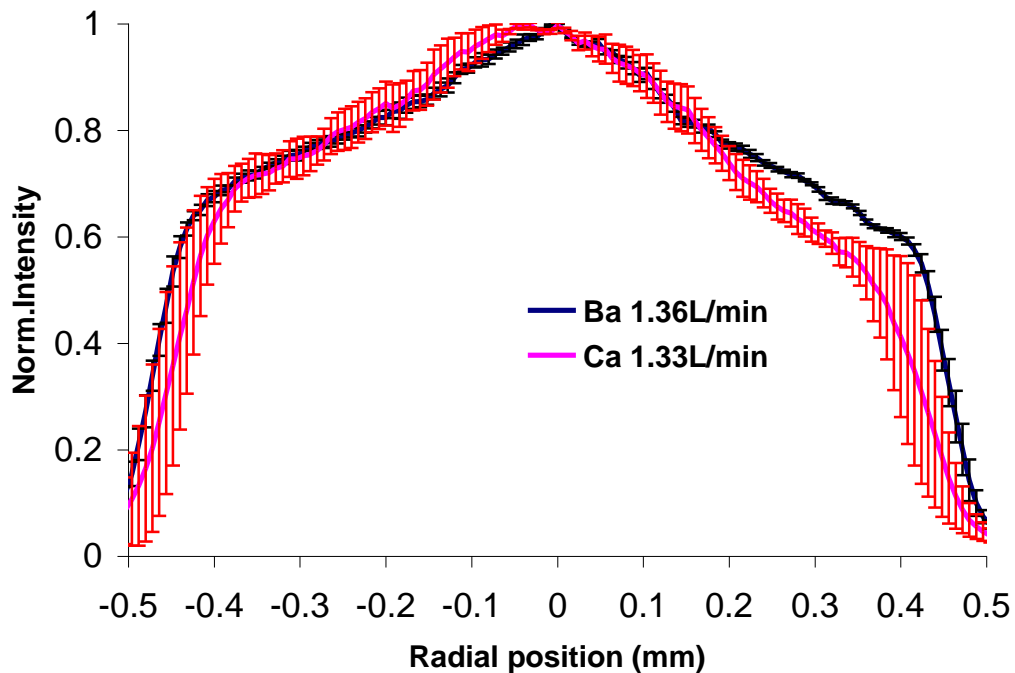
Fig 4.6 Normalized spatial distribution of barium and calcium at the sampling orifice

4.3.3.   Spatial distributions of analytes 10 mm behind the sampling orifice

The radial distributions of barium and calcium ions 10 mm downstream from the sampling cone are significantly different from those recorded at the sampling orifice. Fig 4.7 displays the spatial distribution of barium and calcium ions 10 mm downstream from the sampling cone. With nebulizer flows of 1.33 L/min for calcium ion and 1.36 L/min for barium ion, the difference between radial distributions of the two analytes becomes evident at distance greater than 2.5 mm from the central axis. The lighter calcium ions had a broader radial distribution than that of heavier barium ions.

Therefore, it can be inferred that the diffusion behind the sampling cone was mass-dependent, with the heavier particles favored in the centerline of the expansion beam and diffusing slower than the lighter analyte species.
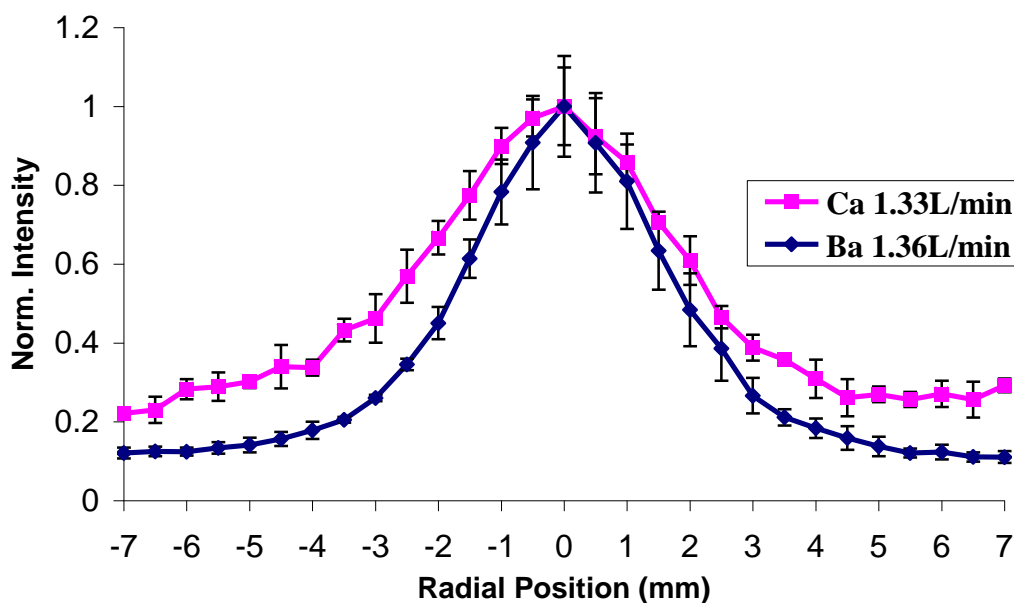
Fig 4.7 Radial distributions of barium and calcium ions 10 mm behind the sampling cone

4.3.4.　Factors impacting the radial distribution of analytes behind the sampling cone

Usually, the plasma incident power, nebulizer flow and matrix compositions are three factors significantly impacting the sensitivity and detection limits of an ICP-MS.[11] The radial distribution of analyte species in the first vacuum stage is largely dependent on the operating condition of the plasma and the matrix compositions.[12] In this section, the radial distribution of barium ions under a series of incident power, nebulizer flow and matrix composition at two different positions behind the sampling cone (marked as Z values, the distance from the sampling orifice to the probing points) were carried out to provide a more detailed description of radial distribution of analyte species in the first vacuum stage when the skimmer cone was not installed.

4.3.4.1. Incident power and nebulizer flow

It has been shown that incident power and nebulizer flow have similar effects on the spatial distributions of analytes upstream from the sampling cone.[10] This phenomenon was verified again on the radial distribution of barium ions behind the sampling cone, as shown in Fig 4.8 and Fig 4.9 with fixed nebulizer flow (1.36 L/min) and variable power, and fixed incident power (1250 Watts) and variable nebulizer flow, respectively. As expected, fluorescence signal intensities were largely dependent on the distance downstream from the sampling cone (different Z values). The fluorescence intensity at Z = 6 is much higher than that in the position of Z = 10. The supersonic expansion behind the sampling cone can be approximated as an axisymmetric semispherical expansion, where the intensities of analytes drop sharply.[13]
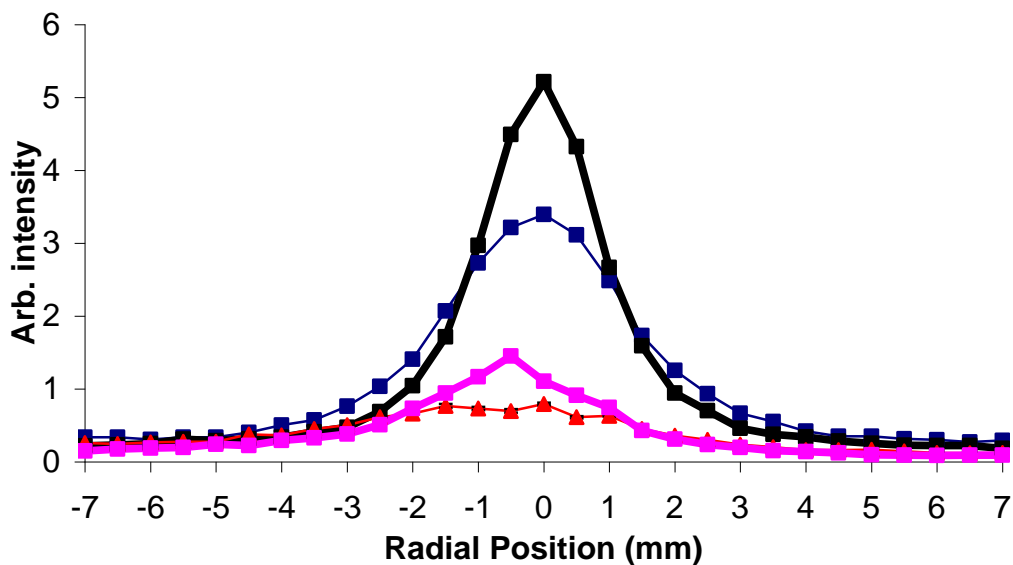
Fig 4.8 Influence of incident power on radial distributions of barium ion behind the sampling cone, the nebulizer flow was 1.36 L/min; (——) 1250 W, Z=6; (——) 1250 W, Z=10; (——) 850W, Z=6; (——) 850W, Z=10
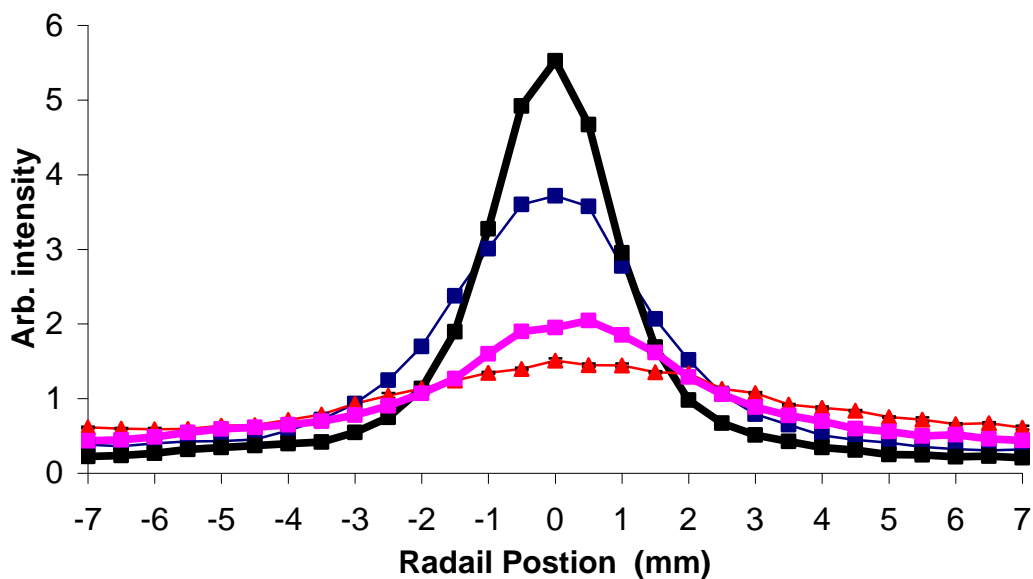
Fig 4.9 Influence of nebulizer flow on radial distributions of barium ion behind the sampling cone, the incident power was 1250 W; (━━) 1.36 L/min, Z=6; (━━) 1.36 L/min, Z=10; (━━) 0.82 L/min, Z=6; (━━) 0.82 L/min, Z=10

4.3.4.2. Matrix composition

When a solution consisting of 10 ppm barium and 400 ppm lithium was aspirated into the plasma under the incident power of 1250 Watts and nebulizer flow of 1.36 L/min, the fluorescence signal of barium behind the sampling cone was suppressed significantly at the center region, while the ion intensity on the edge of the *zone of silence* was enhanced slightly, as shown in Fig 4.10. The trend was not surprising since similar suppression of barium ionic fluorescence intensity caused by the addition of matrix compositions on the plasma axis due to the addition of matrix compositions has been observed upstream from the sampling cone in our lab.[10]
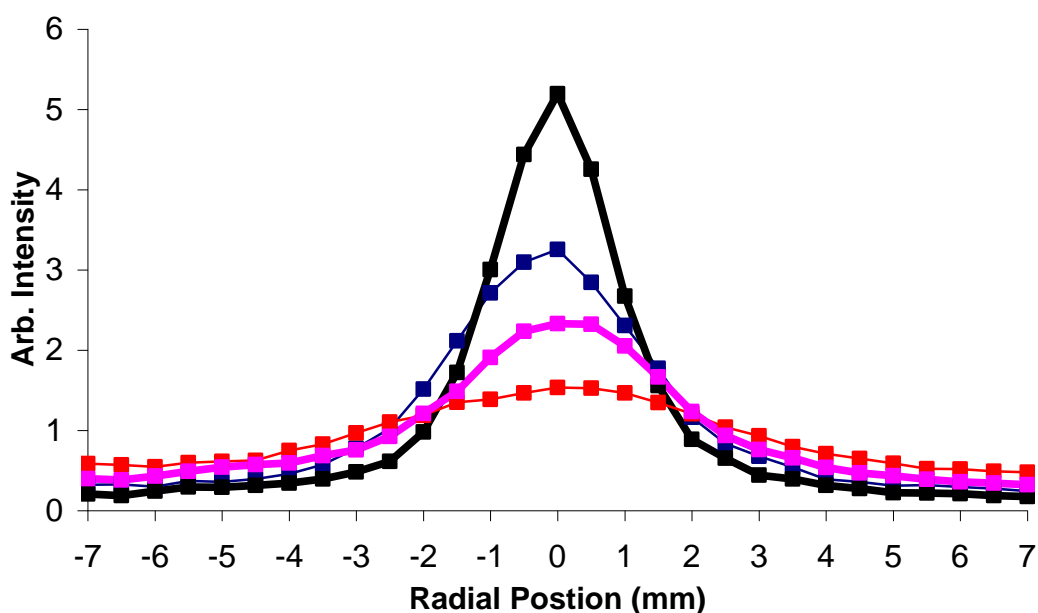
Fig 4.10 Influence of matrix composition on the radial distribution of barium ion behind the sampling cone, the incident power and nebulizer flow were set to 1250 W, 1.36 L/min consistently; (━━━) Z=6, no matrix; (━━━) Z=10, no matrix; (━━━) Z=6, 400 ppm Lithium; (━━━) Z=10, 400 ppm Lithium

4.4. Summary and Conclusions

Relying on the laser induced fluorescence technique, we imaged the spatial distribution of barium and calcium ions at the sampling orifice and 10 mm downstream from the sampling cone under different experimental conditions.

The results showed that the spread of analyte ions in the first vacuum stage of an ICP-MS was mass-dependent, the lighter particles diffuse faster than the heavier ones in the first vacuum stage. This phenomenon indicates that the diffusion behind the sampling cone might be ambipolar, which will be verified by the measurement carried out in the next chapter of this dissertation.

In addition, the radial distributions and intensities of ions behind the sampling

cone were highly dependent not only on the operating conditions of the plasma, such as incident power and nebulizer flow, but also the composition of the aspirated solutions.

4.5. Reference

[1] Robert T., *Practical Guide to ICP-MS*, Marcel Dekker, Inc., New York, **2004**

[2] Chambers D. M., Poehlman J., Yang, P., Hieftje G. M.*, Spectrochimica. Acta Part B*, 46, **1991**, 741

[3] Becker E. W., Bier K., *Zeitschrift für Naturforschung. A*, 9, **1954**, 975

[4] Becker E. W., Beyrich W., Bier K., Burghoff H., Zigan F., *Zeitschrift für Naturforschung. A*, 12, **1957**, 609

[5] Waterman P. C., Stern S. A., *J. Chem. Phys*., 31, **1959**, 405

[6] Stern S. A., Waterman P. C., Sinclair T. F., *J. Chem. Phys*., 33, **1960**, 805

[7] Reis, V. H., Fenn J. B., *J.   Chem. Phys.*, 39, **1963**, 3240

[8] Macedone, J. H., Gammon, D. J., Farnsworth, P. B., *Spectrochimica. Acta Part B*, 56, **2001**, 1687

[9] Macedone, J. H., Farnsworth, P. B., *Spectrochimica Acta part B*, 61, **2006**, 1031

[10] Mills A. A., Macedone, J. H., Farnsworth, P. B., *Spectrochimica Acta Part B*, 61, **2006**, 1039

[11] Montaser, A. Golightly, D. W., *Inductively Coupled Plasmas in Analytical Atomic Spectrometry*, 2nd, VCH Publisher, Inc. **1992**

[12] Macedone, J. H., Mills A. A., Farnsworth, P. B., *Appl. Spectrosc*., 58, **2004**, 463

[13] Scoles, G., Bassi, D., Buck U., Laine D. C., *Atomic and Molecular Beam Methods*, V1, Oxford University Press, **1988**

5. TEMPERATURE AND VELOCITY MEASUREMENT OF ARGON ATOMS AND CALCIUM IONS IN THE FIRST VACUUM STAGE OF AN ICP-MS

5.1. Introduction

To understand ion transmission through the first vacuum stage of an ICP-MS, the supersonic expansion behind the sampling cone needs to be fully characterized.[1] It has generally been assumed that in an ICP-MS supersonic expansion, the argon gas and ionized analytes flow through the sampling orifice without changes in composition, and that the plasma remains neutral.[2] Meanwhile, due to simultaneous drops in number density and temperature, the collision frequency in the expansion falls off sharply. However, there has been some experimental evidence that the plasma is not neutral in the first vacuum stage,[3] and that collisions downstream from the sampling cone in an ICP-MS can change the composition of the plasma.[4] Our group has speculated that the ion transport behind the sampling cone is charged-induced.[5]

Velocity and temperature are two important parameters characterizing the supersonic expansion in an ICP-MS. In this supersonic expansion behind the sampling cone, the velocities of ions or atoms can be resolved into axial and radial velocities. Similarly, the temperature can also be separated as axial and radial temperatures.[6]

Using the Doppler shift of exciting radiation and high-resolution diode laser spectroscopy, previous workers in our lab have measured the velocity of argon metastable atoms in the second vacuum stage of an ICP-MS. Similar work was carried out in the first vacuum stage of an ICP-MS by Radicic et al.,[5] who characterized the velocities and temperature of argon atoms as a function of spatial position within the Mach disk and barrel shock, the nebulizer flow, the RF incident power, the quantity of

water loading, and the plasma and auxiliary gas flows.

In addition, Radicic also compared the velocities of charged calcium ions and neutral argon atoms behind the sampling cone, which showed that the velocity difference between two species was small but significant. Some experimental measurements raised the possibility of charge-induced transport of ions behind the sampling cone. The charged particles seem to undergo a higher acceleration than the neutral particles.[3,5]

The goal of the current experiments is to measure and compare the temperature and velocity of argon atoms and calcium ions on the central axial direction behind the sampling cone. The reasons why we selected charged calcium ions and neutral argon atoms are: 1) both have similar atomic masses, 40.078 amu (calcium) vs 39.948 amu (argon), which eliminate the mass-dependent bias observed in the first vacuum stage in chapter 4; 2) the description of the bath gas, argon atoms, can be used as the baseline for the characterization of other analyte behaviors behind the sampling cone.

In this research, diode laser spectroscopy was used to record the fluorescence wavelength difference between stationary populations of argon and calcium and the same species in the supersonic expansion of the first vacuum stage. Velocities were determined from the frequency shift on the basis of the following equation:

$$V_D = \frac{\lambda_{\max}\Delta\nu}{\cos\theta} \qquad (5\text{-}1)$$

where $\lambda_{\max}$ is the peak excitation wavelength for a motionless population, θ is the angle of the excitation laser relative to the motion of the ion beam, and $\Delta\nu$ is the measured Doppler shift.

Similarly, the temperatures of expanded species were calculated from the Doppler broadened line widths by

$$T = \frac{\Delta v_D}{2} \frac{m}{2(\ln 2)k} \tag{5-2}$$

where Δv_D is line width, m is the atomic mass, and k is Boltzmann's constant. In this research, the measurement does not determine the axial or radial temperature separately. The calculated temperature is a mixture of the axial and radial values.

5.2. Experimental

5.2.1.　Probe species and fluorescence

During this experiment, the fluorescence of two probe species, calcium ions and argon metastable atoms, was recorded under the same experimental operating conditions. Argon metastable atoms in the 4s [3/2] J = 2 state have been verified as a successful probe species in our lab.[8] Fig 5.1 shows the partial Grotrian diagrams of Ar (I) and Ca (II) used in this experiment.
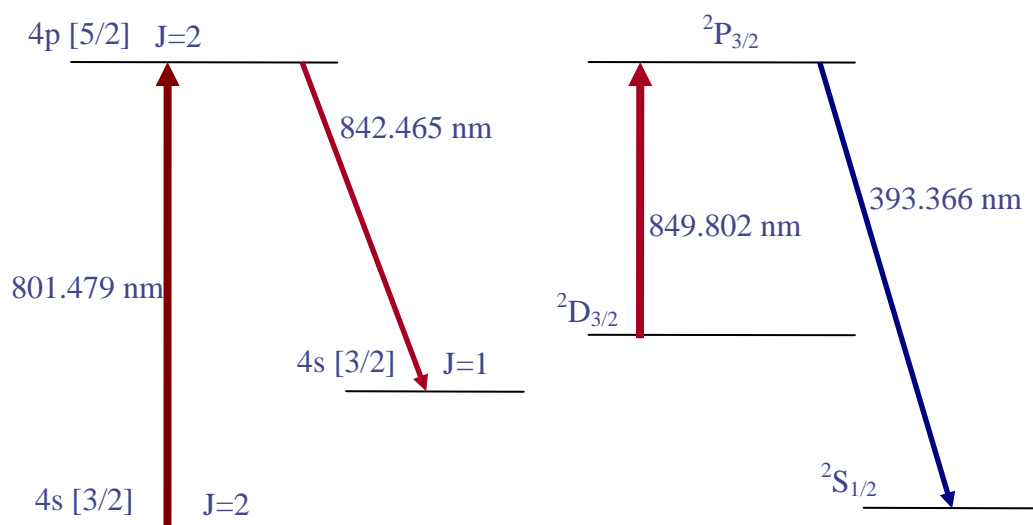
Fig 5.1 Partial Grotrian diagram for Ar I (left) and Ca II (right)

In this research, as in the previous research, it is assumed that the results obtained from the detected argon metastable atoms and calcium ions are representative for all neutral argon atoms and charged calcium ions, respectively.

5.2.2.   Instrumentation

Earlier papers from our lab provide detailed descriptions of the instrumentation and procedures.[5,7] The plasma generator, the load coil, torch and vacuum chamber were the same as described in chapter 2.

Fig 5.2 Instrument schematic

Briefly, as showed in Fig 5.2, the ICP torch and impedance matcher were mounted on a precisely-controlled X-Y-Z stage, so the plasma torch could be aligned

precisely with the sampling cone. Also, the excitation and collection systems were positioned on a motor-controlled X-Y-Z stage, where the z-axis was parallel to the axis defined by the torch and the sampling orifice.

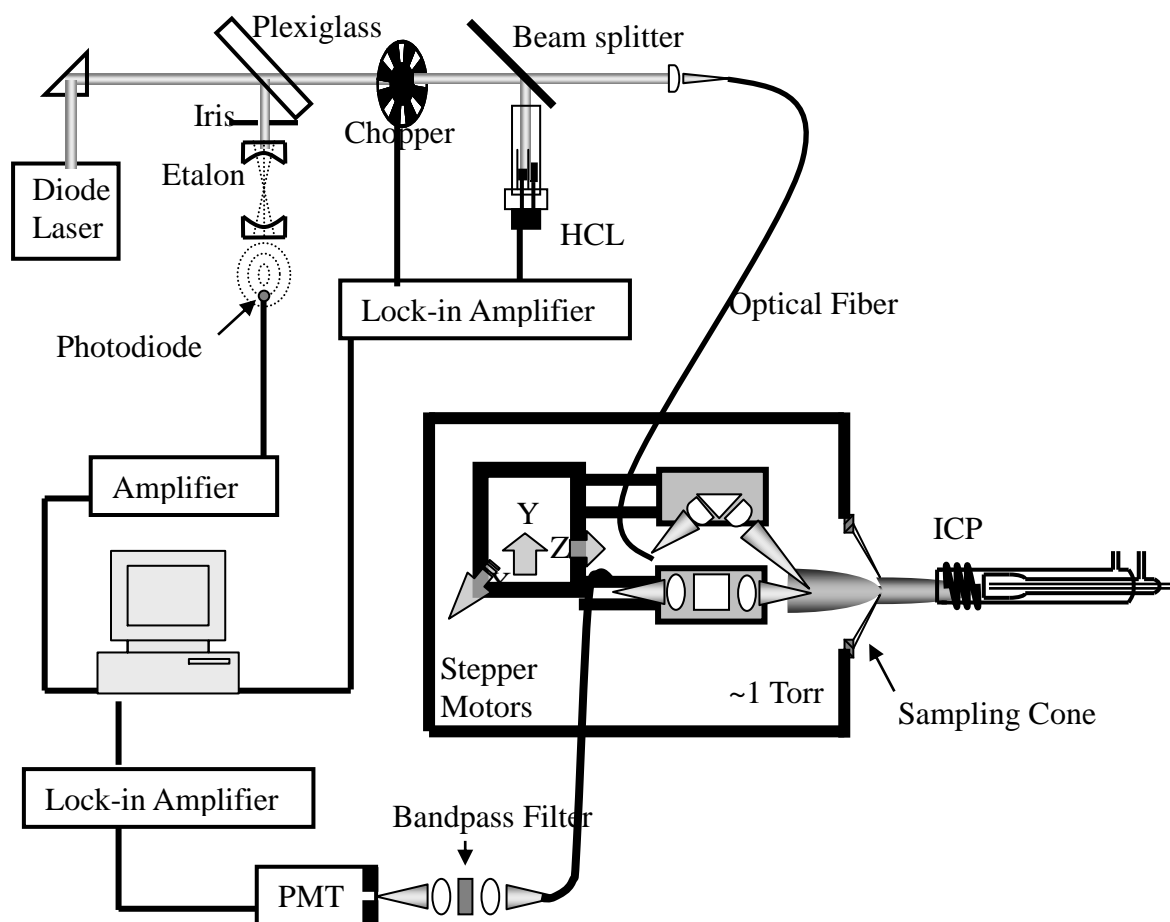The high-resolution excitation laser used for the argon metastable atoms measurement during this experiment was an external-cavity diode laser (2010, EOSI, Boulder, CO), which was connected with a 10-milli-Hz-frequency scanning function generator (HP 33120A, Hewlett Packard, Palo Alto, CA). A plexiglass sheet was used to split a small fraction of the laser beam into a confocal etalon with a nominal free spectral range of 750 MHz. The actual free spectral range was calibrated against the Doppler-free absorption spectrum measured in Rb vapor cell (Rbs2010, EOSI, Boulder, CO). The DC signal from an interferometer photodiode was magnified by a low-noise preamp (SR560, Stanford Research Systems, Sunnyvale, CA) and used as a frequency marker for velocity and temperature calculation.

Then, the laser was chopped (Optical chopper, Scitec instruments, Cornwall England) and a portion was split into an argon-filled hollow cathode lamp (Fe Cathode, Argon gas, WL-22661, Imaging and Sensing Technology, Horseheads, NY; APH 500M, Kepco Power Supply, Flushing, NY). The chopper was also connected with two lock-in amplifiers (SR830 DSP, Stanford Research Systems, Sunnyvale, CA) as the reference for the modulation. Finally, the remaining laser beam was delivered to the vacuum chamber via a 0.4 mm diameter fused silica fiber optic.

When the calcium measurement was carried out, the excitation laser was another tunable diode laser (6000 Vortex Series, New Focus, San Jose, CA). A calcium-filled hollow cathode lamp (P809, Calcium, Photron, Australia) was used to generate the stationary fluorescence signal for calcium ions. The calcium fluorescence was

detected by a photomultiplier tube (R928 Hamamatsu, Bridgewater, NJ) with a monochromator (Instruments SA, Inc., Santa Cruz, CA) which was tuned to 393.4 nm. The calcium fluorescence and argon optogalvanic signals were processed by the two lock-in amplifiers.

Theoretically, to compare the velocity and temperature difference between argon atoms and calcium ions, these two species should be measured at the same time. However, due to limitations in the experimental setup, simultaneous characterization of argon metastable atom and calcium ions was impractical. However, the poor long-term stability of the inductively coupled plasma makes a swift shifting between the measurements of calcium ions and argon metastable atoms of importance. If the switch between calcium and argon measurement is too slow, difference between the two becomes indistinguishable from drift. Therefore, for each experimental run, the switch between calcium and argon measurements was rapid. Variations caused by plasma drift were negligible.

Inside the vacuum chamber, the excitation and collection optics were aligned and collimated precisely, as described in references.[5,8] The geometry of the optics was critical. Both probes were angled at 45° relative to the z-axis.

The laser-excited fluorescence of argon and calcium were both coupled by a 0.4 mm fused silica optical fiber and delivered into a photomultiplier tube, which was connected to a lock-in amplifier. Two interference filters were used to block the emission and laser scattering from the plasma. A 1-nm bandpass filter (642.5 nm, Andover Corp., Salem, NH) was used to isolate the argon fluorescence. For the calcium fluorescence measurement, the filter was replaced by another 1 nm bandpass filter (393.46 nm, Barr Associates, Westford, MA). When the probe was close to the

orifice of the sampling cone, some extra neutral density filters were needed to prevent the signal from overloading the lock-in amplifier.

5.2.3.   Operating conditions

The operating conditions of the plasma, which are listed in table 1, chapter 2, were chosen to run the whole experiments. The analyte solution was 25 ppm calcium, which was made from calcium carbonate powder (AR grade, Mallinckrodt Inc., Paris, KY). A pneumatic concentric nebulizer system was adopted to aspirate the solutions into the plasma. The water loading of this pneumatic system, which was about 29 mg/min, was determined by measuring the mass of tiny water droplets frozen in a cold ($-78^{\circ}C$) glass trap filled with steel wool.

5.2.4.   Data acquisition and processing

The outputs of the three amplifiers, plus the modulating triangle wave from the function generator, were digitized with a multifunction card (PCI-6110, National Instruments, Austin, TX) and processed by the Virtual Bench software (National Instrument, Austin, TX).

Five complete triangle waveform cycles were scanned for each position of the optical stage, including five on the ascending parts of the waveform and five on the descending parts, resulting in a set of ten values for each data point. The fringe spacing was calibrated to 751.3 MHz by the Rb spectrum calibration.[9] Fig 5.3 shows a representative data set for the calcium signals from three amplifiers. An Excel form and Mathcad program have been designed to fit the signals to a Gaussian distribution, which was used to compute exact temperature and velocity values.
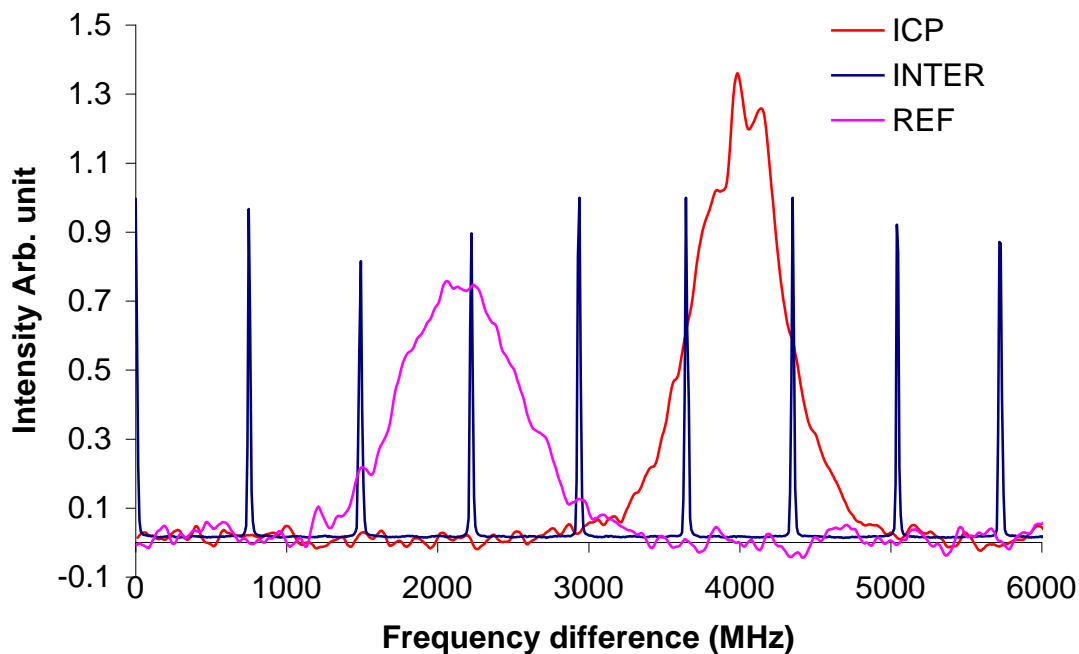
Fig 5.3 Representative signals

5.2.5. Nebulizer flow determination

Changes in nebulizer flow have opposite effects on the signal intensities of argon metastable atoms and calcium ions behind the sampling cone.[10] It is crucial to select an appropriate nebulizer flow. The lower the nebulizer flow, the higher is the argon metastable atom signal. However, when the nebulizer flow decreases, the calcium ionic fluorescence drops dramatically. It was therefore necessary to select a compromise nebulizer flow rate that gave adequate signals for both probe species.

The dependency of signal-to-noise for argon and calcium is displayed in Fig. 5.4. Because high signal-to-noise ratios were necessary for precise velocity and temperature determinations, only a narrow range of nebulizer flow was usable. In this experiment, one nebulizer flow, 1.24 L/min, was used for all measurements.
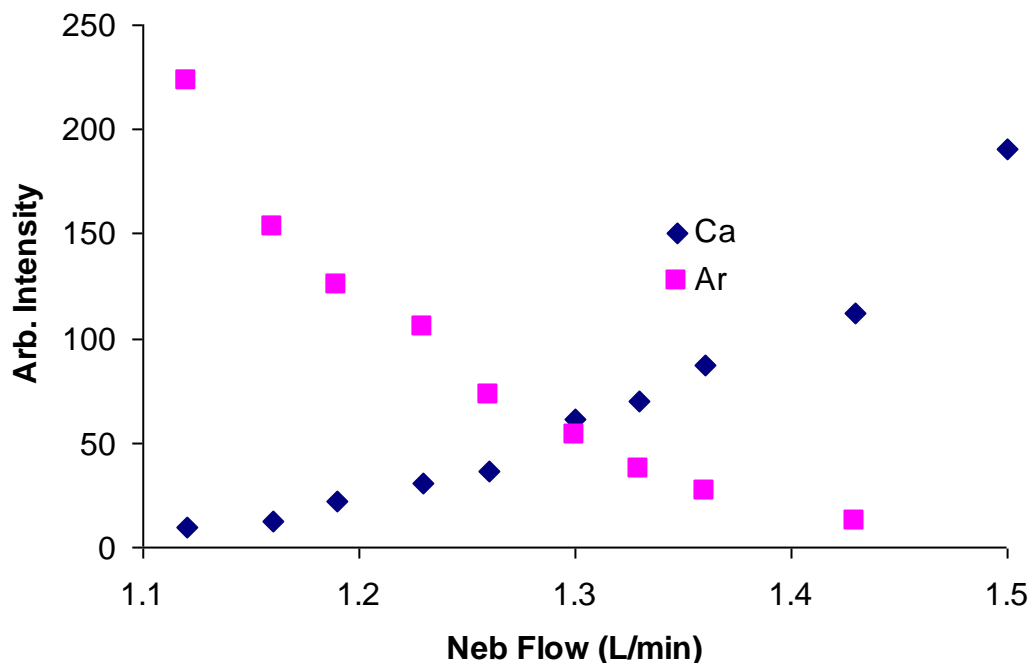
Fig 5.4 Dependency of signal-to-noise for argon atoms and calcium ion

5.3. Results and discussion

During this experiment, the long-term uncertainties of temperature and velocity were calculated and recorded as the error bars. The long term uncertainties are the standard deviations of the triplicate measurements.

It has been calculated [5] that, under our experimental conditions, the distance between the sampling cone and Mach disk is about 17 mm. The focal lengths of the two lenses that were used to deliver the excitation laser and collect the fluorescence signal were ~50 mm. Considering the angle of 45° between the axial direction and focusing lenses, the optical stage had a ~35 mm distance from the sampling orifice and was not in the direct path of the beam. It did not perturb the Mach disk and isentropic expansion in front of it.

5.3.1. Alignment of plasma torch with sampling cone

In our lab, Macedone et al. showed that when the plasma was off-axis with respect to the sampling orifice, the spatial distribution and number intensity of analyte behind the sampling cone changed dramatically.[11] To get high transmission efficiency from the plasma to the skimmer cone, the alignment of the plasma to the sampling cone is crucial.
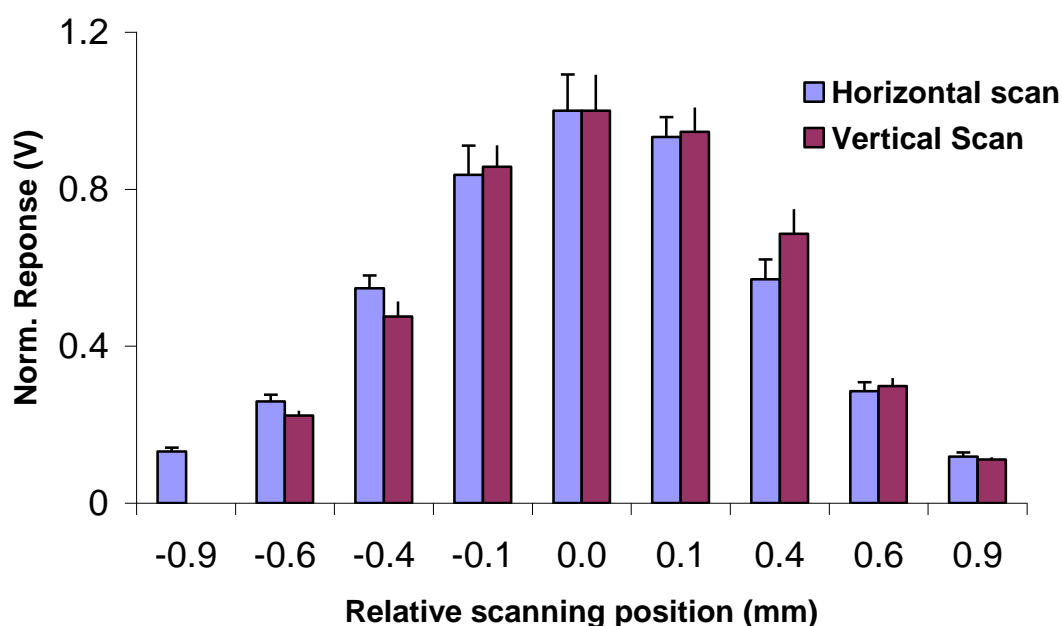
Fig 5.5 Intensity response with the horizontal and vertical scanning of the plasma torch

To align the torch with the sampling cone precisely, the fluorescence intensity variation of calcium ions 10 mm behind the sampling cone was monitored while the plasma torch was scanned in vertical and horizontal directions in small steps. When the plasma torch was scanned along the vertical or horizontal direction, the fluorescence of calcium ions varied dramatically, as shown in Fig 5.5. The cross-point of maximum fluorescence response on the vertical and horizontal axes was defined as

the origin, where the plasma torch and the sampling cone have a good alignment.

Initial efforts in our lab to compare argon and calcium behavior in the supersonic expansion suffered from irreproducibility due to problems with torch alignment.[12] By changing the positions of the plasma torch relative to the sampling cone, we demonstrated the effects of torch misalignment.
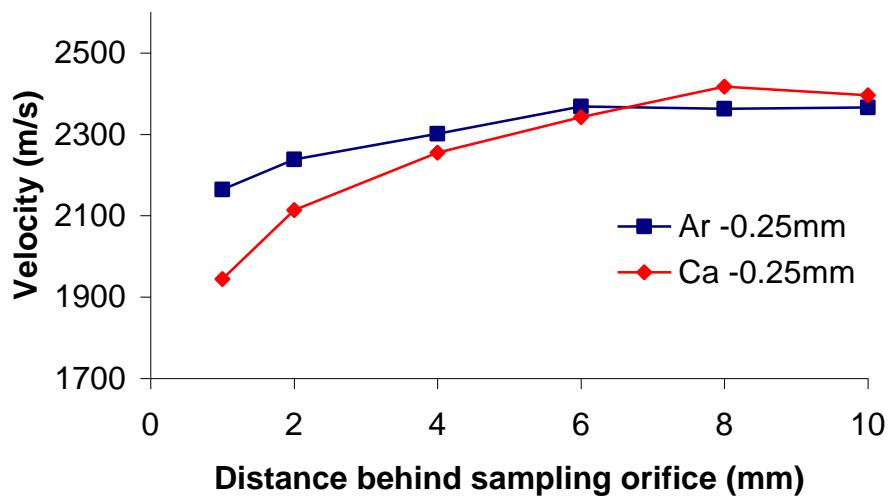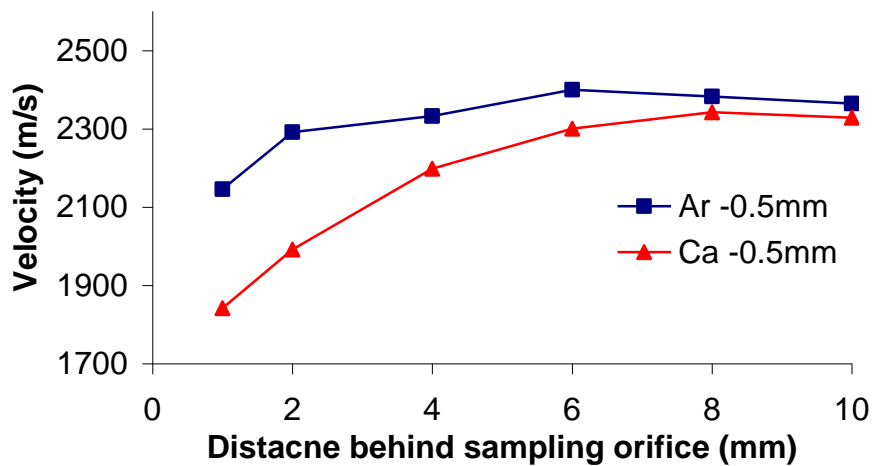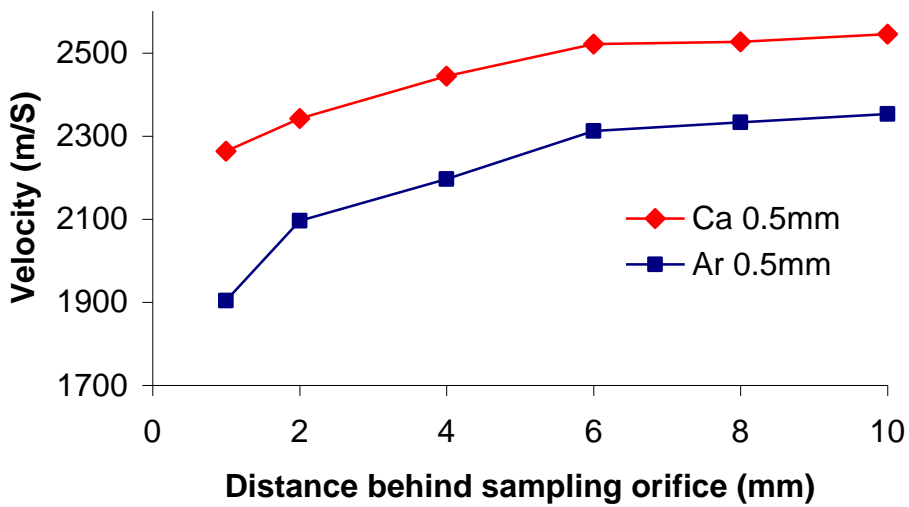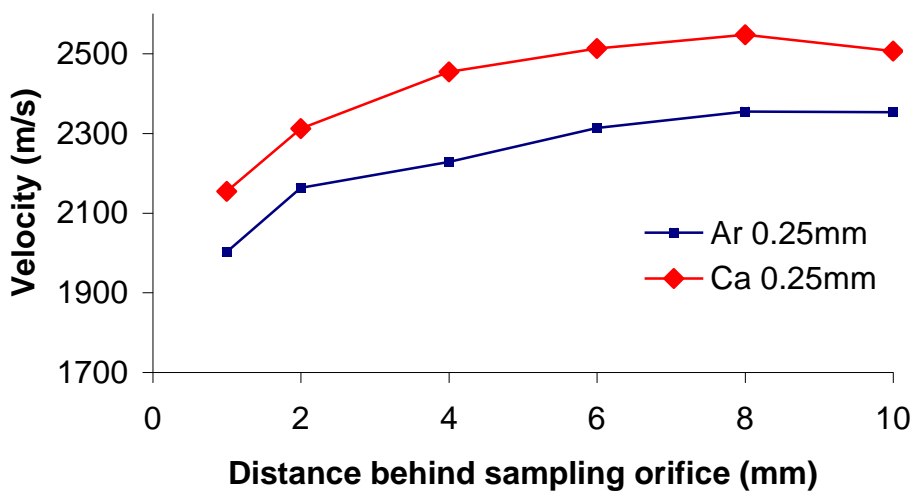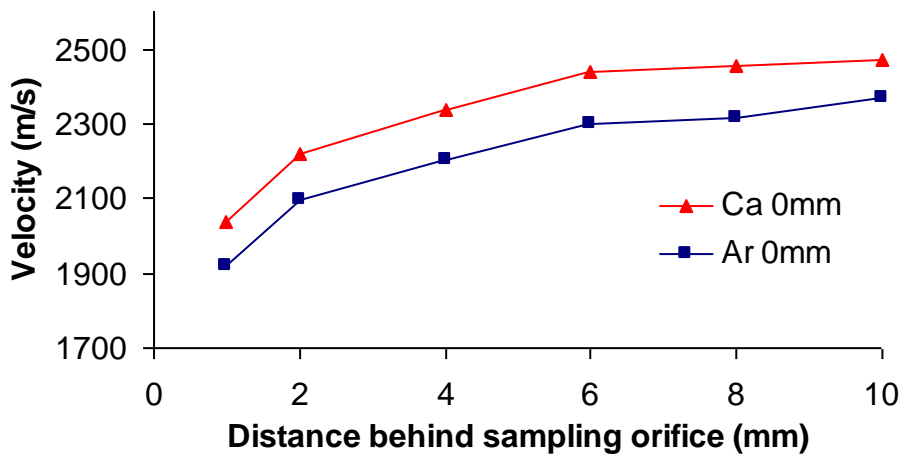
Fig 5.6 Velocity variation of argon atom and calcium ion behind the sampling cone

with off-horizontal-axis scanning (-0.5 mm to 0.5 mm) of the plasma

As shown in Fig 5.6, the velocities of argon atoms and calcium ions downstream from the sampling cone under different horizontal positions of the plasma torch varied dramatically. For the final data, reported in the following sections, the torch and the sampling cone were aligned by the procedure depicted graphically in Fig 5.5.

5.3.2. Temperature measurements

Using equation (5-2) and recorded signals, the temperature of argon atoms and calcium ions were calculated. Fig 5.7 shows the calculated temperature results of the two species at different axial positions downstream from the sampling cone. Apparently, as showed in Fig 5.7, there was no significant difference between the two species at most measured points.
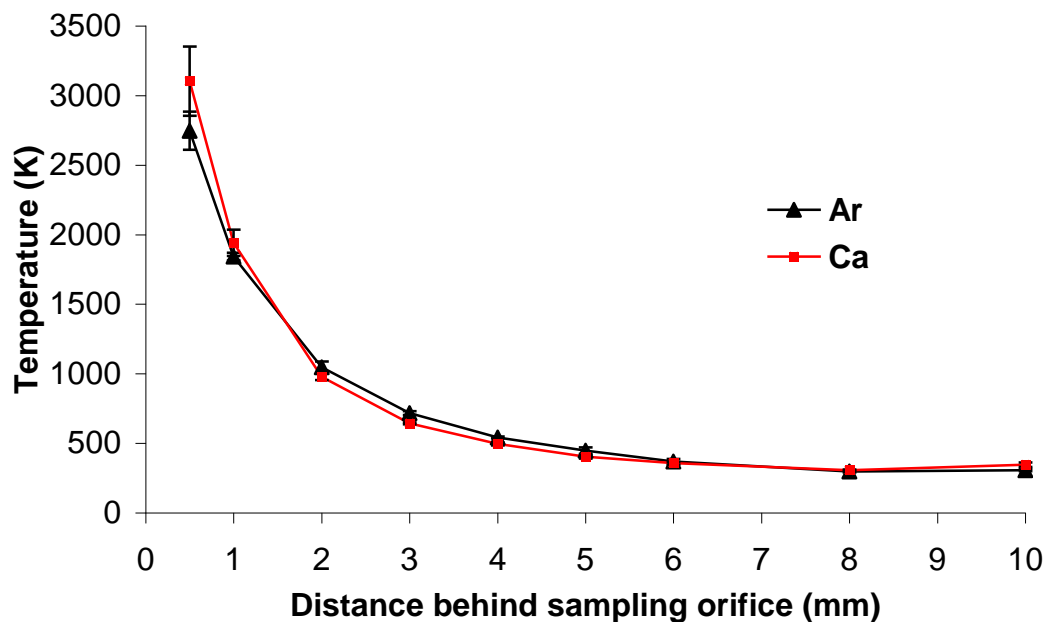
Fig 5.7 Temperature comparison of argon atoms and calcium ions behind the sampling cone

5.3.3. Velocity comparison between argon atom and calcium ion

The velocities of argon atom and calcium ions were calculated by equation (5-1). As shown in Fig. 5.8, both atomic and ionic species were accelerated in the supersonic expansion. Furthermore, the terminal velocities between argon and calcium are significantly different, although the velocities near the orifice of the sampling cone are indistinguishable. The different accelerations can be explained by the ambipolar diffusion of two species, the charged calcium ions and neutral argon atoms.
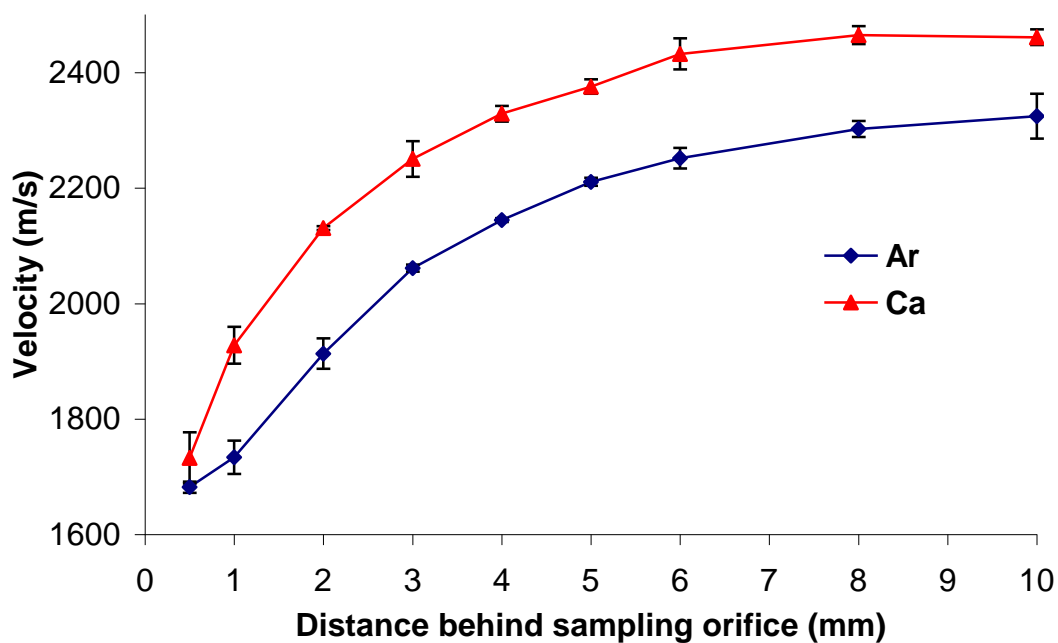
Fig 5.8 Velocity comparison of argon atoms and calcium ions behind the sampling cone

In ambipolar diffusion, the ionic particle is not only accelerated by the supersonic expansion, but also by the electric field generated by the separated positive ions and negative electrons. Behind the sampling cone, the gases are partially ionized. Due to the low mass and high temperature of electrons, which move faster and leave some

positive ions in the initial volume, an outwardly-directed electric field is created and positive ionic particles are accelerated. Therefore, compared with neutral atomic argon particles, calcium ions can get more energy and move faster.

5.4. Summary and Conclusions

The temperatures and velocities of argon metastable atoms and calcium ions in the supersonic expansion were measured by high-resolution fluorescence excitation spectroscopy. The work provided a good supplement of previous characterization of supersonic expansion in the first vacuum stage of an ICP-MS.

Furthermore, the velocity difference between calcium ions and argon atoms is indicative of ambipolar diffusion in this region and provide the experimental data for the simulation model being developed.

5.5. References

[1] Houk, R. S., Zhai Y., *Spectrochimica Acta Part B*, 56, **2001**, 1055

[2] Douglas D. J. French, J. B., *J. Anal. At. Spectrom.*, 3, **1988**, 743

[3] Chambers D. M., Poehlman J., Yang P., Hieftje G. M., *Spectrochim. Acta Part B,* 46, **1991**, 741

[4] Macedone, J. H., Farnsworth, P. B., *Spectrochimica Acta Part B*, 61, **2006**, 1031

[5] Radicic, W. N., Olsen J. B., Neilson R. V., Macedone J. H., Farnsworth P. B., *Spectrochimica. Acta Part B*, 61, **2006**, 686

[6] Scoles, G., Bassi, D., Buck U., Laine D. C., *Atomic and Molecular Beam Methods*, V1, Oxford University Press, **1988**

[7] Olsen, J. B., Macedone J. H., Farnsworth P. B., *J. Anal. At. Spectrom.* 21, **2006**, 856

[8] Patterson J. E., Duersch B. S., Farnsworth P. B., *Spectrochim. Acta Part B,* 54, **1999**, 537

[9] Barwood G. P., Gill P., Rowley W. R. C., *Applied Physics B*, 53, **1991**, 142

[10] Montaser, A. Golightly, D. W., *Inductively Coupled Plasmas in Analytical Atomic Spectrometry*, 2nd, VCH Publisher, Inc. **1992**

[11] Macedone J. H., Mills A. A., Farnsworth P. B., *Appl. Spectrosc.*, 58, **2004**, 463

[12] Radicic, W. N., *Velocity and Temperature Characterization of the First Vacuum Stage Expansion in an Inductively Coupled Plasma - Mass Spectrometer*, **Thesis,** Brigham Young University, **2004**

6. STUDIES OF ION TRANSMISSION EFFICIENCY THROUGH THE SKIMMER CONE OF AN ICP-MS

6.1. Introduction

A typical ICP-MS interface consists of a sampling cone, a skimmer cone and ion focusing lenses.[1,2] The sensitivity and detection limit of an ICP-MS are largely dependent on how many analyte ions are delivered from the plasma to the mass detector through the interfacial region.[3,4] In the first two vacuum stages, the atmospheric-pressure plasma is expanded into a region where the pressure is about 10^{-3} Torr.[5] Due to the large drop in the pressure, only a small portion of analytes can be extracted through the sampling and skimmer cones. The transmission efficiency of the interface between the ICP and MS is poor, typically less than 0.1%, leaving considerable room for the modification and improvement of interface design and arrangements. If matrix components are introduced into the sample solution, the performance of an ICP-MS will be further deteriorated.[6,7]

Although many experimental and computational studies[8,9,10,11] have been carried out on transmission efficiencies of the sampling cone or the whole interface between the ICP and MS, a number of critical issues remain unsolved and prevent us from understanding the ion extraction process completely. Better understanding of the skimming processes, including properties of the shock wave just at the tip of the skimmer and space charge effects behind the skimmer, are critical to improve the design of the interface used between the ICP and the MS.[12]

The existence of the shock wave increases collisions among particles, deviating the skimming process from ideal.[13,14,15] The optimal position of the skimmer cone is partly determined by the location of the Mach disk and can't be predicted by gas

dynamic theory alone. Shock wave formation is a concern no matter where we place the skimmer cone, either inside or outside the zone of silence in the supersonic expansion behind the sampling orifice.[16,17]

Our research group has developed interface designs that allow us to optically measure the ion number densities upstream from the sampling cone, in the first vacuum stage without skimmer cone, and behind the skimmer cone. The size of the zone of silence, the formation of the Mach disk, and the trajectories of atoms in the zone of silence have been investigated in our lab.[18] Unfortunately, due to the limited space between the skimmer and sampling cones, we could not measure densities in the first vacuum stage with the skimmer cone in place. Therefore, the transmission efficiency of the skimmer cone could not be investigated directly.

This section describes the design of a new interface that allows for simultaneous density measurements of analyte upstream and downstream from the skimmer cone under a range of operating conditions. Incident power, nebulizer flow, the pressure of first vacuum stage, and matrix compositions were varied in this research. In addition, by probing and characterizing different species, such as barium metastable ions or argon metastable atoms, we plan to provide a comprehensive image of the shock structure and its location relative to the skimmer tip.

6.2. Experimental

6.2.1. Interface design

A newly-developed home-made interface, shown in Fig 6.1, was used to perform simultaneous measurements of analyte ion number densities upstream and downstream from the skimmer cone.
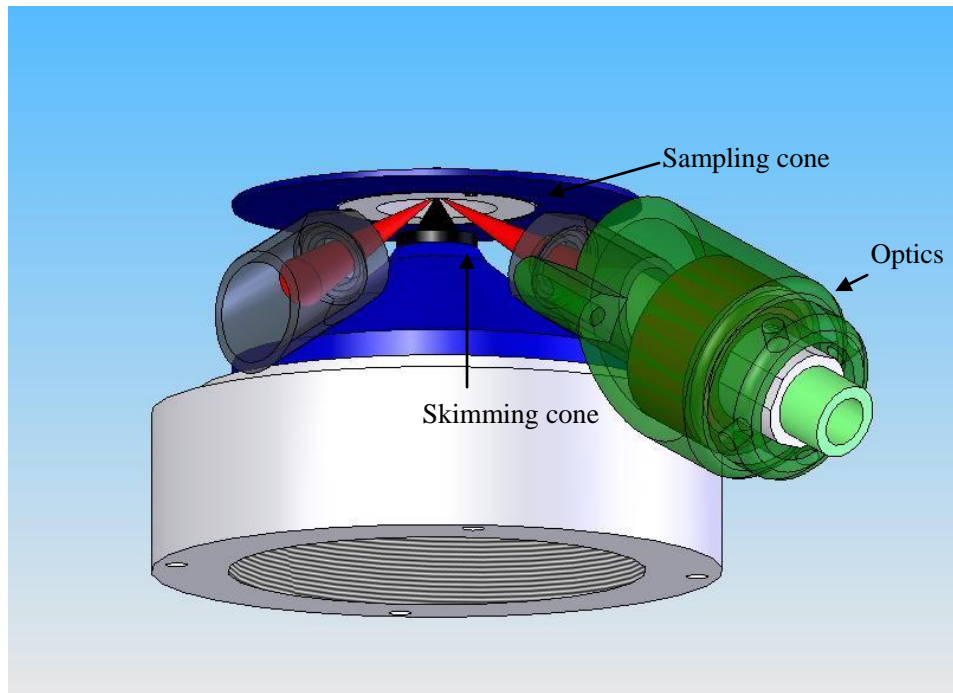
Fig 6.1 Image of the newly-developed interface and optics

The optics in Fig 6.1 can move in three dimensions independent of the skimmer cone. Therefore, the excitation and collection lasers can be focused and overlapped in a large region in front of the skimmer tip. The distance between the sampling and skimming cones is adjustable. This allows us to locate the skimmer tip at any position related to the Mach disc. The fiber and lens used will be described in the following sections.

6.2.2.   Experimental setup

With the exception of the newly designed interface, which mounts the sampler and skimmer, the remainder of the instrumentation used has been described in previous sections and some published papers.[7, 17] The load coil, torch, and sampling cone are identical with those defined in section 2.2.1. New experimental components will be described in detail in the following sections.

The diameter of the skimmer orifice (VG1002-Ni, Spectron, Ventura, CA) is 0.7 mm. The first vacuum stage was pumped by two mechanical pumps. Vacuum in the second vacuum stage was maintained by a turbomolecular pump (TPH330, Pfeiffer Vacuum, Asslar, Germany), which was cooled by circulating cooled water, and backed by a rotary vacuum pump (E2M-18, Edwards High vacuum international, West Sussex, England). The second stage vacuums were monitored by a Penning gauge head (CP25K, Edwards High vacuum international, West Sussex, England) and appropriate vacuum measurement instruments (Series 500, Edwards High vacuum international, West Sussex, England). The backing vacuum, about 0.1 Torr, was monitored by a thermocouple vacuum gauge (Type 0531, Varian Inc., Palo Alto, CA) combined with a readout device (415/969-8811, Duniway Stockroom Corp., MT. View, CA). The optical components used upstream and downstream from the skimmer cone, such as the optical fiber, the collimating and focusing lenses of the excitation and collection optics, the PMTs, were identical, to minimize signal differences in two collection systems.

A dye laser system (Lambda Physik, Ft. Lauderdale, FL) was pumped by a XeCl Excimer laser (LPX 200, Lambda Physik, Ft. Lauderdale, FL). The dye laser, tuned to 455.4 nm, was split by an appropriate 50:50 beam splitter (BS1-455-50-1025-45S, CVI, Albuquerque, NM) into two laser beams. As shown in Fig 6.2, after that, the lasers were focused and transmitted by a 0.4 mm diameter fiber (ASB400/ 440UVPIT, Fibertech Optica, Inc., Kitchener, ON, Canada) and used to excite barium ions upstream and downstream from the skimmer cone.

The excitation lasers were collimated by 25 mm focusing-length lenses (AC127-025-A1, Thorlabs Inc., Newton, NJ) and then focused by 63.5 mm focal-length lenses

(PAC031 Achromatic lens, MgF$_2$ coat 400-700 nm, Newport, Irvine, CA). To

eliminate scattering interferences behind the skimmer cone due to the reflection of

Raman scattering generated in the fiber, a bandpass filter (F10-457.9-4, CVI,

Albuquerque, NM) was inserted between the collimation and focusing lenses of the

downstream excitation probe.
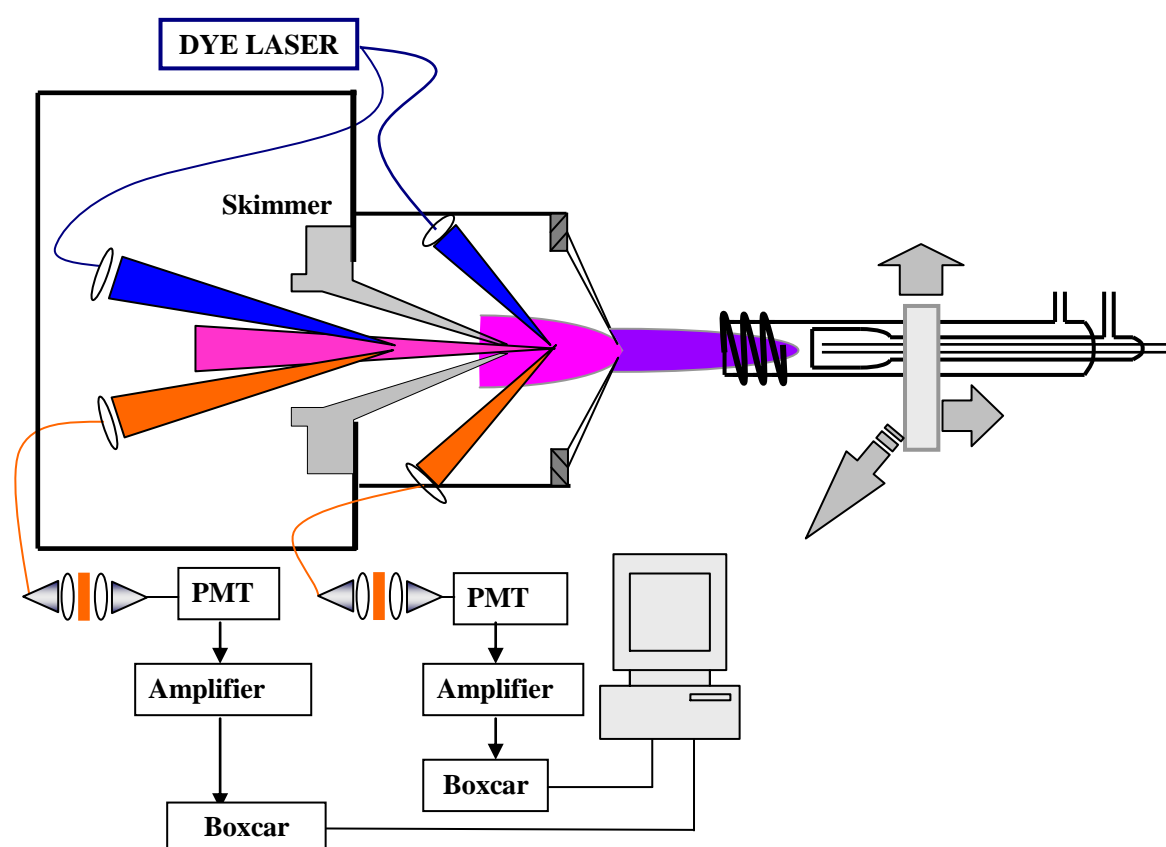
Fig 6.2 Experimental schematic

The optical parts used in the collection systems were identical to those used in the

excitation systems. The fluorescence signals both upstream and downstream from the

skimmer cone were isolated by appropriate longpass filters (600 nm) and bandpass

(614.2/1-25.4-Barr, Barr Associates, Westford, MA) filters successively before they

reached the photomultiplier tubes (R928 Hamamatsu, Bridgewater, NJ). The signals

were then amplified by fast amplifiers (model 310, Sonoma Instruments, Santa Rosa,

CA) and processed by gated boxcar integrators (SR 250, Stanford Research system, Sunnyvale, CA). The boxcars were trigged by a photodiode located in the dye laser cabinet. The signals finally were converted by an A/D converter (PCI-6110, National Instruments, Austin, TX) and recorded on a personal computer.

The downstream laser optics were mounted on a rigid aluminum frame, which was precisely driven by a three dimensional computer-controlled stage. The upstream probe volume was adjusted manually by changing the angle at which the excitation and collection optical axes intersected the center axis of the interface.

6.2.3.   Laser alignment

The lasers upstream and downstream from the skimmer cone were both aligned with a CCD chip extracted from an inexpensive commercial webcam (Quickcam, Communicate Deluxe S7500, Logitech, Fremont, CA). The excitation and collection fibers were backlit with appropriate LEDs, with wavelengths that were close to the excitation or emission wavelengths, respectively. The positions of the downstream focusing lenses were adjusted to give a clear, 1 mm-diameter and overlapped image on the CCD, as shown in Fig 6.3.

Fig 6.3 Laser alignment behind the skimmer cone

The positioning of the upstream optics was more difficult. To precisely define an axial position for the upstream optics, we advanced the downstream optics to -2.5 mm, which meant that the downstream lasers were focused and overlapped 2.5 mm upstream from the skimmer tip. Then the CCD chip was positioned to focus the overlapped image. Finally, the upstream lasers were focused and overlapped on the chip, as shown in Fig 6.4.

Fig 6.4 Laser alignment in front of the skimmer cone

6.2.4. Signal calibration for collection optics

The spatial resolution of the downstream lasers has been characterized precisely in our lab.[19] The results showed that the spatial resolution of the laser probes along the z-axis is about 3.5 mm. To prevent the detection volume from being blocked by the back side of the skimmer cone, we focused the downstream optics 2.5 mm behind the skimmer orifice.

The volume probed was defined by the cross-section of the excitation and collection optics. As shown in Fig. 6.2, the angles of the downstream and upstream lasers relative to the ion beam axis (z-axis) are about 15 and 60 degrees, respectively. Therefore, we should not expect that the volumes these two optical systems collect are the same.

To calibrate the two collection systems with respect to each other, we removed the skimmer cone and advanced the downstream optics to -2.5 mm, which overlapped them with upstream optics, as shown in Fig 6.5. Then, signals from the two systems were collected and a calibration factor was calculated. In using this calibration factor, we have assumed that the averaged ion densities in the collection volumes are the same.
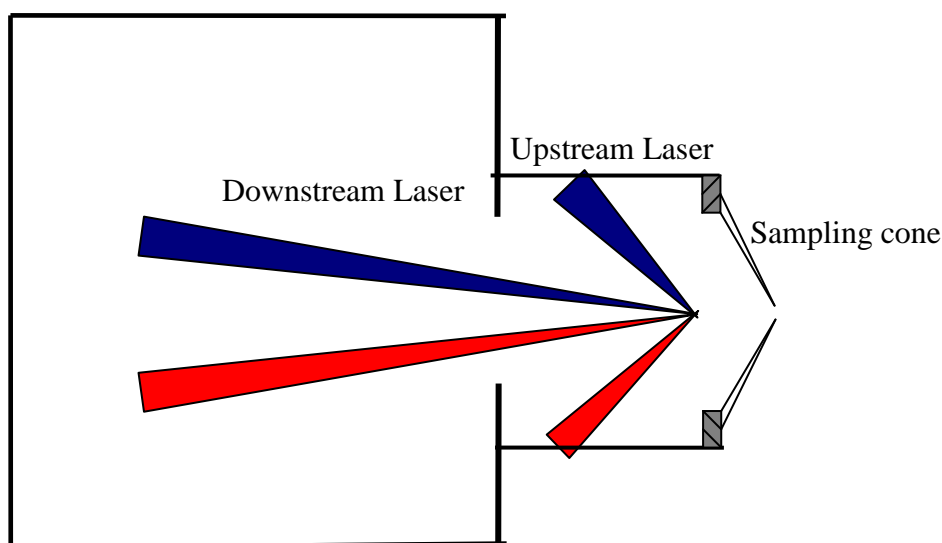
Fig 6.5 Schematic overlap of two lasers

6.2.5.   Analyte and matrix solutions

50 ppm barium was used as analyte in this study. For matrix interference studies, analyte solutions were prepared with 50 ppm barium and 4.8 mM of either lithium or lead, corresponding to 33.5 ppm lithium and 1000 ppm lead. The barium solution was prepared from solid reagent-grade barium chloride (Fisher Scientific, Hampton, NH). 33.5 ppm lithium solutions were prepared from lithium nitrate (solid reagent-grade lithium nitrate, Mallinckrodt, Paris KY). Similarly, 1000 ppm lead was prepared from lead nitrate (Crystal reagent-grade lead nitrate, Chemical MFG. Corp., Redondo

Beach, CA). All the solutions were made with 18 MΩ water (Milli-Q RG, Millipore, Bedford, MA) and aspirated by a concentric pneumatic nebulizer (5601, RF Power Products, Vorhees, NJ) combined with a Scott-type double pass spray chamber.

6.2.6. ICP-MS operating conditions

If not otherwise specified, the operating conditions for the ICP and vacuum interface are listed in Table 6.1. Nebulizer flows were adjusted from 0.82 L/min to 1.50 L/min, and ICP power was changed from 1050 Watts to 1350 Watts.

Table 6.1 ICP/MS operational parameters

ICP power	1.25 kW
Reflected power	< 5 W
Plasma gas flow	12 L/min
Auxiliary gas flow	0.4 L/min
Sampling depth	10 mm
Sampler-skimmer separation	9 mm
First vacuum stage pressure	1.33 Torr
Second vacuum stage pressure	< 3E-4 Torr

The variation of nebulizer flow or incident power can slightly change the pressure of the first vacuum stage. To eliminate any influence of the first vacuum stage pressure on the transmission efficiency of the skimmer cone, which was shown to be a significant factor in a preliminary study, an argon gas inlet was connected with the first stage pump outlet, to adjust the pressure in the first vacuum stage. In these experiments, the pressure of the first vacuum stage was constant at 1.33 Torr as the incident power, nebulizer flow, and matrix compositions were varied.

6.2.7.   Signal collection and data processing

The dye laser was tuned to the appropriate excitation wavelength for barium ground state ions. The energy of the laser was adjusted to saturate the transition. The output from 2000 shots of the dye laser was collected and averaged to produce a single data point. Immediately after that gross signal was recorded, the dye laser was detuned to 450 nm with other experimental parameters unchanged, to produce a background emission. The signals used in the transmission efficiency calculations were net signals, with the emission background subtracted.

6.3. Results and discussions

In this section I report preliminary measurements of the transmission efficiency of barium ground-state ions. Four experimental parameters: incident power, nebulizer flow, matrix composition and first vacuum stage pressure, were varied to demonstrate their influence on the transmission efficiency of the skimmer cone. The error bars show the high and low values obtained.

6.3.1.   Ideal skimming

On the basis of classic gas dynamic theory,[8] if the skimming process is ideal, the number densities at a specific point (x) behind the sampling cone can be calculated by

$$\frac{n_x}{n_0} = 0.161(\frac{x}{D})^{-2} \tag{6-1}$$

where n_x is the number density at x behind the sampling cone, n_0 is the number density at the orifice of the sampling cone, and D is the diameter of the sampling orifice. In this experiment, we positioned lasers 2.5 mm upstream and 2.5 mm

downstream from the skimmer cone. Since the separation between the skimmer and sampler was 9 mm, the distances from the sampling cone of the upstream and downstream optics were 6.5 mm and 11.5 mm, respectively. Using equation 6-1, we can compute the density ratio between these two points:

$$\frac{n_{downstream}}{n_{upstream}} = \frac{6.5^2}{11.5^2} = 31.9\% \qquad (6\text{-}2)$$

Therefore, ideal skimming should produce a ratio between the downstream and upstream signals of around one third.

6.3.2.   Effect of incident power

In previous chapters, it was found that the incident power and nebulizer flow both significantly influence the characteristics of the plasma and transmission efficiency of the sampling cone. By compared with the analyte fluorescence intensities upstream and downstream from the skimmer cone, Fig. 6.6 shows how the incident power affects the transmission efficiencies of the skimmer cone under specific nebulizer flow, 1.16 L/min. The transmission efficiency is defined by the ratio between upstream and downstream signal intensities, corrected for the differences in optical efficiency between the two probes.

.As we can see, variation of the incident power did not change the transmission efficiency of the skimmer cone dramatically, although these values are much less than those predicted for ideal skimming. The real transmission efficiency is only about one ninth that calculated for ideal skimming.
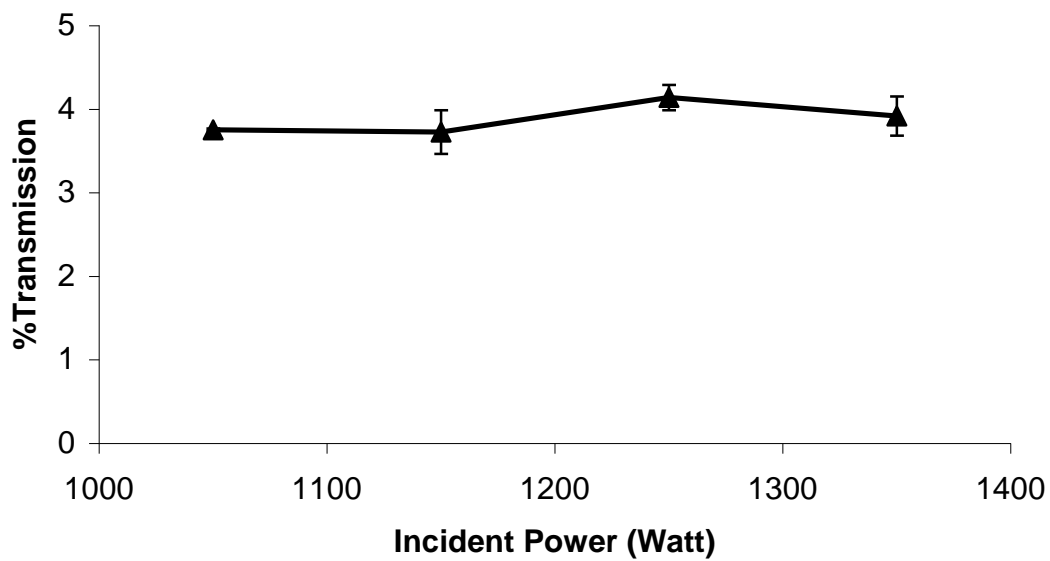
Fig 6.6 Transmission efficiencies of the skimmer cone with different incident power

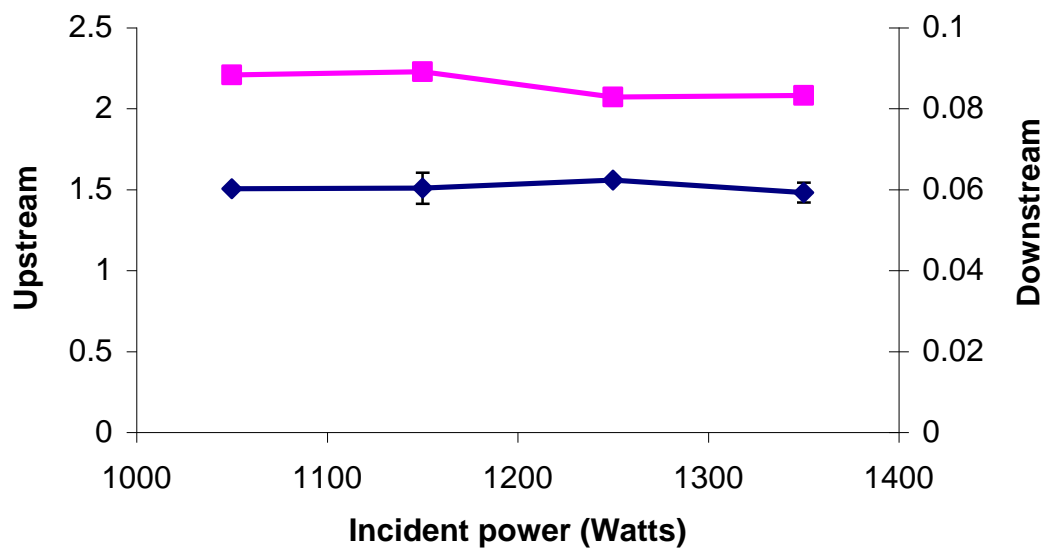Fig 6.7 Signal arbitrary intensities upstream and downstream from the skimmer cone

under different incident power; (——) upstream, (——) downstream

Fig 6.7 displays the signal intensities in front of and behind the skimmer cone. Neither signal changed very much with variation of the incident power. Therefore, the transmission efficiency of the skimmer cone is not changed significantly with the variation of the incident power.

6.3.3. Influence of nebulizer flow

Nebulizer flow is another variable that influences the transmission efficiency of the skimmer cone we tested in this research. The nebulizer flow was changed from 0.85 L/min to 1.50 L/min with fixed incident power of 1250 Watts.

Fig 6.8 shows the variation of transmission efficiency of the skimmer cone under different nebulizer flows. When the nebulizer flows increased from 0.85 L/min to 1.43 L/min, transmission efficiency of the skimmer cone dropped. However, when the nebulizer flow was high, such as 1.50 L/min, the transmission efficiency of the skimmer cone rebounded.
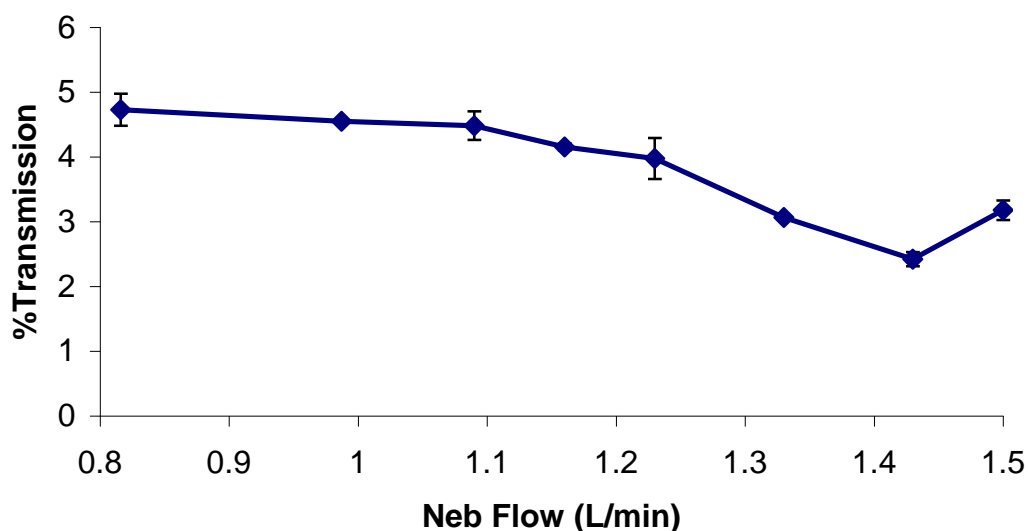
Fig 6.8 Transmission efficiencies of the skimmer cone with different nebulizer flows

A comparison of the upstream and downstream signals gives some insight into the cause of the changes shown in Fig. 6.8. As shown in Fig 6.9, the initial increases in nebulizer flow caused the fluorescence signals in front of and behind the skimmer cone to increase simultaneously. This is consistent with the results observed without the installation of the skimmer cone in our lab.[20] However, the downstream signal

peaked earlier than the upstream, leading to the changes in transmission efficiency shown in Fig. 6.8.
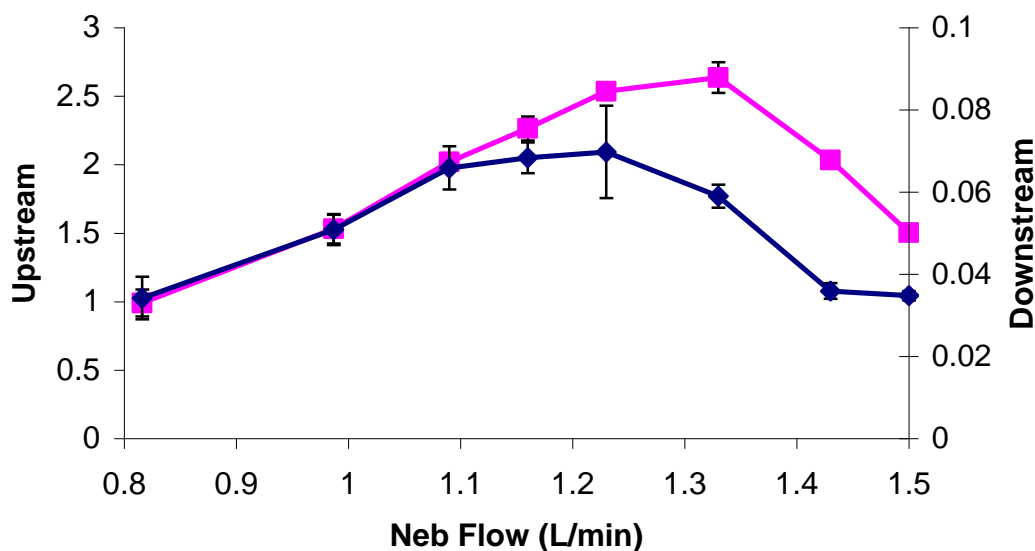

Fig 6.9 Fluorescence intensities upstream and downstream from the skimmer cone under different nebulizer flows. (——) upstream, (——) downstream

6.3.4.   Matrix components

Sample composition is another parameter we tested for transport behaviors of analyte species through the interfacial region of an ICP-MS.[7, 19] In most cases, the matrix components suppress analyte fluorescence signals inside the plasma or behind the sampling cone in the absence of the skimmer cone.

A similar trend was observed upstream from the skimmer cone in this research, as shown in Fig 6.10. When the concentrated matrix components were introduced to the analyte solution, the fluorescence signals upstream from the skimmer cone decreased. However, the transmission efficiencies of the skimmer cone did not change very much because of the simultaneous drops of downstream signals, as shown in Fig 6.11, and 6.12.
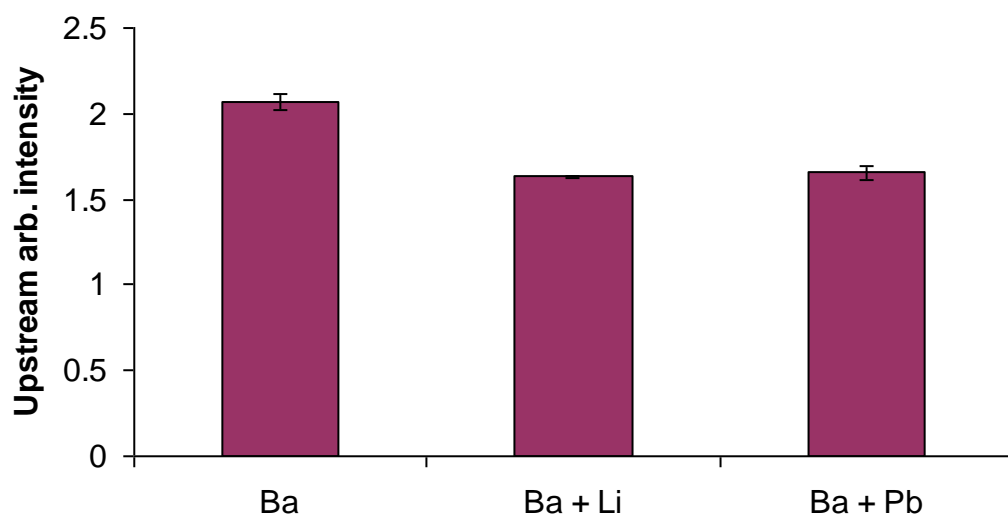
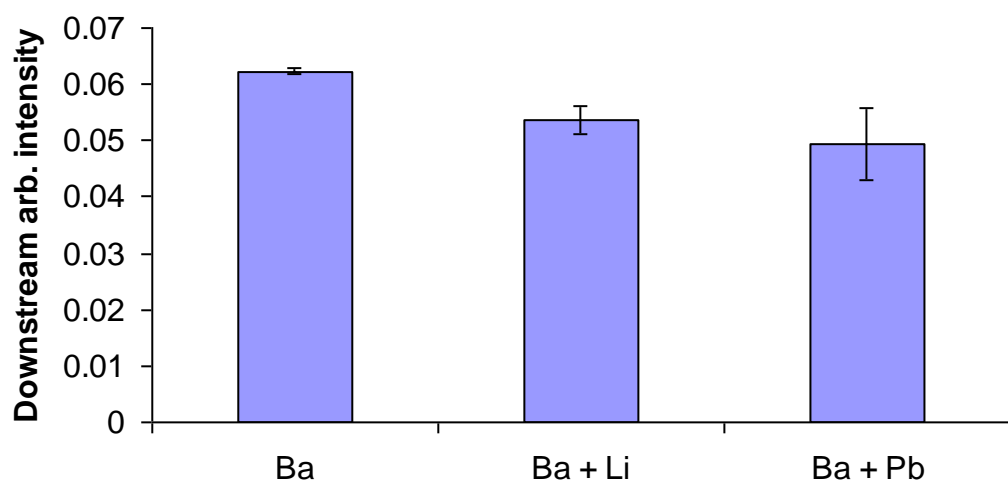Fig 6.10 Upstream signal intensity with matrix compositions

Fig 6.11 Downstream signal intensities with matrix compositions
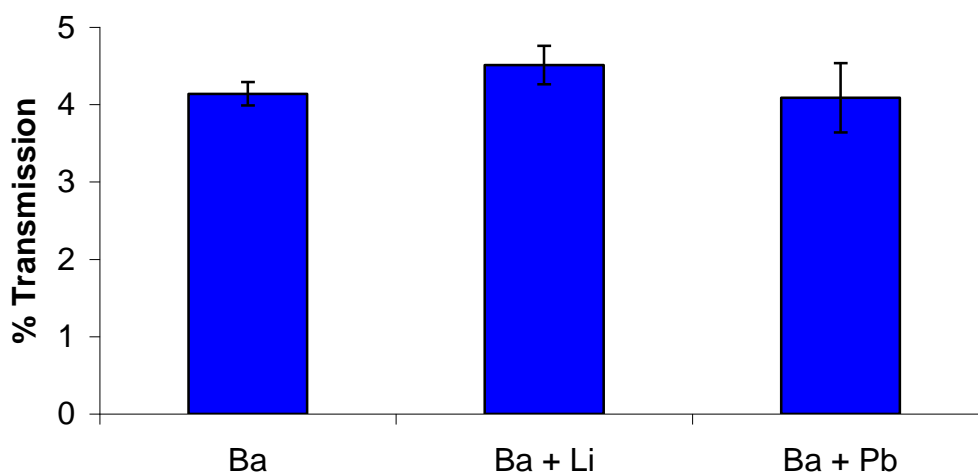
Fig 6.12 Transmission efficiencies of the skimmer cone with different matrices

6.3.5.   Effect of the first vacuum stage pressure

The optimum position of the skimmer cone is determined by the location of the Mach disk.[1] In a typical ICP-MS, the pressure of the first vacuum stage is usually fixed, although the variation of the incident power and nebulizer flow can slightly change it.[21]

In classical gas dynamic theory, it is assumed that when the skimmer orifice is located in the zone of silence, a small change in pressure should have a slight influence on the signal intensity. However, it was reported that this prediction is only true when the nebulizer flow is off.[22]

To avoid excessive interference at the tip of the skimmer cone, the skimmer orifice has to be located in front of the Mach disk.[12] Theoretically, the position of the Mach disk behind the sampling cone can be calculated by

$$\frac{x_M}{D} = 0.67(\frac{P_0}{p_1})^{\frac{1}{2}}$$

(6-3)

where x_M is the position of the Mach disk, P_0 is the pressure of the plasma, and P_1 is the pressure in the first vacuum stage. The atmospheric pressure in our lab (Provo, UT) is about 650 Torr. Therefore, we can calculate the positions of the Mach disk under different pressures of the first vacuum stage, as listed in Table 6.2.

Table 6.2 Variation of Mach disk positions with first vacuum stage

D_0	P_0	P_1	x_m
		1.1 Torr	16.28 mm
1 mm	650 Torr	1.7 Torr	13.10 mm
		2.5 Torr	10.80 mm

On the basis of Table 6.2, considering the highly diffuse character of the Mach disk and the distance change between the skimmer and sampler due to the thermal expansion when the plasma is on, 2.5 Torr was chosen as the maximum pressure used in this study.

Fig 6.13 shows the transmission efficiencies of the skimmer cone under different nebulizer flows and first vacuum stage pressures. The effect of the nebulizer flow was similar to that observed in 6.3.3. When nebulizer flow increased, the transmission efficiency decreased. Furthermore, when pressure of the first vacuum stage was changed from 1.1 Torr to 2.5 Torr, the transmission efficiency of the skimmer cone decreased significantly.

By analyzing signal intensities upstream and downstream from the skimmer cone, we can see why the transmission efficiency of the skimmer cone varied with the first vacuum stage pressure.
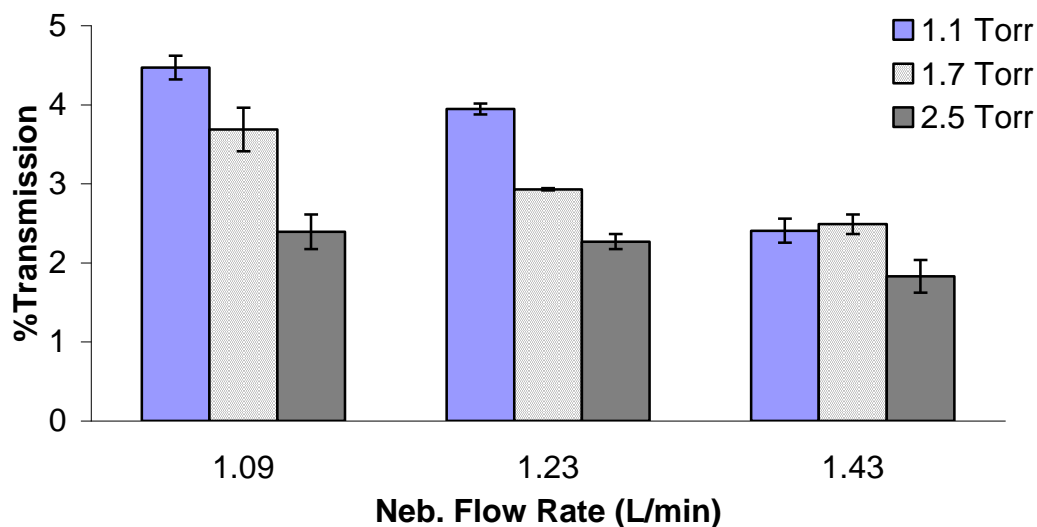
Fig 6.13 Transmission efficiencies of the skimmer cone with the variations of nebulizer flows and first vacuum stage pressures

The upstream and downstream fluorescence signals of barium ground state ions are plotted in Fig 6.14 and 6.15, respectively. The changes in transmission efficiency are caused by increases in the upstream density with increasing pressure, while the downstream signals change much less.
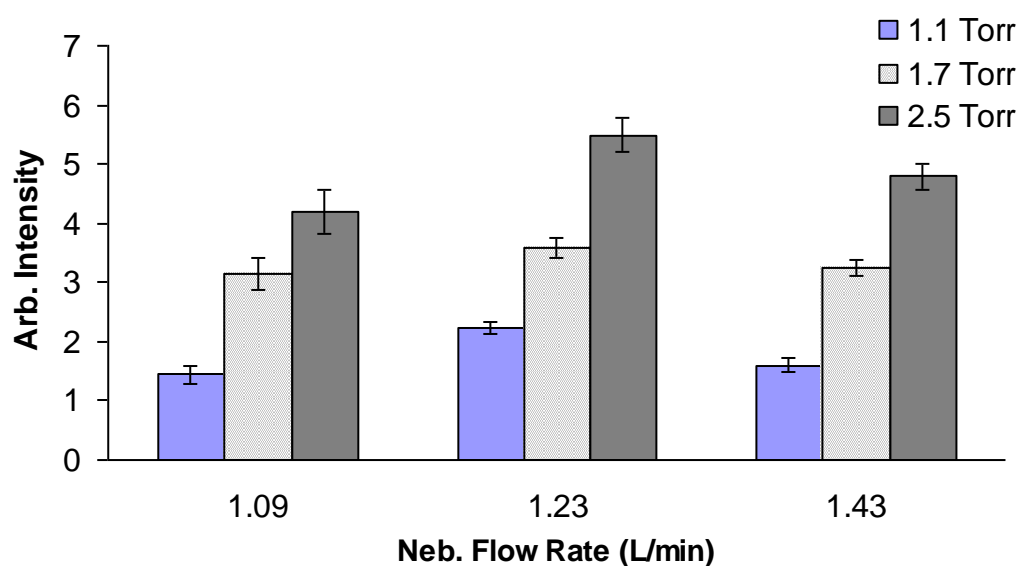
Fig 6.14 Upstream signal intensities with the variation of nebulizer flow and first
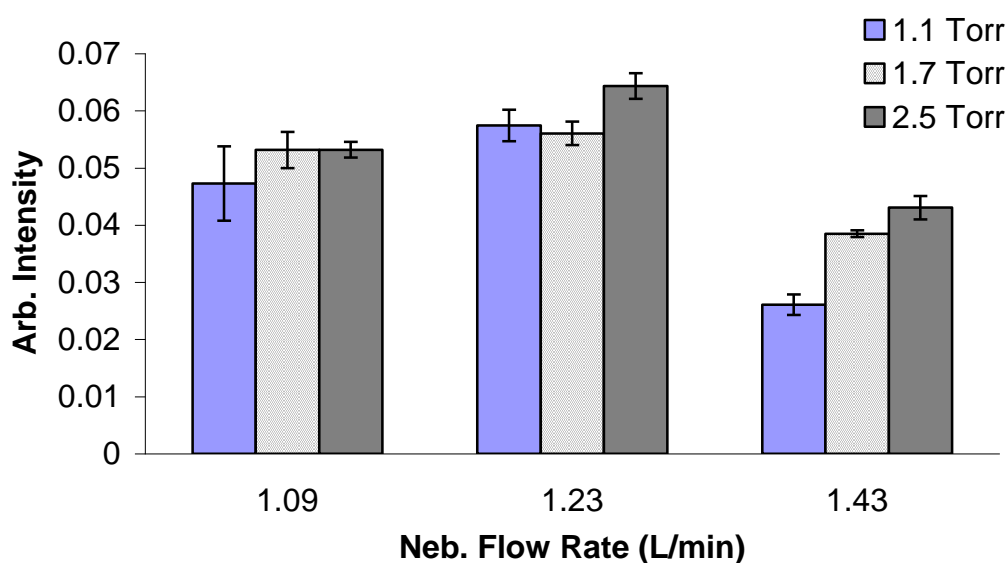
Fig 6.15 Downstream signal intensity with the variation of nebulizer flow and first

vacuum stage pressure

Gray[16] reported that the shock waves in an ICP-MS expansion stage changed with

variation of the first vacuum stage pressure. In our experiments, it appears that the

shock wave at the tip of the skimmer was also intensified with increased first vacuum

stage pressure. Therefore, more analyte particles accumulated in front of the skimmer

cone. The intensified shock wave caused bigger disturbances, which drive the

skimming process further from the ideal. It is also suspected that the recombination

between ionized particles and electrons was strengthened due to the increased

disturbance.

6.4. Conclusion

The experiments described here are the first step of a larger project. On the basis

of the experimental results, we can conclude that the transmission efficiency of the

skimmer cone is impacted by the nebulizer flow and first vacuum stage pressure, but

not by the incident power or matrix components.

Until now, only barium ground state ions have been detected. Therefore, it is premature to conclude which factor dominates the variation of the transmission efficiency of the skimmer cone with current results.

6.5. References

1 Niu H., Houk R. S., *Spectrochim. Acta Part B*, 51, **1996**, 779

2 Sakata K., Yamada N., Sugiyama N., *Spectrochim. Acta Part B*, 56, **2001**, 1249

3 Lim H. B., Houk R. S., Edelson M. C., Carney K. P., *J. Anal. At. Spectrom.*, 4, **1989**, 365

4 Stewart I. I., Olesik J. W., *American Society for Mass Spectrometry*, 10, **1999**, 159

5 Montaser, A. Golightly, D. W., *Inductively Coupled Plasmas in Analytical Atomic Spectrometry*, 2nd, VCH Publisher, Inc. **1992**

6 Tan S. H., Horlick G., *J. Anal. At. Spectrom.*, 2, **1987**, 745

7 Chen Y., Farnsworth P. B., *Spectrochim. Acta Part B*, 52, **1997**, 231

8 Douglas D. J., French J. B., *J. Anal. At. Spectrom.*, 3, **1988**, 743

9 Stewart I. I., Hensman C. E., Olesik J. W., *Applied Spectroscopy*, 54, **2000**, 164

10 Macedone J. H., Gammon D. J., Farnsworth P. B., *Spectrochim. Acta Part B*, 56, **2001**, 1687

11 Sakata K., Yamada N., Sugiyama N., *Spectrochim. Acta Part B*, 56, **2001**, 1249

12 Scoles, G., Bassi, D., Buck U., Laine D. C., *Atomic and Molecular Beam Methods*, V1, Oxford University Press, **1988**

13 Doherty W., *Spectrochim. Acta Part B*, 44, **1989**, 263

14 Campargue R., *J. Phys. Chem.*, 88, **1984**, 4466

15 Houk, R. S., Niu H., *Spectrochim. Acta Part B*, 49, **1994**, 1283

16 Gary A. L., *J. Anal. At. Spectrom.*, 4, **1989**, 371

17 Patterson J. E., Duersch B. S., Farnsworth, P. B. *Spectrochim. Acta Part B*, 54, **1999**, 537

18 Radicic N. W., Olsen J. B., Neilson R. V., Macedone J. H., Farnsworth P. B., *Spectrochim. Acta Part B*, 61, **2006**, 686

[19] Duersch B. S., Farnsworth P. B., *Spectrochim. Acta Part B*, 54, **1999**, 545

[20] Mills A. A., Macedone J. H., Farnsworth P. B., *Spectrochim. Acta Part B*, 61, **2006**, 1039

[21] Chambers D. M., Yang P. P., Hieftje G. M., *Spectrochim. Acta Part B*, 46, **1991**, 741

[22] Chambers D. M., Ross B. S., Hieftje G. M., *Spectrochim. Acta Part B*, 46, **1991**, 785

7. CONCLUSIONS

7.1. Summary

The goal of this work was to better understand the characteristics of ICP affecting ion transmission through the interfacial region between an ICP ion source and a mass spectrometer. The research covered the functions of the plasma as an atomizer and ionizer of the analyte species, the transport behaviors of analytes in the first vacuum stage, and the transmission efficiency of the skimmer cone under different operating conditions and sample compositions.

Relying on laser induced ionic and atomic fluorescence, I modified and set up the experimental instruments used to characterize the specific transmission behaviors of analytes in the interfacial region between the ICP and mass spectrometer, and carried out the following research.

1) I investigated the spatial distributions of barium ground state atoms, ground state and metastable ions at the tip of the sampling cone of an ICP-MS, which showed that the number densities of analyte species just upstream from the sampler cone drop much more abruptly than the classic gas dynamic model predicted.[1,2]

2) I verified that the sampler cone has a significant impact on the spatial distributions of barium analyte in an ICP-MS, and that the existence of the sampler cone disturbs the local thermodynamic equilibrium controlling the atomization and ionization inside the plasma. The sampling cone causes increases in the population of barium singly charged ions, suggesting a previously-unexpected role of doubly charged barium ions in the ICP.

117

3) I found that the spread of ions in the first vacuum stage of an ICP-MS is mass-dependent, that the lighter calcium ions have a wider radial spread than the heavier barium ions after traveling a specific distance behind the sampler cone. These experiments point to a source of mass bias that has not been considered in most applications of ICP-MS.

4) I measured the temperature and velocity of argon atoms and calcium ions in the first vacuum stage of an ICP-MS, showing that the axial diffusion is ambipolar; the charged calcium ions obtain a greater acceleration due to the influence of electric field behind the sampler cone. The ambipolar field may account for some of the mass-dependent behavior described in point 3 above.

5) I preliminarily characterized the transmission of barium ground state ions through the skimmer cone of an ICP-MS, which demonstrated that the nebulizer flow and first vacuum stage pressure seriously impact the transport efficiency of the skimmer cone. The low efficiencies observed in these experiments indicate that there is room for improvement in the overall efficiency of the interface, primarily by refinement of skimmer cone design.

7.2. Future work

Although the experimental results in this dissertation provide some scientific evidence and explanations of several issues of the interfacial region between the ICP and MS, some aspects of ion transmission through the interface are not fully understood yet. The identification of analyte transport processes will help us to explain the non-ideal transmission behaviors of analyte species through the interfacial region between the ICP and mass spectrometer.

7.2.1. Continued work on the skimmer cone

In chapter 6 of this dissertation, I reported preliminary results on the transmission efficiency of barium ground state ions through the skimmer cone of an ICP-MS. Other barium species, such as metastable ions, need to be investigated in the near future. The measurements of barium metastable ions are straightforward since only the excitation and collection wavelengths need to be adjusted. As stated in chapter 3 and chapter 4, by measuring the ratio of metastable ions to ground state ions, we can track temperature variations in the shock waves at the tip of the skimmer cone under different experimental conditions. Recombination of analyte ions and atoms can also be tested by proposed fluorescence measurements.

Another straightforward method to characterize the temperature and velocity variation of analyte particles inside the shock wave is high-resolution diode laser spectroscopy, which has been described in detail.[3,4] It is expected that further research can provide a comprehensive image of the shock waves. All this work will help us to understand the whole transmission process of analyte species through the skimmer cone.

7.2.2. Variation of doubly-charged species in the presence and absence of the sampling cone

As stated,[5] the role of doubly-charged ions inside the ICP will be a fruitful research point for future work. In chapter 3 of this dissertation, the possible explanation of number density increments of barium metastable and ground state ions in the presence of the sampler cone might be largely dependent on the presence of doubly-charged barium species.[6] The following reaction is speculated to shift to left

direction due to the existence of the sampler cone:

$$Ba^+ \leftrightarrow Ba^{2+} + e^- + \Delta E \qquad \text{(7-1)}$$

However, due to the noble gas structure of the doubly charged barium ions and recombination interference behind the sampler cone,[7] neither the conventional laser induced ionic fluorescence technique nor direct mass spectroscopic measurement can be used in this experiment. With the observation of the emission variation of doubly charged species, such as the rare earth elements, it is possible to investigate their number density change under different operational conditions and sample compositions.[8,9] Therefore, we can analyze the influence of the sampling cone on the densities of doubly charged particles and verify our conclusion in the chapter 3.

7.2.3. Velocity comparison of barium and calcium ions in the supersonic expansion

Resorting to the ambipolar diffusion theory, we have explained the velocity difference between argon atoms and calcium ions behind the sampler cone.[10] A possible verification of the simulation model is to measure the velocity of another element in this region. Barium is a potential candidate because of the huge mass difference between calcium and barium. The characterization of barium velocity and temperature can help us test the model and its parameters as described in reference 3. A new high resolution diode laser with specific wavelength range is needed for further investigation.

7.2.4. Argon metastable atom measurement inside the plasma

The mechanisms of atomization and ionization of analyte species in the ICP are

not comprehensively understood. Many researchers have postulated that argon metastable atoms play an important role in the analyte excitation processes.[5,11,12] Spatial mapping of argon and its dependence on the experimental variables will be useful in understanding the mechanism of analyte excitation inside ICP.

Fluorescence images of analyte species provide valuable insights into the nature of the changes in analyte distributions between the sampling cone and the load coil of an ICP-MS. The same experimental scheme may be an alternative for argon species detection. Mapping argon 4s atoms is the only possible choice.

However, due to the high temperature and therefore the fast collision frequencies among plasma species, it is impossible to get good fluorescence signals for argon species. The higher energy levels of argon atoms are split to several energy sub-levels, and the energy is released with a series of fluorescence wavelengths. Therefore, fluorescence measurements at specific wavelengths, as used in analyte species detection, are ineffective due to the high emission background, low florescence quantum yields and unacceptable signal-to-noise ratios.

Absorption depletion imaging is another experimental option for the measurement of argon metastable atoms in the plasma.[13] Although this method suffers from CCD fringe interferences, it has been proven to be a plausible way to detect the variations of argon metastable atoms under different operational conditions and sample compositions.

7.3. References

[1] Mills A. A., Macedone J. H., Farnsworth P. B., *Spectrochim. Acta Part B*, 61, **2006**, 1039

[2] Spencer R. L., Krogel J., Palmer J., Payne A., Sampson A., Somers W., Woods C. N. *Spectrochim. Acta Part B*, 64, **2009**, 215

[3] Olsen, J. B., Macedone J. H., Farnsworth P. B., *J. Anal. At. Spectrom.*, 21, **2006**, 856

[4] Patterson J. E., Duersch B. S., Farnsworth, P. B. *Spectrochim. Acta Part B*, 54, **1999**, 537

[5] Ma H., Taylor N., Farnsworth P. B., *Spectrochim. Acta Part B*, 64, **1999**, DOI: 10.1016/j/sab.2009.04.006

[6] Chan G.C.Y., Hieftje G. M., *Spectrochimica Acta Part B*, 61, **2006**, 642

[7] Macedone, J. H., Farnsworth, P. B., *Spectrochimica Acta Part B*, 61, **2006**, 1031

[8] Arrathoon R., Littlewood I. M., Webb C. E., *Phys. Rev. Lett.*, 31,**1973**, 1168

[9] Littlewood I. M., Webb C. E., *J. Phys. B: Atom. Mol. Phys.*, 7, **1974**, L332

[10] Farnsworth P. B.; Spencer R. L.; Radicic W. N.; Taylor N.; Macedone J. H.; Ma H., The Influence of an ambipolar electric field on the supersonic expansion in the first stage of an inductively coupled plasma mass spectrometer vacuum interface, submitted to *Spectrochim. Acta Part B*

[11] Farnsworth, P. B., Omenetto N., *Spectrochimica Acta Part B*, 48,**1993**, 809

[12] Lehn, S. A., Hieftje, G. M., *Spectromchimica Acta Part B*, 58, **2003**, 1821

[13] Farnsworth P. B., Taylor N., Ma H., Mapping argon metastable atoms in an ICP-MS using absorption depletion imaging, *FACSS*, **2008**